Izu-Bonin rear-arc magmatism: Geochemical investigation of volcanoclastic material

Andreas Sæbø

Master of Science Thesis in Geochemistry and Petrology

Department of Earth Science
University of Bergen

June 2017

ABSTRACT

Studied samples from the Izu Bonin rear arc show a distinct geochemical pattern that resemble the modern continental crust. In contrast to the volcanic front, samples from the Izu Bonin rear arc show enrichment of LREE (La, Ce, Pr, Nd) and higher K_2O at a given SiO_2. This suggest that processes leading up to the geochemistry observed in the rear arc is fundamental in creating the modern continental crust. Additional isotopic and trace element analysis from volcanic material recovered in the rear arc basin between Enpo and Manji seamount chain, will give new insight in the temporal variation in this magmatic regime.

The drilled core from Izu Bonin rear arc represent a time interval of 6 Ma, where the oldest unit (VII) is 12 Ma and the youngest unit (IV) is 6 Ma. Analysis of trace element show a progressively enriched mantle signature. Going from a flat, MORB like pattern in unit VII to an enriched LREE pattern in unit IV. Elemental ratios such as Nb/Zr are higher for unit IV compared to unit VII. For all units analyzed, a high LILE/HFSE ratio is observed. The isotopic composition of Nd and Hf show a decreasing trend towards unit IV, where $^{143}Nd/^{144}Nd$ is going from 0,513068 to 0,512911 and $^{176}Hf/^{177}Hf$ from 0,2832460 to 0,2831803. Better correlation between Pb isotopic composition and Nb/Zr than for Sr and Nb/Zr suggest that the slab derived material is progressively added to the mantle wedge as the mantle becomes more enriched.

These results suggest that the sources involved in rear arc magmatism has undergone a gradual change in the components contributing to the magma. Going from a depleted MORB like magmatism to a more enriched rear arc magmatism coincide with the cessation of back arc spreading in 15 My. A subduction component is added to the magma source as it becomes progressively more enriched.

AKNOWLEDGEMENTS

First, I would like to thank my supervisor Cèdric Hamelin for good guidance on the laboratory and inspiration throughout this project. Also thanks for helping me with questions related to this thesis, feedback and corrections on my writing and for putting together a very interesting project.

A big thanks to Martina Suppersberger Hamre for showing me around the crushing- and thin section lab and how to do proper rock-powder preparations. Thanks to Siv Hjort Dundas for giving me the safety tour in the ICPMS lab and for giving me an introduction on the different methods used in the lab. Also thanks to Yuval Ronen for taken care of my strontium analysis.

I will also thank my family and girlfriend Ingvild for giving me positive thoughts and being there for me whenever I needed motivation.

Finally, I would like to thank my fellow students for making these 5 years worthy. These years would have been much harder without you guys.

CONTENTS

1. INTRODUCTION

The formation and evolution of the continental crust is an important problem of terrestrial geochemistry. In the latter part of the 1960s, S. R. Taylor (1967) proposed the “andesite model” for the origins of continental crust on the basis of similarities between “calc-alkaline” or orogenic andesite formed in island arcs and the” intermediate” bulk composition of this crustal type. Such an observation has been a motivation for studies regarding island and continental arc systems. The andesites of most young oceanic arcs have been found to be more depleted elementally and isotopically than average continental crust, at least at the volcanic front. Thus, geochemical asymmetry in arcs was known prior to the advent of plate tectonics and may be what makes juvenile arc crust “continental”

The Izu-Bonin-Mariana (IBM) arc has been a target for this problematic for many years, but previous drilling efforts have focused mainly on the IBM forearc. Rear-arc IBM magmatic history has not been studied as well as the volcanic front. Previous studies(A. Hochstaedter et al. (2001); (Ishizuka et al.,2003); Y. Tamura et al. (2007)) have also shown that there is a chemical asymmetry between the rear arc and the volcanic front, where the rear arc shows a geochemical pattern that is more similar to the average continental crust. By establishing whether and why arc-related crust has inherent chemical asymmetry, testing models of mantle flow and the history of mantle depletions and enrichments during arc evolution is essential. The generation of crust develops its “continental” geophysical signature in velocity and seismic structure that are similar beneath both the volcanic front and rear arc but is heterogeneous in chemical composition.

Magmas at the volcanic front are rich in fluid-mobile, recycled slab components that swamp the mantle. These magmas are also depleted in mantle-derived fluid-immobile elements that they are dissimilar to “average continental crust” in detail(Y. Tatsumi & Kogiso, 2003). This is not the case in the rear arc. The diminished slab signature and lower degrees of mantle melting create crust that is more typical of the continents and allow the temporal history of the mantle source to be tracked more easily.

IODP 350 expedition drilled in the Izu rear-arc region in the west of the modern volcanic front to recover a complete record of rear-arc volcanism from the present back to its likely inception in Early Oligocene or Eocene times. Drilling is the only way to obtain information about volcanic eruption, sedimentation, and stratigraphy in oceanic arcs without looking through the effects of collision and accretion (e.g. (Haeckel et al.,2001); (Wiesner et al.,2004)). This potential was realized during earlier ODP drilling in the Izu forearc, e.g. (Gill et al.,1994). The forearc turbidites preserve a faithful record of arc evolution, which parallels that seen in tephra (e,g.,(Straub, 2003); (Bryant et al.,2003)) The cores recovered from the Izu Bonin rear arc represent volcanoclastic material erupted by the nearby volcanoes.

In this study, volcanic materials from the volcano bounded basin between Enpo and Manji will be analyzed in order to answer the questions related to how this rear arc/volcanic front geochemical asymmetry has been made in terms of mantle evolution in this time period. A large part of this project will be geochemical analysis including trace elements and isotopic ratios with collaboration with Japan Agency for Marine – Earth Science and Technology (JAMSTEC).

The main objective for this thesis will be to analyze the drilled core recovered from the rear arc basin. Both isotopic and trace element study will hopefully give valuable support and insight in the geochemistry of the rear arc. Investigation of these cores will hopefully give geochemical signals that reflect the magmatic processes in the rear arc.

2. THEORETICAL BACKGROUND

2.1 General

The International Ocean Drilling Program (IODP) expedition 350 went to the Izu-Bonin-Mariana (IBM) arc system to investigate the rear arc part of the subduction system, which would give valuable insight in missing parts of convergent margin processes. There have been expeditions in this area before, but expedition 350 site 1437 is the only study concerning the rear part of the IBM arc. IBM results from 50 Ma of subduction of the Pacific plate under the Philippine plate(Robert J Stern, Fouch, & Klemperer, 2003, pp. 533-543)

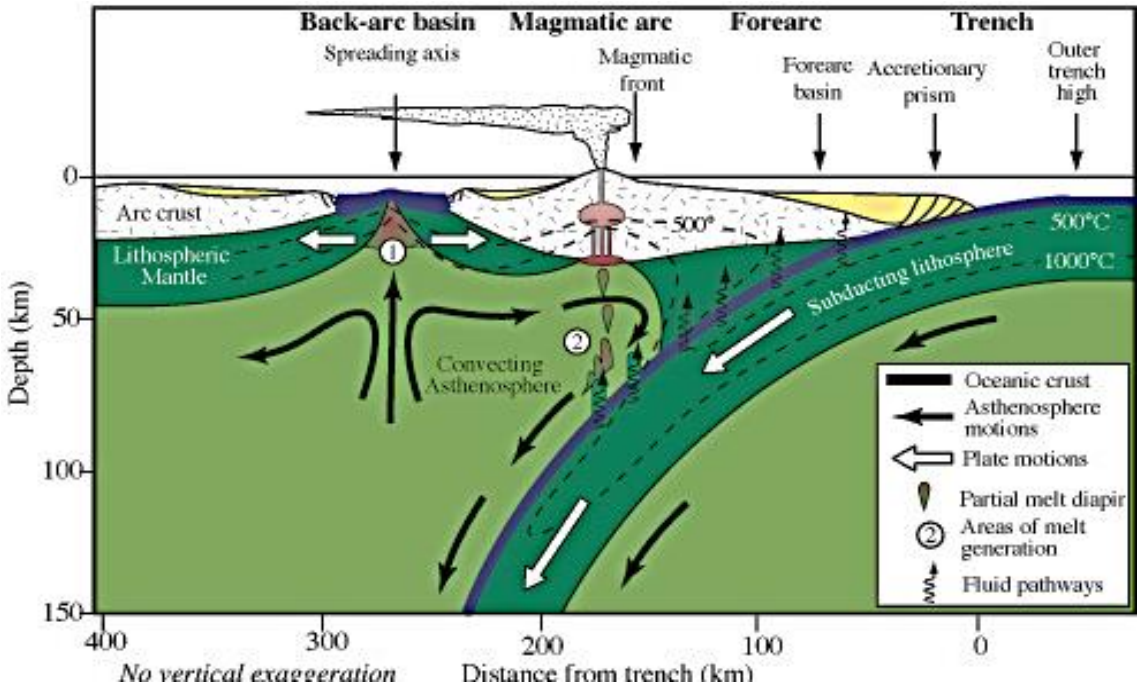

Figure 1 *This figure show a general overview of a subduction zone. The rear arc is located between the back-arc basin and main magmatic arc. Figure taken from (Robert J. Stern, 2002)*

Izu-Bonin can be divided in two distinct segments. Separating them is the Sofugan tectonic line. From here it will be represented as the Izu- and Bonin-segment, where Izu lies in north and Bonin in south.

Site U1437 is in the Izu rear arc, which is the part behind the main chain of volcanoes. Results from site U1437 are expected to give a better overview of the area and eventually a better understanding of Izu arc magmatism and genesis of continental crust. Drilled holes from this

site are unique. By drilling in the volcanoclastic material here, it is possible to track the temporal evolution by investigating the changes in chemistry.

The history of IBM is young and therefore well understood(Robert J Stern et al., 2003). Studies in this area goes back to 1890, when (Petersen, J,. 1890) identified boninites. Boninite is an extrusive, mafic igneous rocks that are extremely depleted in compatible immobile elements and have enrichments in incompatible fluid mobile elements. Further work by (Crawford, 1989, pp. 1-49) suggested that these rocks was the first rocks to be produced in a subduction zone. Geochronological work on the IBM igneous basin and boninites done by (M.A.Cosca et al.,1998) and (B. Taylor & Natland, 1995, pp. 67-96) suggest that the IBM subduction zone is of Eocene-Oligocene age.

Many features related to subduction zones, like fore arc, active arc, rear arc and back arc, are available to study here. IBM arc system is located relatively far from the continental margin. Its location close to Japan makes it easier to study. There is limited continental processes like glaciation and alluvial products that may affect the mantle, oceanic crust and fluid interactions are crucial to get proper samples and avoid contamination(Robert J Stern et al., 2003). The lack of these continental processes near the arc make it easier to study the arc infrastructure.

2.2 Intra Oceanic Subduction Zone

The IBM subduction zone is an intra oceanic convergent margin, which means that the arc crust formed here is built on oceanic crust rather than continental crust(Robert J Stern et al., 2003). In intra-oceanic convergent zones, the overriding plate is the oceanic crust.

Intra-oceanic subduction zones are not so widespread and not so easy to study as continental arcs, but they do bring new information concerning the subduction processes. These types are thought to be the first stage to produce the continental crust(Robert J Stern et al., 2003). Although there are many processes that leads to continental growth, subduction of oceanic crust beneath oceanic crust is the better geochemical match of all these growth processes.

To get a view of the processes dominating in the rear arc it is crucial for the area to be enclosed from other parts of the arc system (Yoshihiko Tamura, 2014). Izu rear arc basin lies between two seamounts, namely Manji and Enpo seamount chains. This is ideal because the basin is shielded bathymetrically. The enclosing bathymetry of the site U1437 is one of the two types of basin types recognized in arc environments. (Smith & Landis, 1995) divided arc basins in two main types; fault-bounded and volcano-bounded basin. Volcano-bounded basins are characterized by small, irregular basins between volcanoes. Between the volcanic chains,

basins are much larger. These volcano-bounded basins were and are evolving as the seamount chains are evolving. In the case of site U1437, the basin between Enpo and Manji is volcano-bounded. The primary accommodation of sediments to this basin is controlled by these volcanoes(Yoshihiko Tamura, 2014).

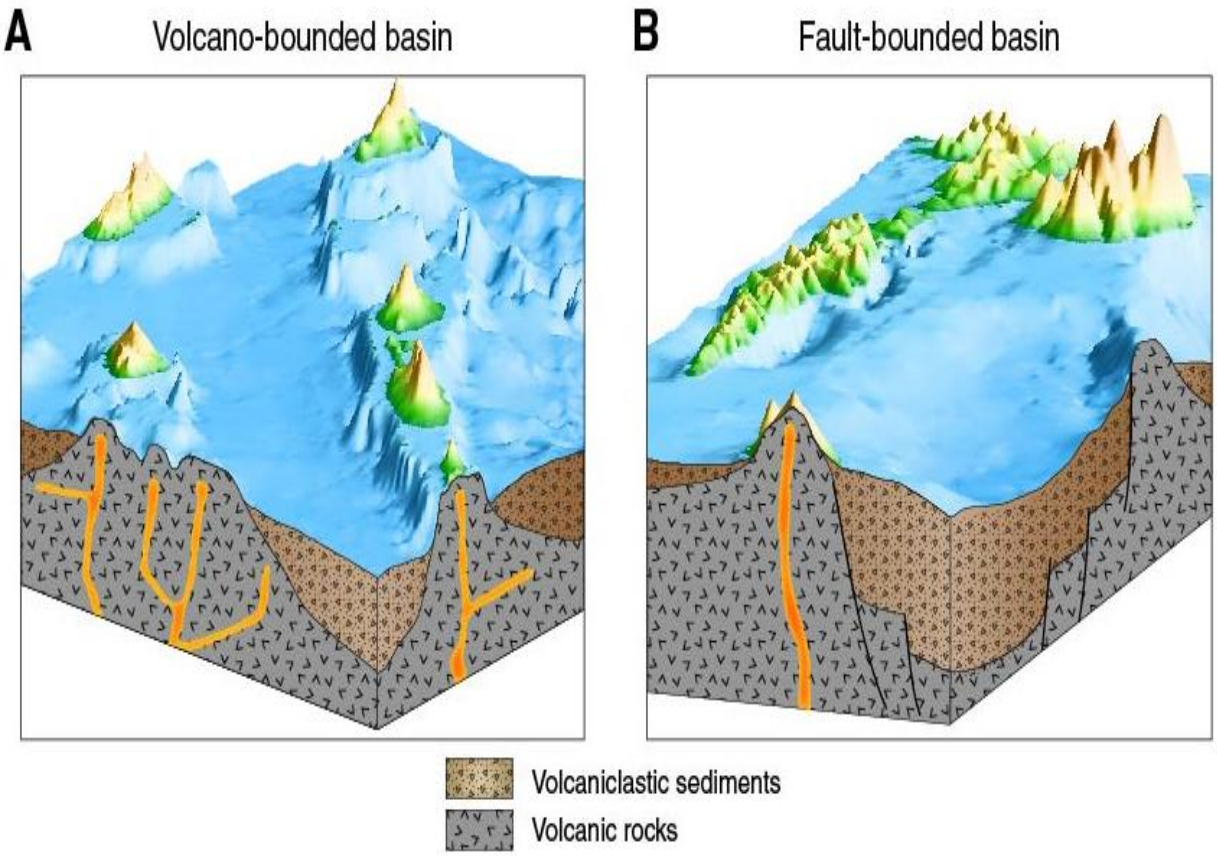

Figure 2 *Cartoon showing the difference between a volcano bounded basin and a fault bounded basin. Figure taken from (Yoshihiko Tamura, 2014)*

Limitation of arc front volcanoclastic density currents means that site U1437 is dominated by volcanoclastic mainly produced by rear arc magmatism (Yoshihiko Tamura, 2014). In this way, results from the rear arc area will reflect the temporal variations related to mantle evolution.

Since the overriding plate is the oceanic crust, resulting magma and volcanic rocks will be much less contaminated than magmatic rocks formed at continental arcs. Thus, compositions from rocks at island arcs are accurately recorded and indicative by the processes in the mantle wedge.

On average, the composition of continental crust is andesitic(White, 2013, pp. 533-543). Since we know continental crust is formed in subduction zones, they should represent the earliest stage of andesite generation, as (S. R. Taylor, 1967) proposed with the andesite model.

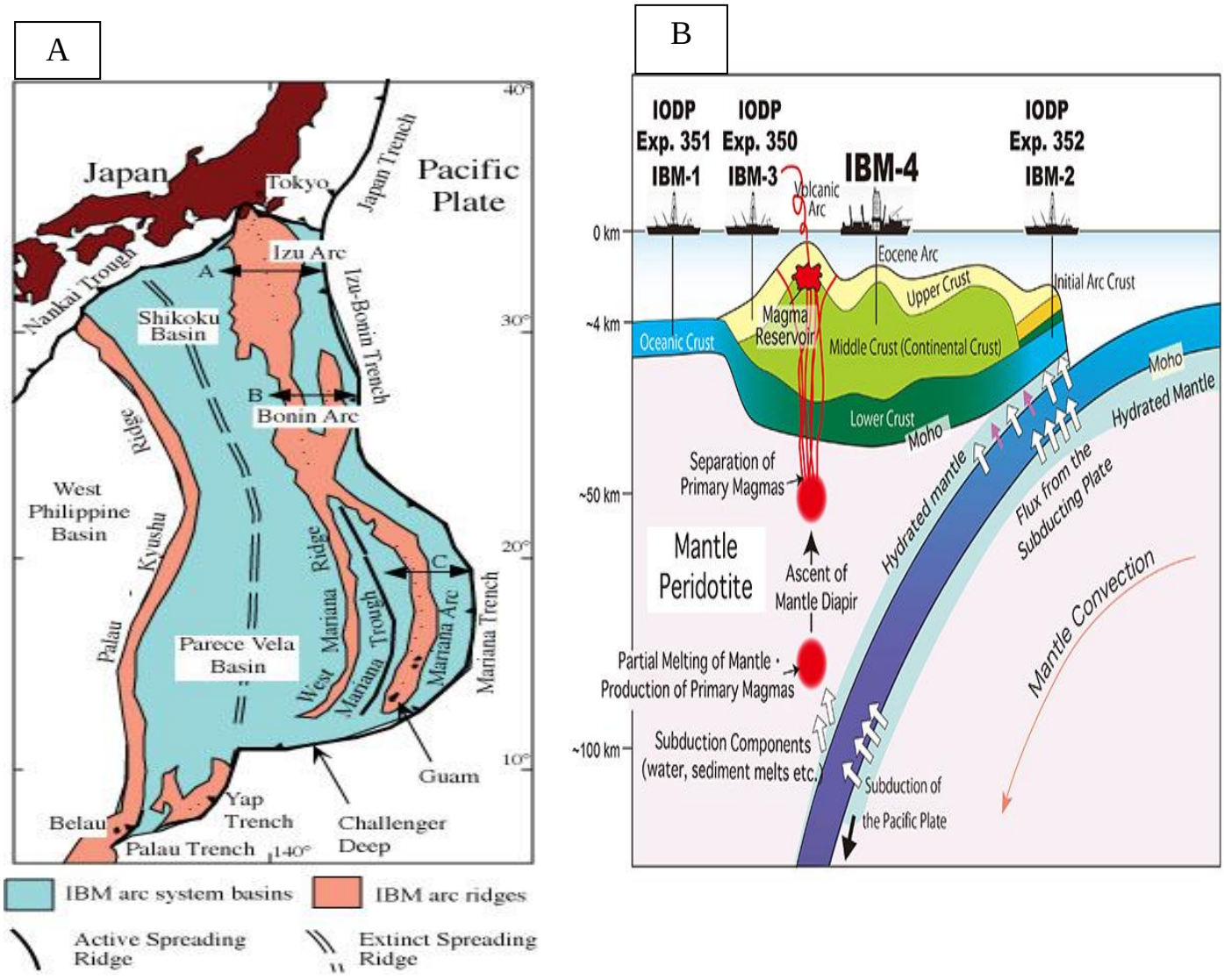

Figure 3 **A.** *Modified figure from (Robert J Stern et al., 2003).This map show an overview over the IBM subduction zone and its tectonic domains.* ***B.*** *The Izu Bonin subduction zone. From (Arculus et al., 2015).*

2.3 Geological history of the Izu Bonin

The arc system extends approximately 2800 km from the island of Honshu in north to Guam in south. IBM arc system is located on the eastern part of the Philippine Sea Plate (PSP) in the western Pacific. In north we find the only subduction triple junction on the planet. It is composed of the Japan, Izu and Sagami through. IBM arc system contains of three segments, Izu in north, Bonin- and Mariana Island in the south part. The Izu and Bonin parts are separated by the Sofugan Tectonic Line (STL)(Bandy & Hilde, 1983). Together, all three segments form a volcanic zone in N-S direction. To the east of the IBM system, we have the deep trenches. Here the Pacific Plate(PP), the oldest seafloor on the planet, is being subducted under the Philippine Sea Plate. West-northwesterly subduction of cretaceous aged pacific plate is occurring at relative velocities of 40-60 mm per year (Robert J Stern et al., 2003).

By dating the rocks formed the IBM subduction system, it is believed and well documented that the subduction zone is of Eocene age(M.A.Cosca et al.,1998). IBM has always been under strong extensional forces which have led to components like the Paulau-Kyoushu Ridge (PKR) and the IBM trench. The extensional forces are a direct consequence of the sinking subducted slab. This process is referred to as trench roll-back. This backward motion of the slab leads to thinning of the overriding plate, and eventually to rifting. The PKR represents the oldest component and IBM trench the youngest(Robert J Stern et al., 2003).

Early formed arc was remarkable for both its width and composition, being dominated by boninittic and island arc tholeittic rocks(O. Ishizuka et al., 2003).

2.3.1 Subduction Initiation

Subduction can be initiated in many ways, as proposed by Robert J. Stern (2004), where he classified the possible ways of how subduction can be initiated.

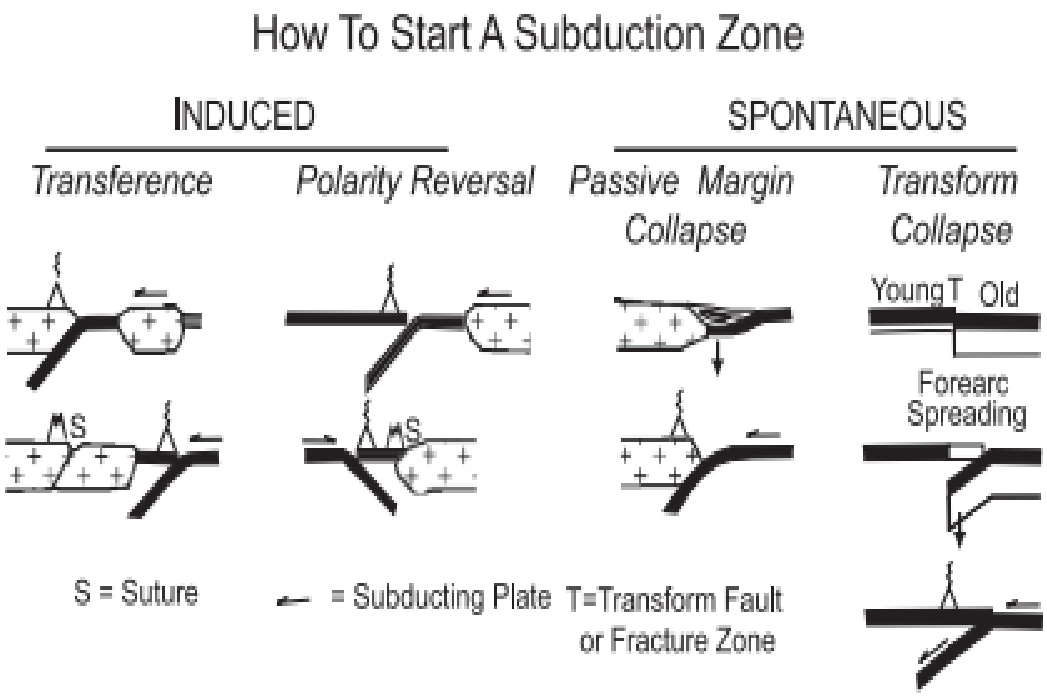

Figure 4 *The classification scheme of Robert J. Stern (2004). Shows the 4 ways subduction can be initiated.*

The great difference in lithospheric density between PSP and PP led to subsidence because of the different ages of these plates. Because of this subsidence, the transform fault or fracture zone collapsed under the big pressure. This resulted in production of the first arc magma around 49-48 Ma. During this period, magmatic activity localized along the present magmatic arc which led to cooling of the fore arc region. The transition from lithospheric subsidence to a subduction zone happened because of this. Age data shows that “true subduction”, the downgoing motion of the lithospheric plate, initiated at approximately 43 Ma. This transition may be a consequence of the remobilization of the plates(Robert J Stern et al., 2003).

Arc magmatism and formation of the first mature arc dominated until approximately 30 Ma, when the first episode of back-arc spreading occurred and created the Shikoku basin in north and Parece Vela basin in south. Spreading teared apart the first arc, producing two arcs

separated by the Shikoku basin. The remnant arc on the west of Shikoku is Paulau-Kyoshu Ridge. The spreading lasted until 15 Ma.

When back-arc spreading waned, resurgence of arc magmatism became the dominating process. This period produced basaltic to rhyolitic magmatism in the Izu rear-arc until approximately 3 Ma. This led to the formation large seamount chains, which has attracted great interest concerning the formation of the continental crust. The magmatism of the rear arc will be discussed later.

2.4 Elemental Behavior During Subduction Processes

To be able to determine magma sources and how the magmas evolve with time, chemical analyses is an important tool. Both trace elements and isotope ratios can reveal important information.

Trace elements correspond to elements with a concentration less than 0,1 %(less than 1000 ppm) of the total weight. Despite their low concentration and the fact that they have no specific influence on the minerals assemblage, they are very important magmatic tracers. These elements can substitute for major elements, by having similar ionic radius and charge, or they can fit in the crystal lattice of a mineral. For example, Ni is a compatible trace element in olivine and Cr in spinel. How easily this happens is determined by the ionic potential, which is the charge to radii ratio.

$$Ionic\ potential = \frac{Charge}{Radii} \qquad Eq.1$$

In what degree an elements is partitioned between two phases α and β is determined by the partition coefficient D;

$$D^{\alpha\text{-}\beta} = \frac{C^{\alpha(mineral)}}{C^{\beta}(melt)} \qquad Eq.2$$

In geochemical investigations, the two phases α and β are usually melt and mineral, respectively.

Based on the value of D, it has been useful to divide elements into two main groups. Those having $D \geq 1$, are considered as compatible elements. From the equation, we see that these partition in the mineral. If $D << 1$, it is an incompatible element.

Two kinds of incompatible elements can be distinguished. A plot of elements, where the x-axis is ionic radius and y-axis is ionic charge, show different groups of elements. Those with high charge to radii is called high field strength elements (HFSE). Opposite, those with low charge to radii is called large ion lithophile elements (LILE). Presence of LILE (K, Sr, Ba, Cs, Pb etc) in subduction zone magmas indicate that the magma has been added a continental component. This suggest mixing between mantle and continental components.

Investigations of mantle evolution, heavy radiogenic isotopes are often used. An important property these isotopes have in common is that the do not fractionate during magmatic

fractionation processes like melting and crystallization. In this way, they are an excellent tool to investigate sources involved in the resulting magmas.

2.4.1 Rb-Sr

Rubidium-strontium system is used for both geochronological dating and isotope geochemistry. Rb is producing Sr through beta decay. As a neutron from the Rb nucleus is transformed to a proton and electron, the electron is sent out as radiation. In this way, the daughter nucleus gain a proton and giving a higher atomic number. Decay of Rb to Sr through beta-decay can be written like this;

$$^{87}Rb \rightarrow {}^{87}Sr + \beta^-$$

It is a common property of certain elements to substitute for other elements. This is also the case for both Rb and Sr. In minerals like mica, amphibole and k-feldspar, Rb readily substitutes for K. Common minerals where Sr concentrates because of substitution with Ca, is plagioclase and apatite.

Both Sr and Rb are incompatible elements because of their large ionic radius. Rb is slightly more incompatible. This property is well used for discrimination between mantle derived magmas and continental magmas. When production of small degrees of melt, Rb is concentrated in melt, compared to Sr. Thus, the melt will have a high Rb/Sr ratio and the residual melt will have a low Rb/Sr ratio. Growing over long period of time, a high and enriched $^{87}Sr/^{86}Sr$ signature will be produced.

Addition of being incompatible, both Rb and Sr are soluble in fluids. During subduction, water is released from the subducting slab, and it carries soluble ions into the mantle wedge. Such elements which are carried with fluids are called non-conservative elements. Island arc magmas are therefore known to have a high Rb and Sr content.

2.4.2 Sm-Nd

Neodymium is produced by alpha decay from its parent Sm. This decay process can be written as; $^{147}Sm \rightarrow {}^{143}Nd + {}^{4}\alpha$

Samarium nucleus emits a helium nucleus to produce neodymium. Both Sm and Nd are light rare earth elements (LREE) and incompatible. When melting occurs, Nd is more enriched in the melt than Sm. The Sm/Nd ratio will decrease in the melt produced. The residue on the other hand, will increase in Sm/Nd. Comparison with the Rb-Sr system, they are negatively correlated. The reason for this negative correlation is that the daughter isotope is more incompatible than the parent in the Sm-Nd system. This is not the case in the Rb-Sr system.

ε-notation is used as a convention to make the measurements easier to deal with. Simply put, εNd is a number that tells how much Nd is enriched in a melt. It is defined by;

$$\varepsilon Nd = \left[\frac{(143Nd/144Nd)i}{(143Nd/144Nd)CHUR} - 1\right] \times 10^4 \qquad Eq.3$$

CHUR is an abbreviation for Chondrite Uniform Reservoir, and is the average composition of a chondrite.

Generally, positive εNd indicates depleted mantle and negative εNd is enriched mantle. High Nd is indicative of slab melting processes and not the presence of fluids. In this way, it is possible to distinguish between the two important processes in subduction zones, hydration and slab melting.

2.4.3 Lu-Hf

Lutetium belongs to the rare-earth elements. Due to lanthanide contraction, ionic radius decreases along the REEs. Since Lu is the last element in the group, it has the smallest ionic radius and thus least incompatible. Hafnium is not a REE, but in the same group as zirconium and titanium. Because of this, Hf share a lot of similar properties as Zr. Both Lu and Hf are relatively insoluble and immobile elements.

By beta decay, ^{176}Lu produces ^{176}Hf. This beta decay equation can be written as followed;

$$^{176}Lu \rightarrow {}^{176}Hf + {}^{-}\beta$$

As for εNd, εHf indicate wether there is an enrichment or a depletion. It is defined as the equation shows;

$$\varepsilon Hf = \left[\frac{(176Hf/177Hf)sample - (176Hf/177Hf)chondrite}{(176Hf/177Hf)chondrite}\right] \times 10^4 \qquad Eq.4$$

Lu-Hf system show many similarities with Sm-Nd system, but fractionation between Lu and Hf is greater than for Sm and Nd. This results in greater variation in $^{176}Hf/^{177}Hf$ than $^{143}Nd/^{144}Nd$.

2.4.4 Pb

Pb is produced by three different decay series. Radioactive parents ^{232}Th, ^{235}U and ^{238}U gives daughter isotopes ^{208}Pb, ^{207}Pb and ^{206}Pb, respectively. All these decay series have different half-life and this is the reason why Pb dating and Pb isotopic analysis is so useful.

Lead is a transition metal. As with Sr and Nd it is also an incompatible element, but not as much as its parents uranium and thorium. Since these are incompatible elements means that they are concentrated in the earth's crust.

As Sr, also Pb is highly soluble in fluids. Pb is transported by water released from the subducting slab and carried into the mantle wedge. These two elements are good proxies for fluids in subduction zones. Compared with MORB and OIB (Ocean Island Basalt), island arc basalts generally have elevated $^{207}Pb/^{204}Pb$ isotopic ratios. This is due to the incorporation of sediments in subduction zone magmas.

2.5 Subduction Factory

This section will discuss the different aspects of subduction. How it is a part of the dynamic processes on Earth, the nature of subduction zones and the how the different components in a subduction zone is affecting the resulting rock type.

2.5.1 Earth dynamic and mantle convection

The Earth is a dynamic planet. Since Alfred Wegener came up with the idea of continental drift in 1912, why plates move has been one of the major questions in recent times.

Plates move because of mantle convection. This convection is generated by internal heat produced in the mantle by radioactive breakdown of elements like K, U and Th. This heat creates a thermal gradient between the surface and the deep mantle. Warm material rise to the surface, cools and sinks. In this way, convection cells are produced in the mantle.

New techniques such as seismic tomography and geochemistry has led to hypotheses regarding the mantle convection cells. According to single convection cell model, the upper part of the mantle should be colder and the deep part should be warm. At subduction zones, cold lithospheric plates are brought down in the mantle. These areas are colder than normal. At mid-ocean ridges, high degrees of melting produce areas that are warmer than normal. These varying temperature anomalies can be seen in seismic tomographic models, by measuring both P- and S- wave velocities. Based on this, the shallow mantle temperature anomalies do not agree with the idea of a single convection cell model.

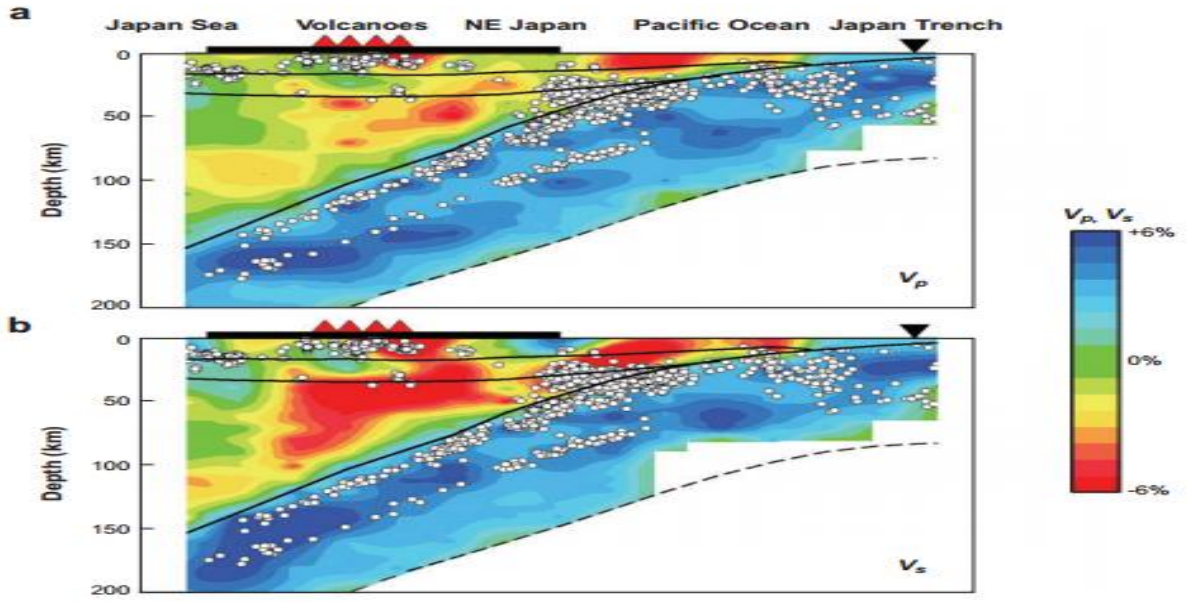

Figure 5 *V_p and V_s indicating hot and cold regions in a subduction zone. Figure from (Zhao et al.,2007)*

Analyses of mid-ocean ridge basalts(MORB) and ocean-island basalts(OIB) show opposite chemistry. MORB is depleted in the most incompatible elements and OIB is enriched in the most incompatible elements. Since both MORB and OIB are not contaminated by continental crust, the do rely on some information on the mantle source, from where they are derived. MORB provides information on the upper depleted mantle source and OIB on the lower (enriched) mantle source. These results indicate that the mantle is layered, but how this is affecting mantle convection is still under debate.

Subduction zones are important for the mantle convection (Stern 2007). The driving force for plate tectonics is about 10% ridge push. Greater density of the lithosphere, about 1,5%, than asthenosphere. Slab pull and slab suction is estimated to be around 90% of the driving force of plate tectonics. In the great picture, plate tectonics is just a surface expression of mantle convection.

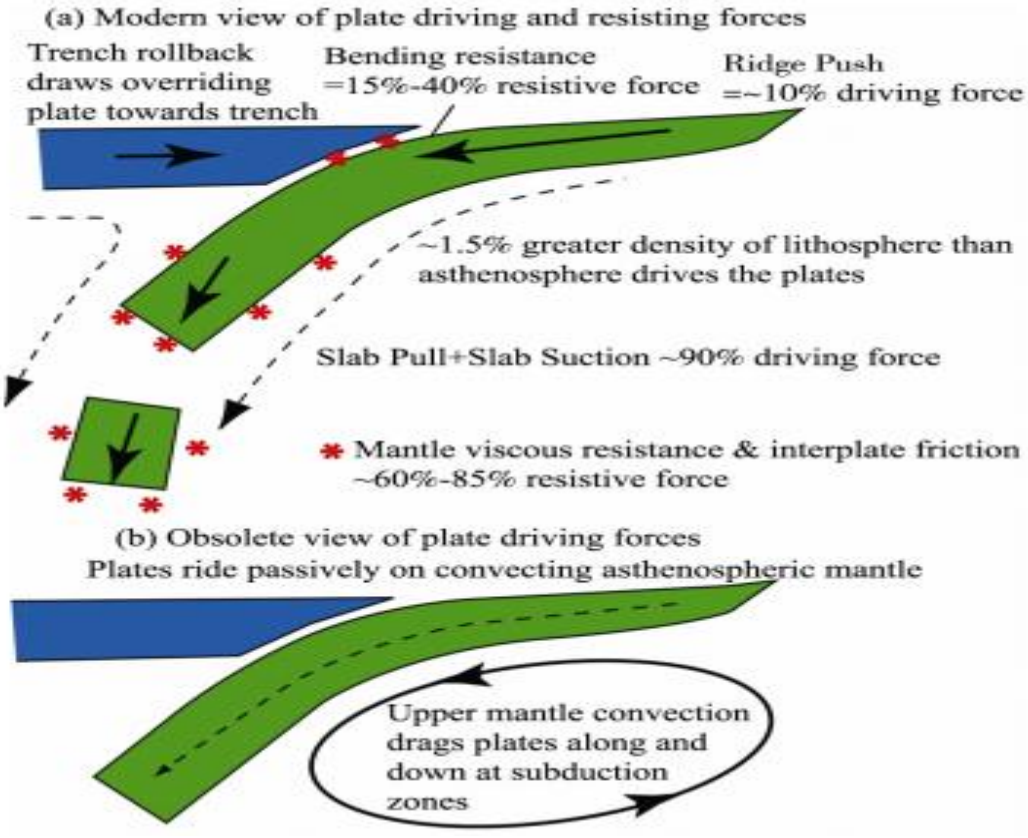

Figure 6 *Modern view of the resisting and driving forces in a subduction zone. Figure from (R. Stern, 2007).*

2.5.2 Geochemistry of subduction zones

The process of subduction combine many components such as mantle wedge, fluids, lithospheric mantle and sediments. All these components are exerted to high pressure and temperature. This makes the subduction zone processes very complex.

Comparison between subduction angle and volcanic arc width shows a negative correlation. In other words; steep angle gives small arc width. Estimated from geophysical tools such as seismic tomography, most arc volcanoes are situated 110-170 km above the subducting slab, independent on the dip of the slab. This limited region of 110-170 km suggests that arc petrogenesis is produced by important pressure-temperature dependent processes like dehydration and melting.

As the slab descends into the mantle, it is heated and squeezed, thereby changing the mineralogy and volatile contents of sediments, crust and mantle lithosphere. Arguing the most important agent in subduction zone magma genesis is the presence of fluids.

When temperature and pressure are increased, H_2O is released from the slab. Water comes from pore spaces in sediments and from the crystal lattices of hydrated minerals such as amphibole and serpentine. At high temperature and pressure, water becomes super critical. This allows water to dissolve additional elements. In island arc basalts, the enrichment of fluid mobile incompatible elements is a geochemical fingerprint.

P-T diagrams show that the subducting slab is too cold to melt at these shallow depth. Thermal gradient of the slab does not cross the solidus. What happens is that water released from serpentine and some amphiboles in the shallower part of the subduction zone, reacts with the lherzolitic mantle wedge. This reaction form an amphibole called pargasite. Most of the water in the upper mantle is bounded up in pargasite. When pargasite is formed, the geothermal gradient of the slab crosses the wet solidus and melting can occur.

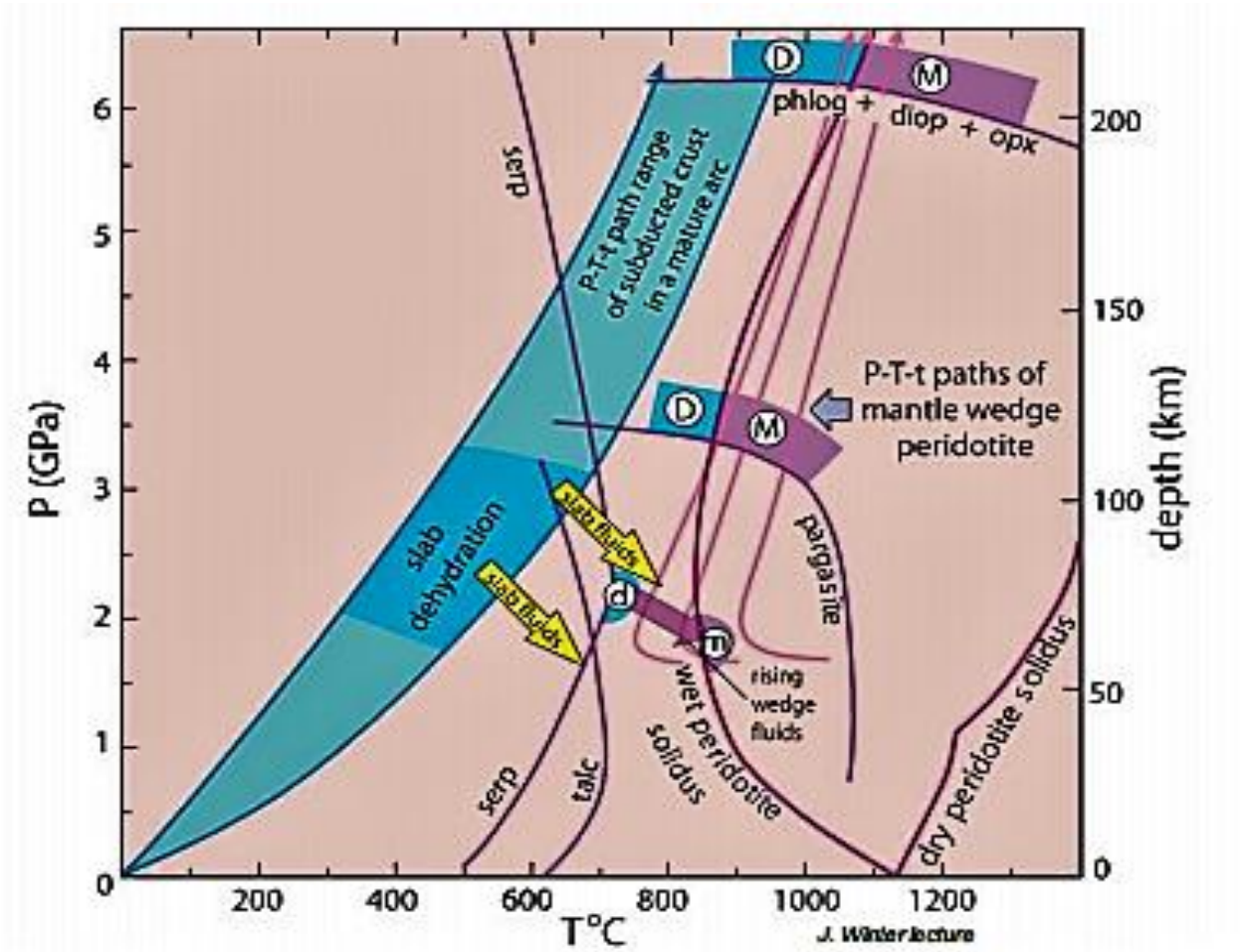

Figure 7 *P-T diagram showing the importance of water in subduction zone environments. Figure from (Winter, 2010).*

Experimental studies from (Bureau & Keppler, 1999) have shown that silicate melts are miscible with hydrous fluids under the specific pressure and temperature conditions found in subduction zones.

Spatial and temporal variations are found in the distribution of island arcs. The so-called K-h relationship is the comparison of K_2O content with the distance from slab surface or the Wadati-Benioff zone. It shows that K_2O is increasing away from the trench side and thus K_2O is increasing with the distance from the slab surface(Dickinson, 1975).

Even though there are several processes leading to the formation of magmas in a subduction zone, basalt still dominates among the rock types in these areas, as shown in figure 9. There are some places where andesites dominate and basalt is rare. Overall, convergent boundaries are dominated by basalts and andesites. Basalts are more widespread but andesites are concentrated and are typical for convergent boundaries.

2.5.3 Components of a subduction zone

The mantle wedge is the triangular region above the slab and under the island arc. It is here the inputs from the slab is mixed with the mantle. Opposite to hot magma-regimes such as mid-ocean ridges and hot-spots, subduction zones are cold. This region of the mantle moves with the sinking plate, something called induced convection. The interaction between moving mantle, rising fluids and sinking slab defines the subduction factory.

The addition of aqueous fluids leads to melting in the mantle wedge. This type of melting is called flux melting and happens because water lowers the melting point of the mantle. The distinctive chemistry of arc lavas come from the addition of fluids. These fluids can transport ions. With the P-T conditions in the subduction zone, super critical fluids can dissolve additional elements. The typical island arc magma is enriched in large-ion lithophile elements (LILE) like Sr, Cs, Rb, K, Ba etc.

Fluids can also come from pore water stored in sediments. Even though most of the sediments are scraped off in an accretionary prism, some is subducted. Typically, sediments are enriched in Sr having a high $^{87}Sr/^{86}Sr$ and low $^{143}Nd/^{144}Nd$. As mentioned, water can come from pore spaces in sediments. Also, sediments begin to melt further down in the subduction zone. It is important to mention that type of sediments vary with latitude and climate. This will affect the final composition of the rock. For example, sediments in the Mediterranean Sea are mostly evaporitic. This give an unusual chemistry on the arc volcanoes formed here. In other regions, sediments can be deep sea clay, terrigenous silisiclastic sediments and carbonates.

The overriding plate with its sediments is called the slab. This plate can affect the processes leading to the resulting magma in several ways. The age of the incoming plate can vary on Earth. An old plate, such as the Pacific, is dense and thick. On the other hand, the Nazca plate is much younger, and thus it is less dense and less thick. Age of the incoming plate is also directly correlated with the sediment content.

2.5.4 Recycling of residual waste material

Not all the material is going to produce arc magmas, but a lot of it is recycled into the deep mantle. What is recycled is called waste material. This material of the subducting slab is brought further down in the mantle. As both pressure and temperature increases with depth, chemical modification occurs via processes like melting and dehydration. As some of the oceanic crust is mixing with mantle wedge to produce arc basalts, mafic lower crust along with sediments is recycled. Waste material and residues produce distinct geochemical reservoirs within the mantle(Yoshiyuki Tatsumi, 2005). Evolution of the mantle will thus be affected by this input over time. Understanding subduction zones is therefore important to understand both the evolution of continental crust and mantle.

Crust and sediments are being recycled down in the deep mantle. Since processes like dehydration and melting occurs, the chemical state of the slab will be changed through time. When this residual slab enters the deep mantle, it will affect the chemical state of the mantle and produce mantle heterogeneity. Oceanic island basalts and mid-ocean ridge basalts show a wide diversity in isotopic composition. It is proposed that different geochemical reservoirs are producing this diversity. Depleted MORB mantle (DMM), enriched mantle 1 (EM1), enriched mantle 2 (EM2) and high-μ mantle (HIMU) together with primitive mantle are the endmembers that may explain isotopic diversity of ocean basalts(Yoshiyuki Tatsumi, 2005).

Isotopic studies of MORBs show that DMM is the distinct geochemical reservoir of the upper shallow mantle. Enriched mantle types are associated with hot spots. The enriched signature may be a result of the recycling process of subduction zones, where the residual slab brings modified material to the deep mantle. Input in the mantle from the slab concern sediments, altered oceanic crust and mafic lower crust.

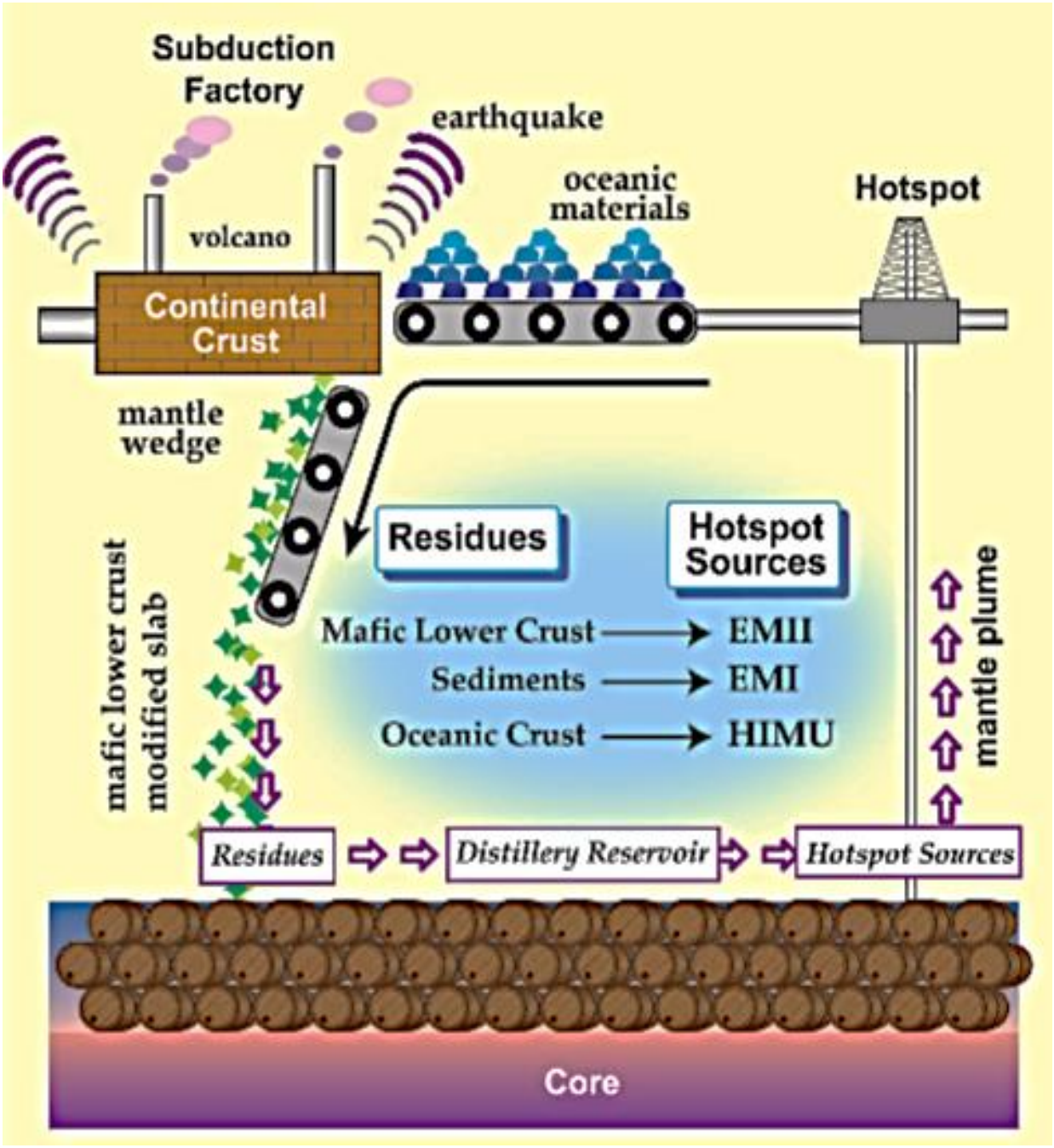

Figure 8 *A cartoon showing how the subduction factory works. Oceanic material is brought down in the mantle. As P-T conditions increase, water and fluid-mobile elements are added to the mantle wedge. Conservative elements are brought further down as residues. These residues may be the sources for hotspots. From (Yoshiyuki Tatsumi, 2005)*

2.6 Generation Of Continental Crust

Earth is the only planet in our solar system which as two types of crust; oceanic and continental. Over geological times, it has been shown that the proportion of continental crust has not been constant (Yoshihiko et al.,2016). Earth`s production of continental crust has been essential for life to exist. It has been showed that subduction zones, makers of continental crust, has major impact on Earth`s climate and thus life(Hubisz, 2014, pp. 452-465).

Divided in two main parts, the continental crust consists of mafic lower crust and felsic upper crust. On average, it has an andesitic composition.

The origin of the first continental crust is still a debated problem. How it has evolved to modern day continental crust is also a focus of recent studies Several hypotheses are presented as models to show the evolution of continental crust growth. Is it formed from early extraction from the mantle (e.g. Fyfe (1978), Reymer and Schubert (1984), Armstrong (1991)) ? Long term steady state growth (Hurley & Rand, 1969) ? Episodic growth (S.R.Taylor et al.,1981)?

As stated earlier, andesitic magmas are characteristic of convergent plate boundaries. It is therefore important to investigate convergent plate boundaries to understand the production of continental crust.

Although andesites are characteristic for convergent zones, basalt still dominate the eruptive products. How is andesite produced? Melting of basaltic magma can give an andesitic magma. If this is extracted, basalt will still dominate in volume because of the small proportion of melt produced. Removal of this basaltic lower crust will make andesite the dominant part. Removal of the lower basaltic crust can happen by delamination.

Locality	B	B-A	A	D	R
Mt. Misery, Antilles (lavas)[2]	17	22	49	12	0
Ave. Antilles[2]	17	(42)		39	2
Lesser Antilles[1]	71	22	5	(3)	
Nicaragua/NW Costa Rica[1]	64	33	3	1	0
W Panama/SE Costa Rica[1]	34	49	16	0	0
Aleutians E of Adak[1]	55	36	9	0	0
Aleutians, Adak & W[1]	18	27	41	14	0
Little Sitkin Island, Aleutians[2]	0	78	4	18	0
Ave. Japan (lava, ash falls)[2]	14	(85)		2	0
Isu-Bonin/Mariana[1]	47	36	15	1	< 1
Kuriles[1]	34	38	25	3	< 1
Talasea, Papua[2]	9	23	55	9	4
Scotia[1]	65	33	3	0	0

[1] from Kelemen (2003a and personal comunication).
[2] after Gill (1981, Table 4.4) B = basalt B-A = basaltic andesite
A = andesite, D = dacite, R = rhyolite J. Winter lecture

Figure 9 *Figure from (Winter, 2010) showing rock distribution in island arcs.*

Geotherm is a well-known term that defines how rapidly the temperature increases down in the Earth. It varies from different tectonic environments. It is a fact that the geotherm was much steeper and hotter in the Archean. This would favor slab melting instead of dehydration processes. With today's geotherm, dehydration processes dominate in the upper part of the slab.

There are several experiments based on interaction with melts to produce andesite. High pressure experiments from (Rapp, Shimizu, Norman, & Applegate, 1999) showed that a reaction between silica-rich melt from slab melting and magnesium-rich mantle produce andesite. But even though andesite is produced, it does not mean that it has the characteristic isotopic and trace elemental pattern observed in all convergent andesites. An article written by (Y. Tatsumi, 2003) supplies with geochemical results that confirms with the high pressure results from (Rapp et al., 1999). Y. Tatsumi and Kogiso (2003) used geochemical modelling to show that andesites indeed inherit the characteristic geochemical trace element pattern.

A new hypothesis from (Yoshihiko et al., 2016) relates crustal thickness to magma type. Izu - Bonin is used as an example. This article proposes how andesitic crust can be produced in

modern intra oceanic subduction zones. Gravimetric and seismic measurements show differences in crustal thickness between the two segments of Izu-Bonin. Crustal thickness of Izu is estimated to be around 10-20 km and of Bonin, approximately 35 km. In other words, the southern part of the two segments has the thicker crust. Comparing these with dominant magma type, it is concluded that thin crust has andesite as dominant product and thick crust has basalt as dominant product.

Interaction between mantle and slab melts produces a mix of melts that rises diapiric under the arc crust. When this melt diapir reaches the base of the crust, it stalls. When this happens, the internal heat of the diapir is reduced. Because of the different crustal thickness of Izu and Bonin, stalling of this diapir will happen at different depths. This means that fractional crystallization is being exposed for different pressure. This will affect the final crystallized mineral assemblage and thus on the resulting rock type.

(Yoshihiko et al., 2016) did a study on how the crustal thickness affect the rock composition. According to (Yoshihiko et al., 2016), primitive arc magmas has following values; Mg# = 70 and $FeO^*/MgO < 1$. In addition to different crustal thickness between Izu and Bonin, it is observed different values of SiO_2 at similar Mg# and FeO^*/MgO(Yoshihiko et al., 2016).

Calc-alkaline magma and high Mg# andesites could not be produced from basaltic primary magmas through fractional crystallization. But they can be produced from andesitic primary magmas, which implies shallow origin.

Water (H_2O) plays an important role in subduction zones. It is the reason why melts are formed here. At high H_2O content, magmas can produce more evolved magmas, in other words higher saturation of silica(SiO_2). For example, an anhydrous lherzolite at 1GPa will produce basaltic melts. If the H_2O content for the same lherzolitic source were higher, it would be able to produce magmas with higher Mg and SiO_2.

Magmas get more silica-rich at decreasing depth and more silica-poor at increasing depth.

Looking at phase diagrams of olivine, pyroxene and silica, we can see how their representative fields change in order of increasing pressure. At low pressure and hydrous conditions, liquidus field of Mg-olivine(Fo) expands relative to enstatite field(pyroxene). At some point, enstatite incongruently produces primary andesitic melt.

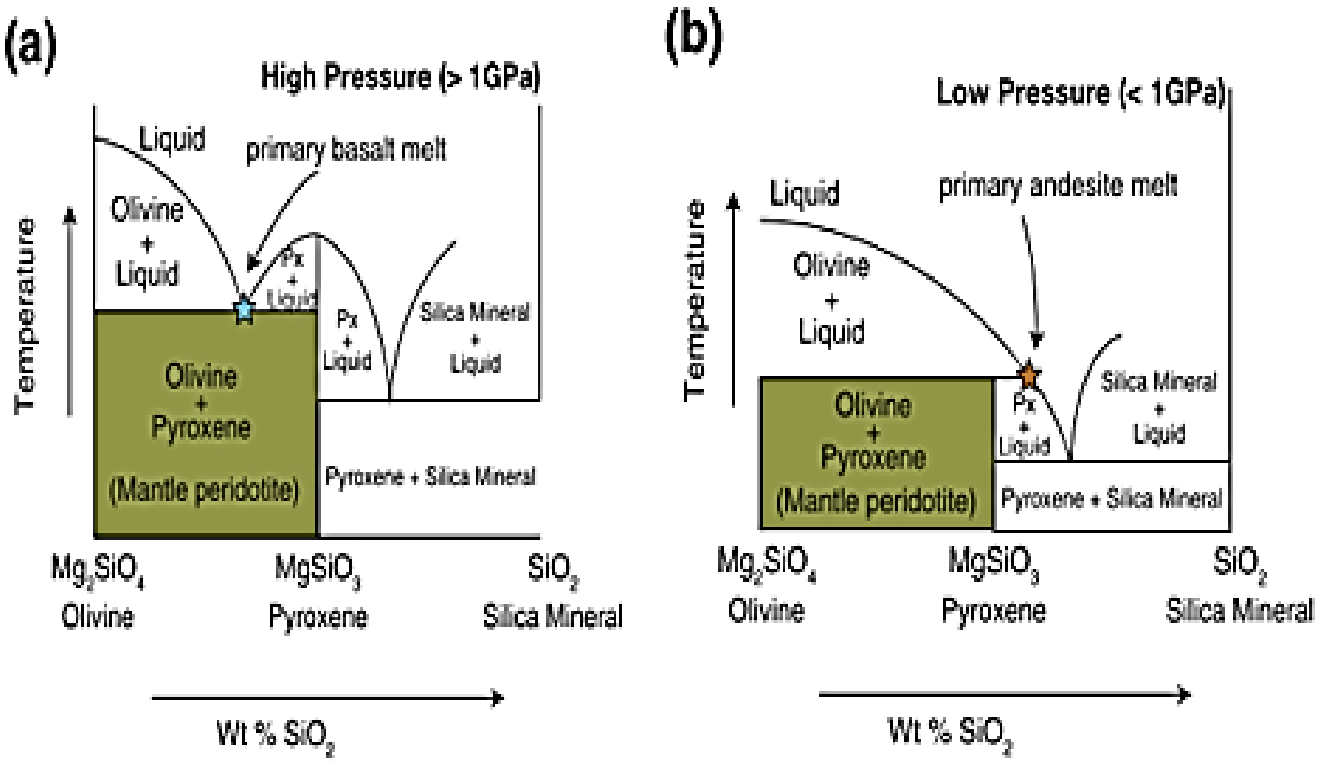

Figure 10 *The phase diagram for Olivine-Pyroxene-Silica is shown with different pressures. Notice how the Olivine+Pyroxene stability field changes with pressure. Figure from (Yoshihiko et al., 2016).*

Interestingly, average continental crust has the composition of andesites. This observation has led to evidence that subduction zones may be where continental crust is being formed. To make andesitic continental crust, like the modern, delamination between initial basaltic arc crust and the extracted felsic melts must happen. Otherwise it is a mainly basaltic arc crust, which is not the real case

2.7 Rear Arc Magmatism

Rear arc part of the Izu – Bonin is defined as the volcanoes behind the main arc and comprise all volcanic rocks with Neogene age (23-3 Ma). These rocks include the east-northeast trending basalt to rhyolite seamount chains ranging from 17-3 Ma. Further east lies an extensional zone. This wide zone consists of two different suites; volcanic rocks in the back-arc knoll zone which have ages younger than 3 Ma, and rocks represented by the active rift, that is younger than 1,5 Ma. To get an overview, these rocks have been divided in two different magma suites based on geochemical environment. These are the east-northeast trending seamount chains and rift type magmas in the extensional zone which is younger than 3 Ma.

All these Neogene rocks lies on arc crust. Worth mentioning is that the most western part of the seamount chains lie on oceanic crust produced in the opening of the Shikoku Basin.

Geochemically, differences between arc front/rear arc seamount chains can be distinguished from the rift type rocks. These geochemical differences are directly connected to the sources which these rocks formed. Hypotheses for this difference in geochemistry:

1) A change from flux (H_2O) melting to pure decompression melting, due to rifting initiation
2) Changes in the slab-derived input of geochemical signal
3) Change in the thermal structure of the underlying mantle

Geochemical arc asymmetry is observed in island arc systems. This is also the case in IBM arc. IBM comprise a 2800 km volcanic chain in the western Pacific. Izu arc segment represent 700 km. This northern part of IBM is characterized by intervals of spaced volcanoes which is dominated by basalt, between these volcanoes, regular submarine calderas are dominated by rhyolites.

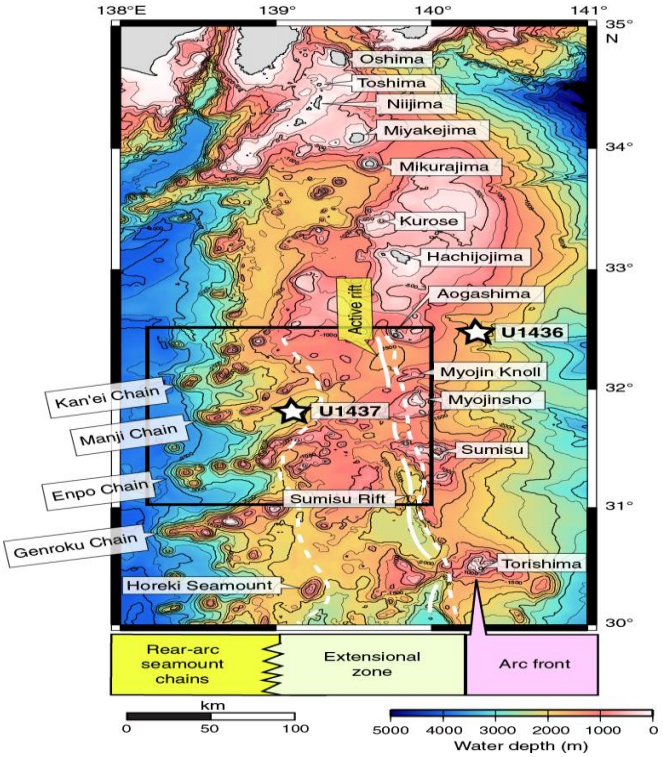

Figure 11 *Tectonic domains of Izu-Bonin. From (Yoshihiko Tamura, 2014)*

Arc asymmetry can be seen, based on major trace elements and isotopic ratios, as mentioned. (Gill,1981) noted that variation of K_2O vs SiO_2 was one of the most important in understanding the variation in subduction related magmas. This variation is observed in Izu arc and is clearly asymmetry across the arc. An increase in K_2O from the trench towards the rear arc indicated that there should be change in the source of these magmas. Arc front is mainly low-K and rear arc is medium-K to high-K.

This asymmetry is also observed when looking at trace elements and isotopic ratios, as mentioned. Looking at rare earth elements, arc front shows strongly depletion of incompatible LREE relative to both MREE and HREE. Rear arc on the other hand shows an enriched pattern of incompatible LREE relative to MREE and HREE.

Depletion of LREE compared to HREE indicates that the source for volcanic front magmatism is depleted, which means that the major magmatism is sourced from the mantle. However, the enriched source for the rear arc is yet to be understood.

These asymmetric patterns can be used as distinguishable factors between arc front and rear arc rocks. In addition to this, K_2O and REE patterns of rear arc show striking similarities with the average continental crust(Rudnick & Gao, 2014). This may be indicative that the magmatic processes at rear arc is the best fit for generation of continental crust.

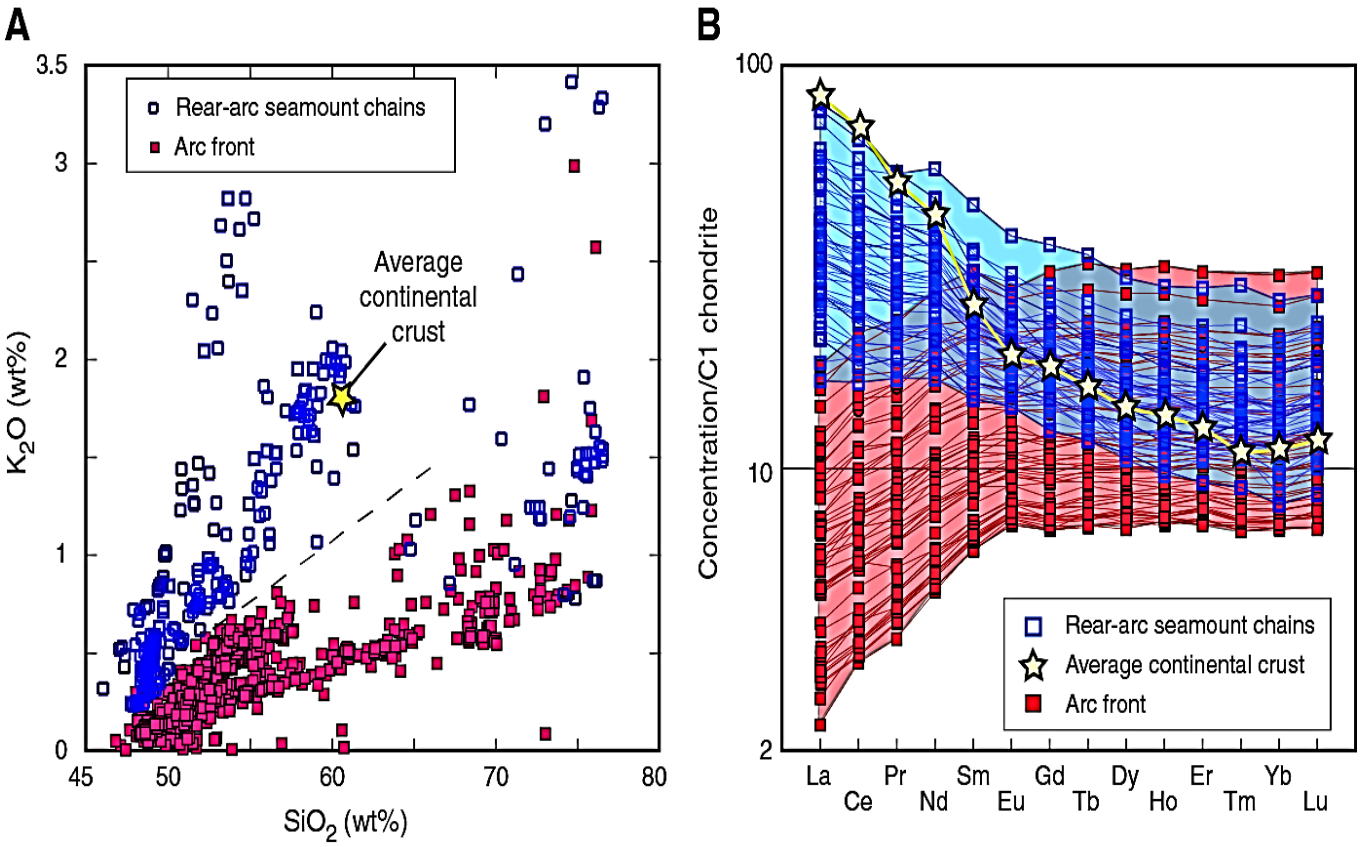

Figure 12 *Figures showing the chemical heterogeneities between arc front and rear arc. To the left, variation in K_2O with SiO_2. Chondrite normalized REE patter to the right. Major element data are taken from (Yoshihiko Tamura & Tatsumi, 2002) and the references therein. REE data are taken from (R. N. Taylor & Nesbitt, 1998), (A. Hochstaedter et al., 2001) and (Osamu Ishizuka et al., 2003).*

The rear arc seamounts are enriched in alkali, high field strength elements (HFSE) and other incompatible elements. Important to notice is that rear arc rocks have low abundance in Sr and Pb compared to the arc front. Isotopic ratios also show difference between rear arc and arc front. For example, heavy radiogenic isotopes as $^{143}Nd/^{144}Nd$ and $^{177}Hf/^{176}Hf$ are showing higher values in the rear arc compared to arc front. This correlate well with the REE pattern shown in figure 12.

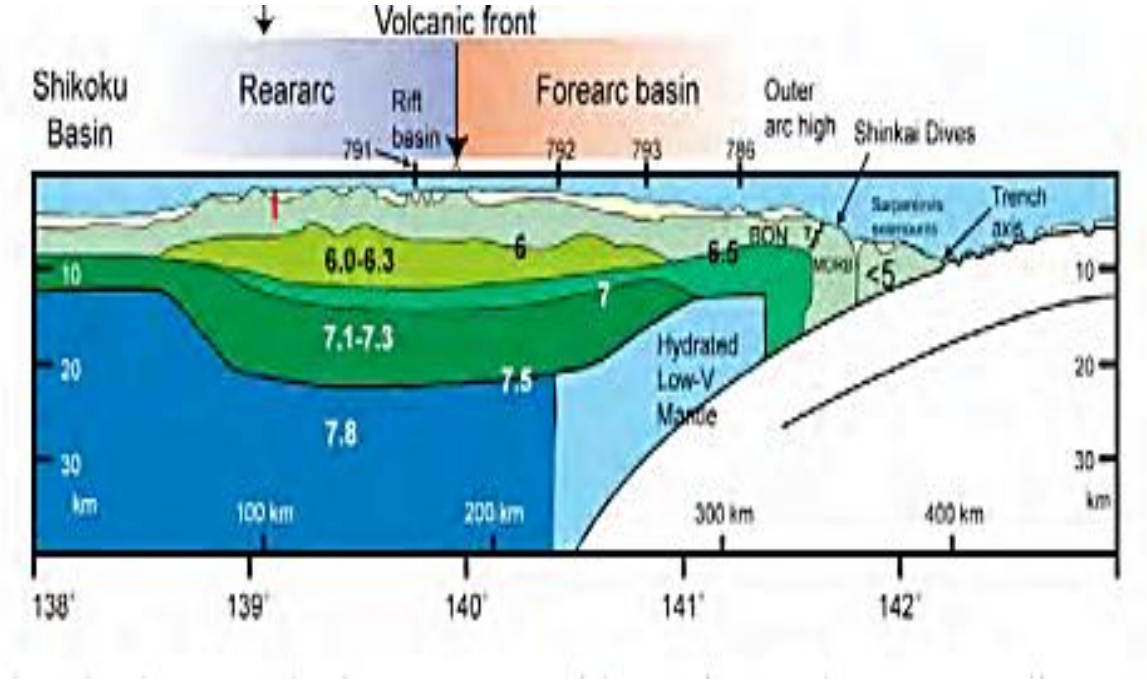

Figure 13 *This figure show the similar velocity between the fore arc basin and the rear arc. Although the rear arc and fore arc is similar in seisimic and velocity, they are chemical heterogenous. Figure taken from(Suyehiro et al., 1996).*

These observations of asymmetric arc crust led to many new questions concerning the generation of the continental crust. Steady state generation of continental crust produce crust that is similar in seismic and velocity beneath the volcanic front and the rear arc. Chemically, the volcanic front and rear arc is different.

“From the Beginning” is the hypothesis that propose the heterogeneity was established from the Eocene arc inception through the Neogene. On the other hand, “From the Middle” propose that the heterogeneity is established after the cessation of Shikoku Basin, only in Neogene.

The different hypotheses regarding this chemical heterogeneity may be explained by two main hypotheses; “From the Beginning” and “From the middle”. These can be tested only by the recovering of Eocene to Oligocene tephras and turbidites. The time interval of samples in this study will reveal if the rear arc magmatism was in change relative to the volcanic front.

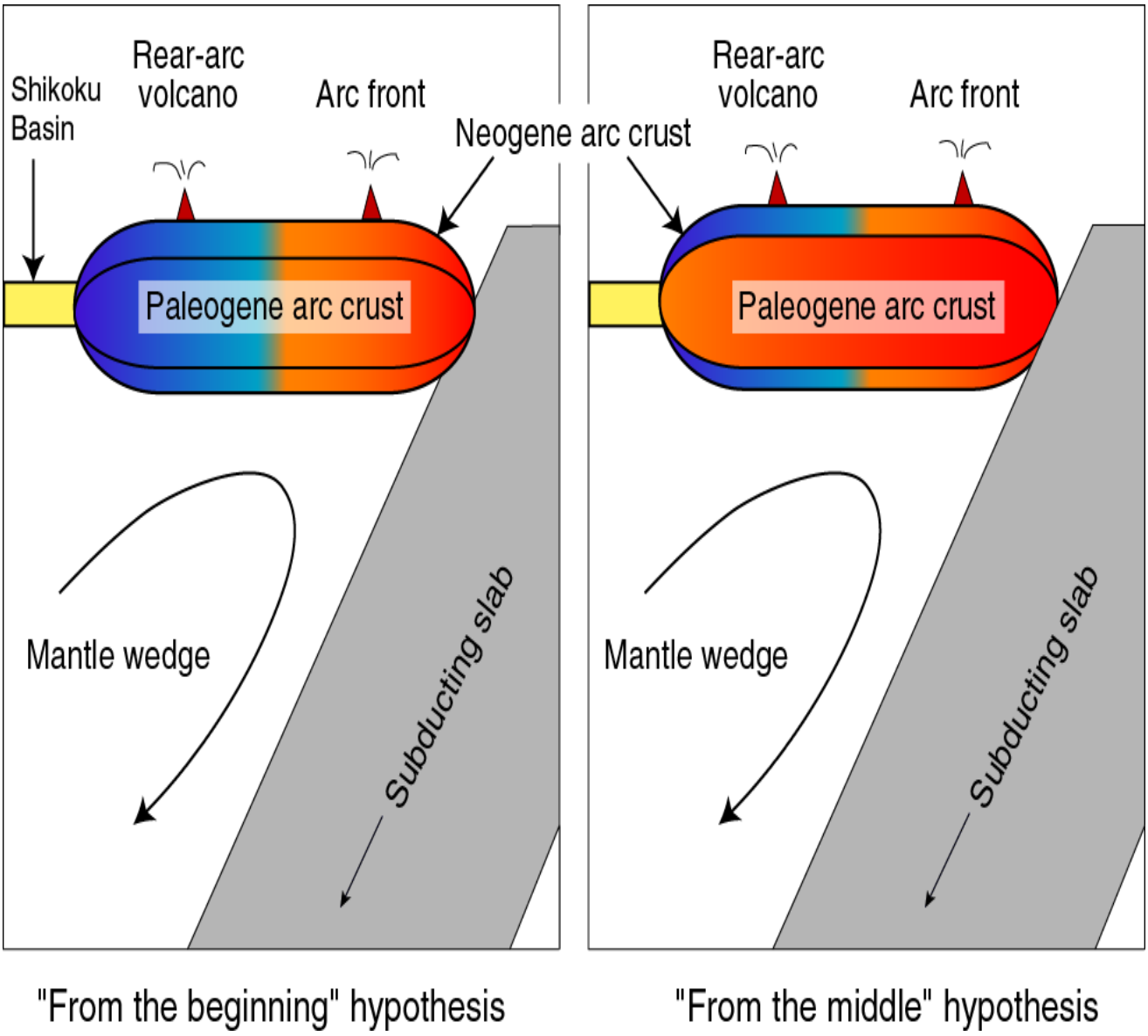

Figure 14 *The two main hypotheses concerning the chemical heterogeneity in the Izu Bonin arc. Figure taken from (Yoshihiko Tamura, 2014)*

By drilling a hole into the volcanoclastic material deposited in the basin between Enpo and Manji, it is possible to track the geochemical processes dominating in this area. Recovering of volcanoclastic material gives the opportunity to look at the temporal record. In this basin, sediments are mixed with volcanic products from the nearby volcanoes. It is the volcanic product that has the geochemical signal reflecting the magmatic processes in this area.

2.8 Lithostratigraphic Column

Expedition 350 drilled 3 holes at site U1437 between seamount chains Enpo and Manji. These 3 holes, B – D – E, make up a coherent consecutive stratigraphic column. Total length of the column is 1806,0 mbsf. Part A and C of the column is not considered because they were not useful due to practical defects with the cores. It was drilled several times because the cores were not long enough to penetrate through all volcanoclastic material at once. When core A was brought up from the sea, core B was set out to penetrate even further down.

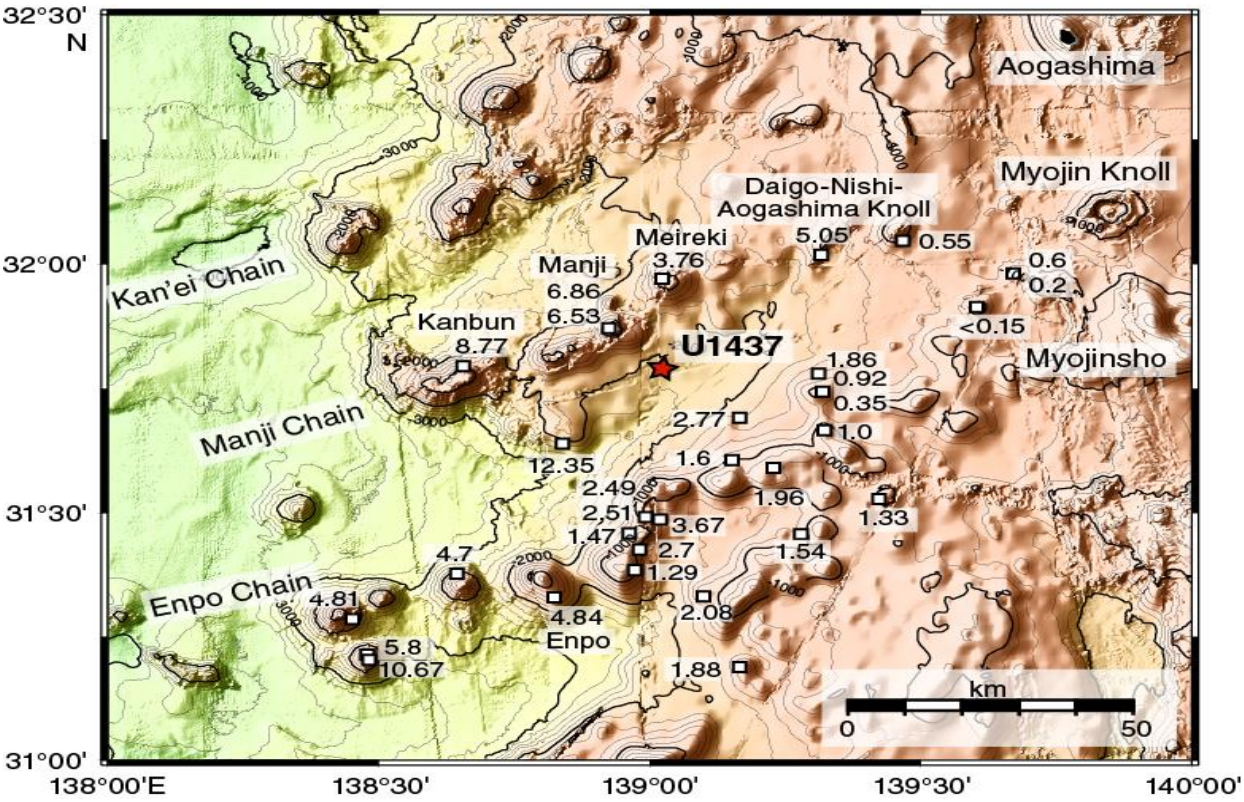

Figure 15 *Site U1437 is shown in this figure, as it lies between Enpo and Manji seamount chain. Taken from (Yoshihiko Tamura, 2014)*

Hole U1437B is the uppermost part of the 3 holes. It goes from 0-439,1 mbsf and consists of core sections 1H-55X. Hole U1437D is the middle part of the holes. It covers the length of 427,2-1104,6 mbsf and consists of cores 2R-73R. Hole U1437E represent the lowermost part of the holes and it goes from 1104,6-1806,5 mbsf. Cores 4R-79R belong to this hole.

Since the site is located between two seamount chains, in a volcano bounded basin, it is reasonable that the 3 holes is dominated by sediments and volcanic rocks from those

volcanoes. Post-cruise work with the column show that it mainly consists of tuffaceous mudstone/ mud with some intervals of volcanoclastic layers. In a certain part of the column, the volcanoclastic column is interrupted by an intrusive rhyolitic-dacitic sheet.

Based on descriptions and characteristics of the column it is divided in 7 units. Each of these units are unique and differ from the others. The uppermost 1300 m of the colums consists of 5 units. 3 of these (I, III and V) are dominated by tuffaceous mudstone with interlayered volcanoclastic layers. Remaining 2 units (II and IV) consists of the same tuffaceous mudstone and the interlayered volcanoclastic layers, but here the volcanoclastic layers dominate over the tuffaceous mudstone.

Further down in the hole (lowermost 500 m), volcanoclastic layering become more frequent and clasts become coarser. This part of the hole is represented by units VI and VII. Unit VI is interrupted by a 1,2 m intrusive sheet of rhyolitic-dacitic composition named igneous unit 1.

2.8.1 Unit IV

- Interval: 350-U1437D-64R-1, 8 cm, to 350-U1437E-6R-3, 122 cm
- Depth: 1017.88–1120.11 mbsf
- Lithology: lithified evolved tuff and polymictic lapilli-tuff with subordinate tuffaceous mudstone
- Age: ~6.2–7.5 Ma

Unit IV is 102.23 m thick, of which 59.20 m (58%) was recovered and described, and includes 132 intervals of tuff (31.14 m), 34 intervals of polymictic lapilli-tuff (14.53 m), 2 intervals of polymictic lapillistone (0.46 m), and 80 intervals of tuffaceous mudstone (13.07 m).

Polymictic tuff and lapilli-tuff dominate over tuffaceous mudstone in Unit IV. Unit IV is characterized by normally graded dark green coarse sand–sized tuff, polymictic lapilli-tuff, and minor polymictic lapillistone (78% of the described thickness of the rock). Of these, fine-grained green tuff intervals and the polymictic lapilli-tuff intervals are the most distinctive. Tuffaceous mudstone intervals form a minor part of the unit (the remaining 22% of the described rocks), becoming more common toward the base (Yoshihiko Tamura, 2014).

2.8.2 Unit V

- Interval: 350-U1437E-6R-3, 122 cm, to 28R-1, 0 cm
- Depth: 1120.11–1320.00 mbsf
- Lithology: monomictic reversely graded lapilli-tuff with mudstone, tuffaceous mudstone, minor evolved tuff, and rare lapilli-tuff and lapillistone
- Age: ~7.5–9 Ma

Unit V is characterized by distinctive intervals of monomictic reversely graded lapilli-tuff with mudstone and the absence of significant thick polymictic lapilli-tuff. In contrast, the base of Unit IV and the top of Unit VI are the bottom and top of thick (>70 cm) polymictic lapilli-tuff intervals, respectively.

Tuffaceous mudstone constitutes 98 m of Unit V with an average interval thickness of 27 cm, making up 69% of the unit. The intervals of evolved tuff are on average 6 cm thick and compose 15% of Unit V, and lapilli-tuff (of all types) accounts for 16% of Unit V. The upper part of Unit V is dominated by tuffaceous mudstone. Lower in Unit V, volcaniclastics become more abundant than the tuffaceous mudstone. The lithofacies occurring in Unit V are divided into (1) monomictic reversely graded lapilli-tuff with mudstone, (2) tuffaceous mudstone, (3) evolved tuff, and (4) lapilli-tuff and lapillistone(Yoshihiko Tamura, 2014).

2.8.3 Unit VI

- Interval: 350-U1437E-28R-1, 0 cm, to 42R-3, 60 cm
- Depth: 1320.00–1459.80 mbsf
- Lithology: dominated by intervals of matrix- and clast-supported polymictic and monomictic evolved pumice lapilli-tuff, lapillistone, and minor tuff-breccia; dark tuff; minor tuffaceous mudstone and sandstone
- Age: older than ~9 Ma and extends to at least 10.97–11.85 Ma

Unit VI is characterized by more tuff and lapilli-sized volcaniclastic intervals (89% of the described intervals) and less tuffaceous mudstone (11%) than Unit V (31% volcaniclastics, 69% tuffaceous mudstone). The top of the unit is marked by the first appearance of multiple intervals of matrix-supported polymictic lapilli-tuff and continues downward through intervals dominated by tuff and lapilli-tuff. Unit VI is intruded by igneous Unit 1, which is a rhyolite-dacite sheet. The bottom of the unit is marked by the first dense glass-rich interval of Unit VII.

The unit includes 116 intervals of lapilli-tuff (total of 50.49 m), 134 intervals of dark gray and green tuff (32.35 m), 44 intervals of tuffaceous mudstone (10.95 m), 7 intervals of clast-supported polymictic lapillistone (4.6 m), and 5 intervals of matrix-supported polymictic and monomictic tuff-breccia (1.88 m) (Yoshihiko Tamura, 2014).

2.8.4 Unit VII

- Interval: 350-U1437E-42R-3, 60 cm, to 79R-3, 83 cm
- Depth: 1459.80–1806.50 mbsf
- Lithology: lithified; black, evolved lapilli-tuff and lapillistone; tuff and evolved tuff; and polymictic evolved lapilli-tuff, lapillistone, tuff-breccia, and consolidated volcanic breccia
- Age: older than 10.97–11.85 Ma

Unit VII is distinguished from Unit VI by the dominance of medium to extremely thick coarse-grained intervals, such as lapilli-tuff, lapillistone, tuff-breccia, and volcanic consolidated breccia (195 intervals). The dominant lithofacies is black, evolved lapilli-tuff and lapillistone. The other voluminous lithofacies is nongraded, nonstratified, very poorly sorted, polymictic lapilli-tuff, lapillistone, tuff-breccia, and volcanic breccia that commonly contain a large variety of angular andesite pebble and cobble sized, some with quenched and peperitic margins, and alteration halos in the surrounding sediment. Graded and stratified lapilli-tuff and lapillistone are subordinate, tuff is common (70 intervals), and tuffaceous mudstone is extremely rare (1 interval) (Yoshihiko Tamura, 2014).

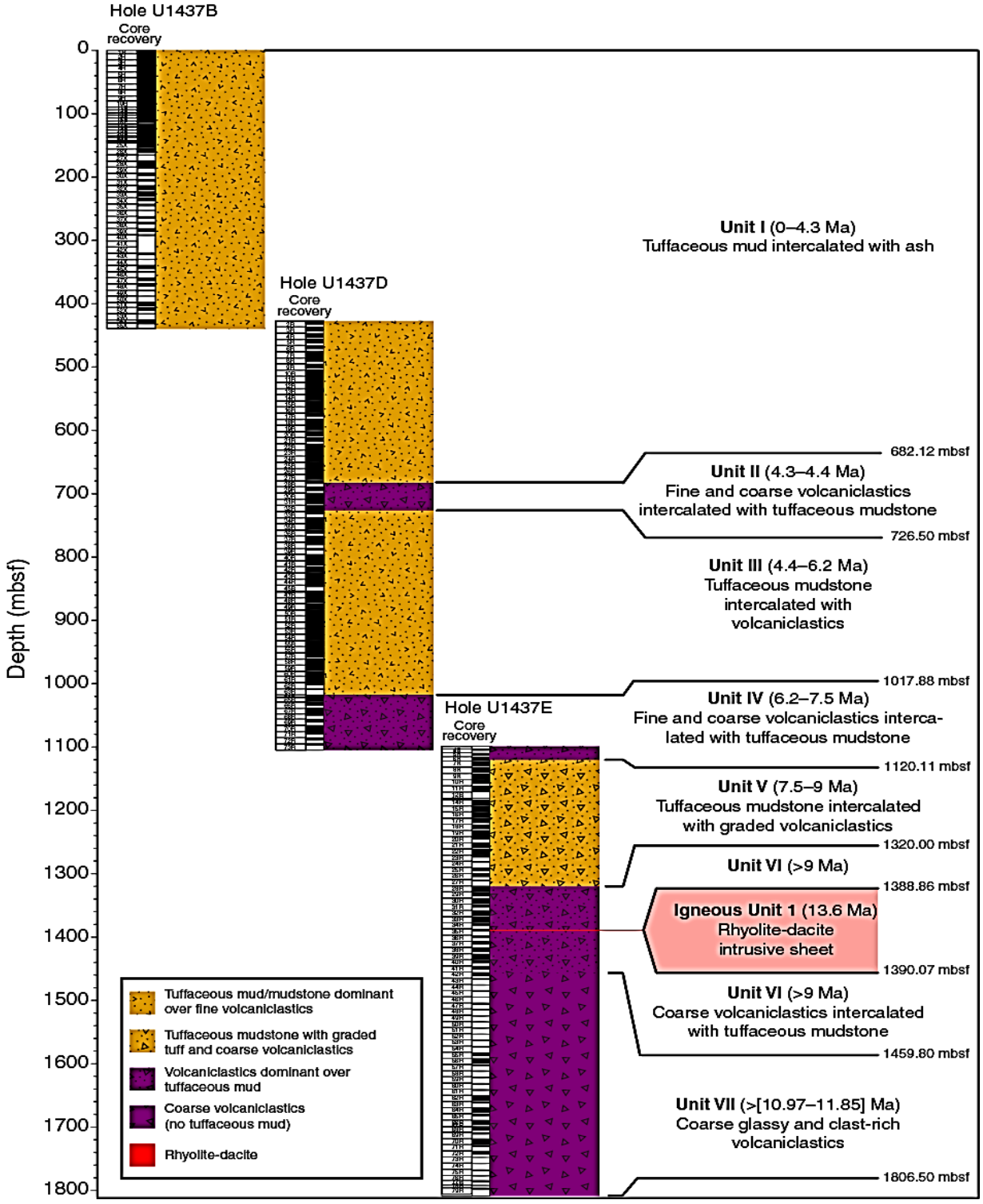

Figure 16 *The lithostratigraphic column drilled in the volcano bounded basin between Enpo and Manji seamount chains. Studied samples comprise unit IV, V, VI and VII. Figure from (Yoshihiko Tamura, 2014).*

3. METHODLOGY

3.1 Introduction

All 14 samples in this project were taken by the IODP expedition 350 in western Pacific in 2014. Samples analyzed in Bergen Geological Facility come from following holes on site U1437; hole U1437D and hole U1437E. This work is done in collaboration with the D/V *Chikyu* group in JAMSTEC, Japan. Samples from holes U1437D and U1437E were analyzed for trace elements including REE and strontium(Sr), neodymium(Nd), lead(Pb) and hafnium(Hf) isotopes. This was done by combining rock powder preparations, ion-exchange chromatography, ICP-MS, MC-ICPMS and TIMS.

3.2 Sample preparation

To get samples in gravel-sized particles, preparations including sawing, picking and milling had to be done. Diamond saw was used to cut them in smaller parts. Each sample was cut in two. One part to be analyzed for isotopes and trace elements. The other half was taken care of in case a thin-section was needed. After each time the saw was used, washing of the saw itself was performed to minimize eventual contamination. After using the saw, the samples were crushed and sieved.

After crushing and sieving, the samples were put under the microscope. Here the aim was to pick the most homogenous and fresh parts of the rocks. Avoiding cut marks from the saw or big crystals.

Before picking, equipment that was used was washed and cleaned with distilled water and ethanol. It was dried with kimtech paper. The grains were put in small centrifugal tubes. This work was done until we could get ≈ 1 g per sample. Due to alteration, some of the samples were hard to pick and the final quantity was reduced to 500 mg.

Thorough cleaning of the agate mills was done by washing them in ethanol and distilled water. The frequency was set on 30 s/m and time on 6 min.

3.3 Ion-exchange chromatography

3.3.1 Basics Of Ion-Exchange Chromatography

When dealing with heavy radiogenic isotopes, it is necessary to purify the element of interest before taking it to the mass spectrometer. Many of these elements have masses that are close to each other, as for example ^{176}Hf and ^{176}Yb. As the mass spectrometer identify the elements by their mass-to-charge ratio it can be difficult to perform isotopic analysis due to mass interferences. The concept of ion exchange chromatography is to separate elements of similar masses by their affinity to specific resins.

Chromatography is a chemical tool used to separate elements from a mixture. It is based on the elements different partition coefficients, which is defined as the ratio of the elements concentration in the phases. See equation;

$$K = \frac{[S2]}{[S1]}$$, where S2 and S1 are substrates. *Eq. 5*

The most used type of chromatography in isotopic geochemistry is ion-exchange chromatography. It includes a mobile phase, the dissolved sample, and a stationary phase, the resin. As the sample goes through the column elements will be attracted to the resin depending on their affinity, described by *K* (see eq. 5). Those who have a higher affinity (higher *K*) will be eluted the last. The resin contains of porous beads made by organic polymers. The relative selectivity of the resin is based on the elemental properties of the ion in the mobile phase. An observation is that relative selection of the resin is governed by the size of the hydrated radius as well as the charge.

Below there is a figure showing the acid dependency(*K*) for some alkali elements. As mentioned earlier, K represent the partition coefficient for element at a certain acid concentration. This figure is based on experimental studies from Horwitz and Chiarizia (1992)

Sr affinity to the resin increases with the concentration of HNO_3. Sr can be efficiently separated from elements like K, Ba, Ca, Cs etc. To get a Sr fraction clean as possible, it would be beneficial to use high concentration of HNO_3.

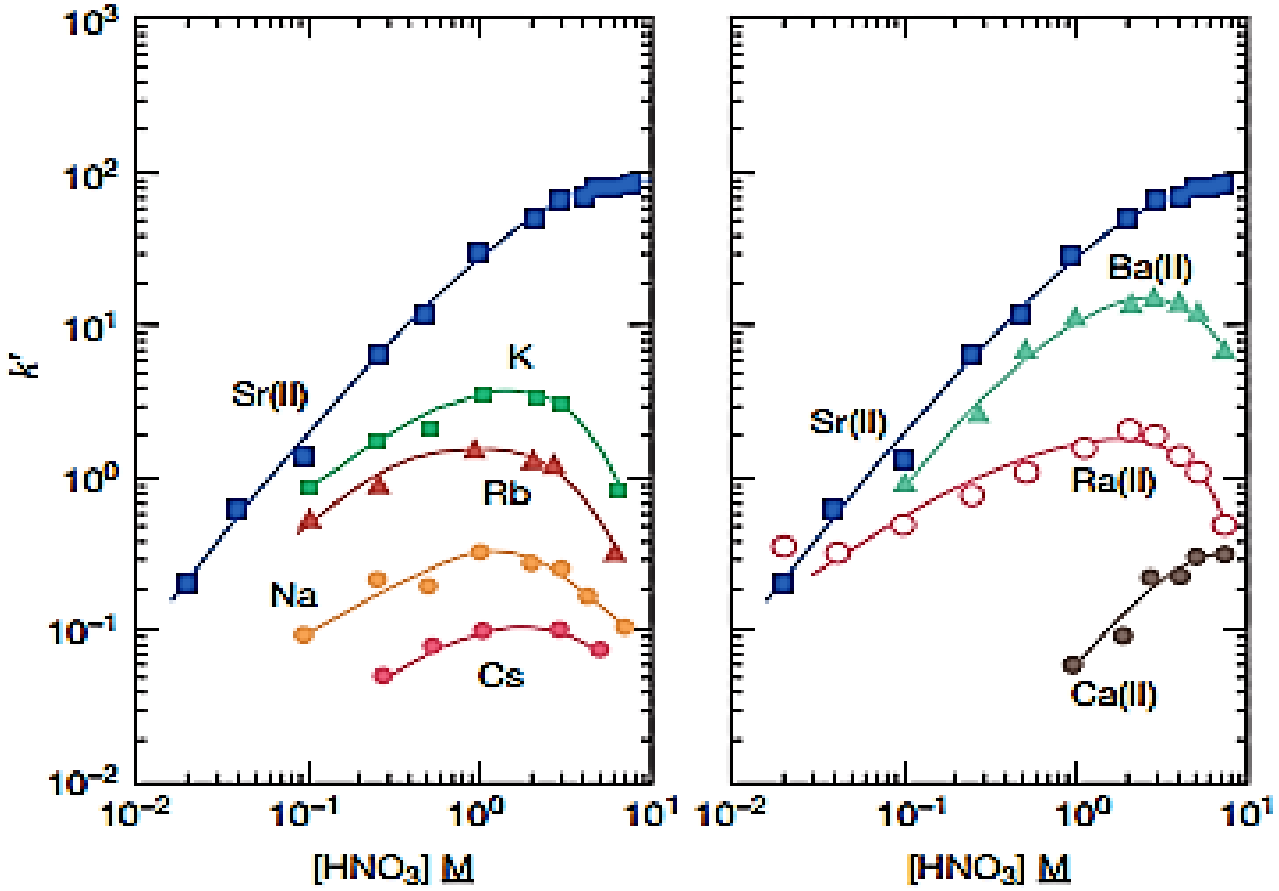

Figure 17 *Partition coefficient to Sr resin when different concentrations of HNO_3 is added. Figure from (Horwitz & Chiarizia, 1992).*

3.3.2 Separation And Purification Of Elements

Clean lab is an over pressurized room where we perform chemical separations. All leaching, dissolutions and chemical separations were carried out in a class 1000 air filtered room at the institute for earth science at Bergen university. Handling and processing of the samples during chemical separations were done under class 100 laminar flow hoods. Reagents used for leaching, digestion and separation were kept in Teflon bottles. All sample materials were leached in screw-top Savillex™ vials.

The samples which came from the agate mill was weighed before the first step, which was leaching. Leaching removes potential alteration signature by dissolving alteration minerals.

For the samples from Izu-Bonin, two leaching methods were used. Strong leaching for the Pb and Sr fraction and a weaker leaching for Hf-Nd fraction.

The powders were put in Teflon beakers prior to leaching. To prepare for Pb separation, strong leaching was done by adding 6M HCl to the beakers. This was then put in a 120°C

ultrasonic bath for 20 minutes. Next step was to take out the liquid phase containing alteration products. Then we added ultrapure H_2O to the beakers. First shake and let it settle, then again took out the liquid phase. The result was finally dried overnight.

After the samples were dried, they were ready to be dissolved. This was done by adding HF and HBr to the beakers in a ratio of 3:1. This solution was then evaporated. The addition of HF is necessary because the highly reactive fluoride ion(F^-) is attacking the silicated network building up the minerals. After dissolution and drying, the samples were re-dissolved, by adding 1 mL of 0,5M HBr.

3.3.3 Pb

The columns used for Pb separation contained a AG1X8 200-400 mesh type resin. The first step was to clean the column, by adding in the following specific order; 0,25M HNO_3, 6M HCl, 0,5M HBr and rinsing with ultrapure H_2O in between acids. Next step was to load the samples on the column, in 1 mL of 0,5M HBr. The Hf-Sr-REE fraction was collected as the Pb was retained in the resin. Pb was then collected by adding 2,5 mL of 6M HCl. When the samples were dried and free of any liquid, new cleaning of the columns was done before the second purification of Pb.

3.3.4 Hf-Sr-REE

Columns used here contained a AG50W type resin. Hf-Sr-REE-fraction from the Pb separation was first re-dissolved in 6M HCl, and then dried again. Before loaded on to column, the fraction was taken up in 1M HCl + 0,15M HF. Also, conditioning of the column was done by adding 6 mL of 1M HCl + 0,15M HF. The sample was loaded on the column in 1,5 ml of 1M HCl + 0,15M HF.

By adding 1,5 mL of 1M HCL + 0,15M HF, Hf-Ti-fraction was collected. After collection of Hf-Ti, column was cleaned with 0,5 mL of 1M HCl + 0,15M HF and 8 mL of 2,5M HCl. Next step was to collect Sr. This was done by adding 5 mL of 2,5M HCl to column. After collection of Sr, the column was cleaned with 6 mL of 2,5M HCl. The LREE was thereby collected by adding 5 mL of 6M HCl. After the collection and separation of Hf-Sr-REE, the columns were cleaned. This was done in this specific sequence: 6 mL of 6M HCl, 6 mL of 2,5M HCl and 6 mL of ultrapure H_2O.

3.3.5 Hf-Ti separation

The Hf-Ti fraction collected from Hf-Sr-REE separation was put on hotplate and dried. This fraction was re-dissolved 3 times in 2 mL of 6M HCl and then loaded on LN column. As for all other separations, conditioning of the column was done before the samples was introduced. We then added 6M HCl + 50µL of H_2O_2 (10 mL in total) to clean the column. Addition of the acid mixture containing H_2O_2 is oxidizing Ti^{3+} into TiO_2. Collection of Hf is done by adding 5 mL of 2M HF.Cleaning the column by adding ultrapure H_2O and 6M HCl is done before doing this separation sequence again.

3.3.6 Nd

Nd is a rare-earth element and was in the REE-fraction from Hf-Sr-REE separation. The column for this separation process was containing a LN-spec type resin. It was dried and re-dissolved in 0,25M HCl. Conditioning of the column was done by adding 3 mL of 0,25M HCl. The sample was loaded on the column with 0,3 ml of 0,25M HCl, and thereby added a new 0,3 mL of 0,25M HCl to column. After this, cleaning of the column was done by adding 2,4 mL of 0,25M HCl. The Nd was collected by adding 2 mL of 0,3M HCl. After collection, column was cleaned by adding 4 mL of 6M HCl and 4 mL of 0,25M HCl.

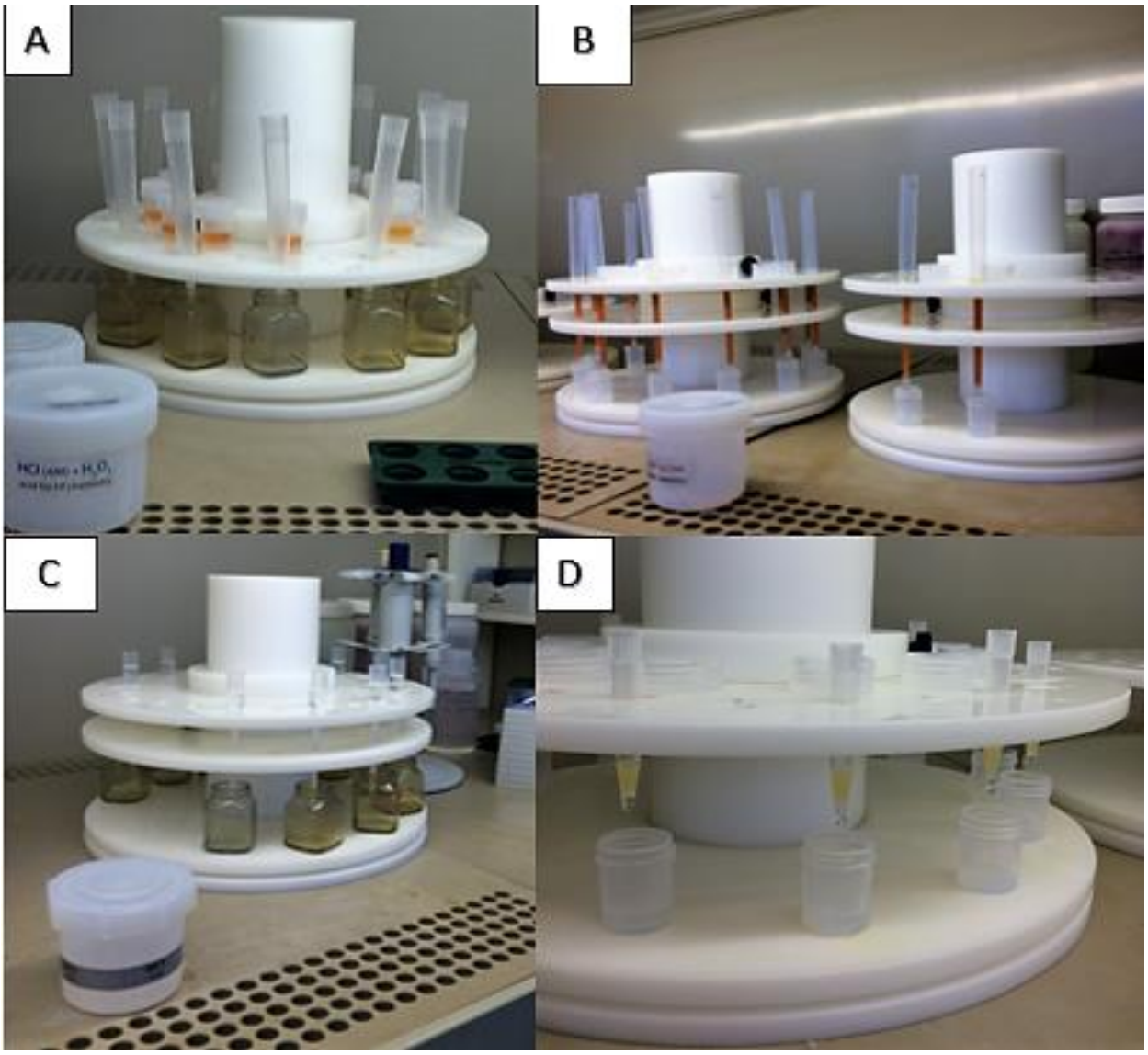

Figure 18 ***A****. Hf-Ti separation. Sample ready to be loaded on column. Characteristic color of oxidized* TiO_2 ***B****. Hf-Sr-REE separation.* ***C****. Nd purification* ***D****. Pb purification*

3.4 Inductively Coupled Plasma Mass Spectroscopy

3.4.1 Basics Of ICPMS

The mass spectrometer is an important tool in modern geochemistry. It is used in geochronology, quaternary geology, environmental geology etc. The way it works is that ions are being deflected by a magnetic field according to their mass-to-charge ratio. The mass spectrometer can be divided in three different sectors; ion source, mass analyzer and the detector.

1) The ionization process: The sample is ionized when passing through a plasma.
2) Acceleration: All ions produced are accelerated in an electric field.
3) Deflection: This effect is based on the elements mass-to-charge ratio. Lower ratio, more deflection.
4) Detection: The ion beam is arriving in a faraday cup where it is transformed into an electric signal.

In an ICP-MS the sample can be introduced to the mass spectrometer as an aerosol by using a nebulizer. In a ICP-MS argon gas is flowing in concentric channels of the ICP torch. The coil to this torch is connected to a radio-frequency generator. A spark is applied to the flowing argon through the torch, and because of this, electrons will be stripped of the argon atoms. In this way, a beam of electrons and argon plasma is produced. The ions produced is caught in an oscillating magnetic and electric field to produce a plasma. This holds up 10 000 K. Electron produced from the ionizing of argon is attracted to a positively charged plate, and forms in this way a beam of electrons. Elements from the sample will be hit by the electron beam. Those with enough kinetic energy will knock off electrons and produce positively charged ions. These positive ions will be repelled from the highly positive charged ionization chamber and thus be accelerated. Beam of electrons will enter different slits that have different voltages. The different voltages in the slits produces a gradient in which the ion beam can accelerate even more. Before going into the magnetic sector, the ion beam is focused by lenses.

Formation of ions in the start chamber produces a beam where all ions has the same kinetic energy. Kinetic energy is given by;

$$E = \frac{1}{2}mv^2 \qquad Eq.\ 6$$

These ions enter the ion separation chamber. A magnetic field exposes a force on the charged particles according to the formula;

$$F = qv\ x\ B \qquad Eq.7$$

This force is perpendicular to the ion beam moving direction. The laws of physics say that this will force the charged particles in circular paths. Moving particles in a circular path will be exposed to centripetal force by the formula;

$$F = m\frac{v^2}{r} \qquad Eq.8$$

Combining these equations and solve for the mass/charge-ratio, we get;

$$m\frac{v^2}{r} = qv\ x\ B \quad \rightarrow \quad (m/q) = \frac{B^2r^2}{2v} \qquad Eq.9$$

This equation relates mass to charge ratio with accelerating potential, magnetic field and the radius of the curvature. The mass to charge ratio is what determines what is being studies and thus makes it to the detectors. Other mass spectrometers use two types of focusing, called double-focusing. In addition to magnetic filter just described, it has an electrostatic filter. It works in the same way, but here the ions are separated by their kinetic energy rather than their mass to charge ratio. This double focusing gives better resolution on resulting signal.

Instead of using both these types of filters in one instrument, many uses what is called a quadropole mass analyzer. Four rods where two have the same charge. The ions will either be resonant or non-resonant with the oscillating signal produced in the quadropole. Ions that make it through will be detected.

The ions produced will be detected or “collected” in metal cups. These cups are designed to prevent free electrons to escape. Most common method is the Faraday cup. These cups have electrons going through them and will thus neutralize the ions when they collide.

The ion current is determined by measuring the voltage developed across a resistor. In the same time electrons from the cup is flowing in this direction and neutralize the ions. To get results to the computer, the electrical signal in voltage is converted to digital signals and can be transferred to the computer.

Usual resistance used on modern mass spectrometers are 10^{11} ohm. If the ion current is 10^{-11} A, it will produce a signal of 1 V.

Multiple isotopes can be measured at the same time. A multi collector mass spectrometer is composed of many cups. Positions of the cups can be adjusted by computer. The distance between the cups varies after what isotopes are interest.

Not all ion currents are strong enough to be detected. In such cases a multiplier is used. It works in a way such that the signal can be 100 times higher. Ion current collide with a charged dynode. These collide and produces free electrons and these will move down a potential gradient as an electron cascade.

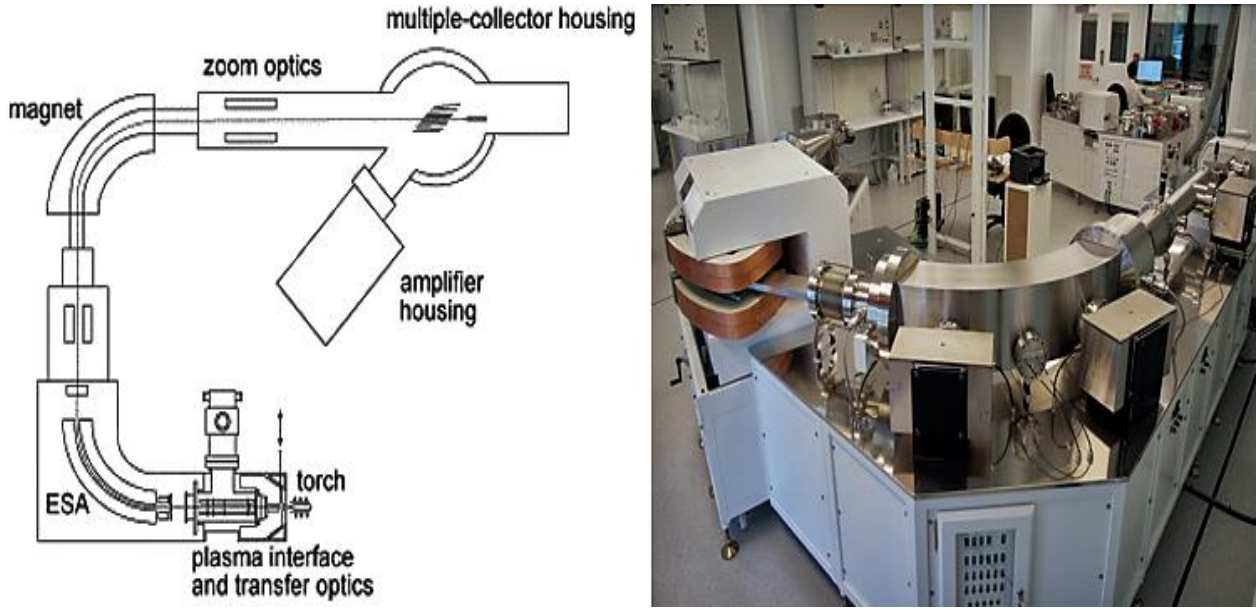

Figure 19 *This figure show a shematic view of a MC-ICPMS. Picture on the right show how it looks like in a mass spectrometry lab. From* http://pcigr.eos.ubc.ca/instrumentation/multi-collector-icp-ms/ *and* *http://cobblab.blogspot.no/2012/09/enter-george-weve-spent-many-nights.html*

3.4.4 Accuracy and Precision

To obtain good results from analytical work, it is necessary that the result is of high accuracy and precision. Accuracy can be defined as the closeness of a measured value to a standard or known value. Precision on the other hand is defined as the closeness of a number of measurements to each other. Best results have both high accuracy and precision, but it is also possible to have good precision without having accuracy.

When working with heavy radiogenic isotopes in a MC-ICPMS, as for example Nd and Hf, having good precision on the behalf of accuracy is often the case. When the isotopes are detected in the faraday cups, measured electric signal is related to the number of element of interest in a standard, which is measured before and after the analysis itself.

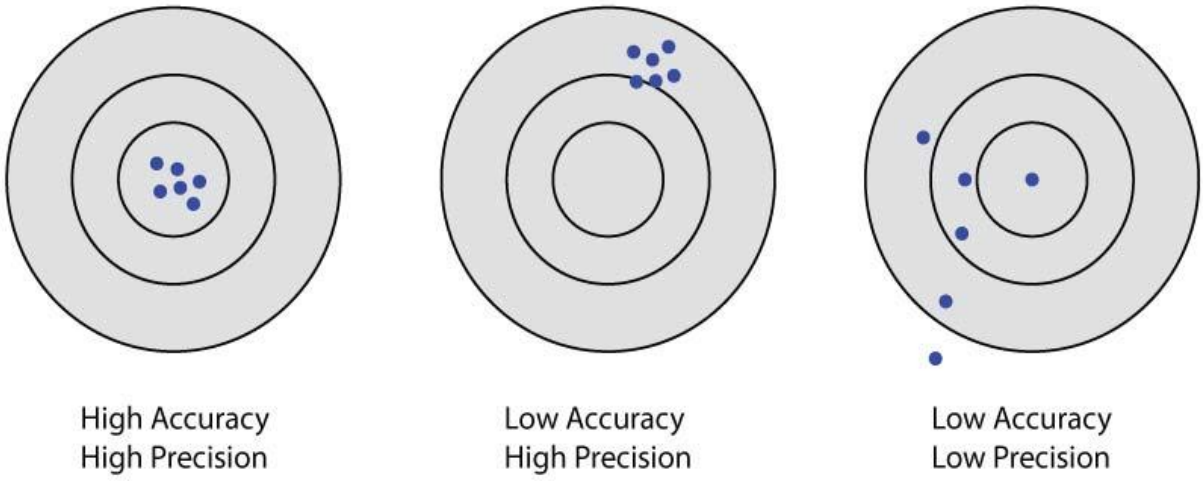

Figure 20 *Cartoon showing the difference between accuracy and precision. From https://online.science.psu.edu/chem101_sp1/node/6357*

3.5 Thermal Ionization Mass Spectroscopy

3.5.1 Basics Of TIMS

Thermal ionization mass spectrometer is an instrument used to determine isotopic ratios. It is based on the same mechanics as ICPMS. The main difference is the ion source. As mentioned earlier the ICPMS is driven by a plasma torch, TIMS on the other hand uses a hot filament to ionize different elements. This is done by heating a metallic ribbon to such temperatures that it ionizes the sample. The metallic ribbon is usually composed of Re(Rhenium).

When ions are produced, they are accelerated through an electric potential gradient of 10 000 volts. Several slits and electrostatic charged plates focuses the ion beam. Entering the magnetic sector the ion beam are separated into different beams on basis to their mass to charge ratio. The ion beam with the correct mass to charge ratio is going to the collectors. Here ions will collide with the collector and produce voltage, which will be sent to computer.

Certain limitations of TIMS compared to ICPMS makes the latter one more useful. Ionization energy vary for different elements. Based on this, TIMS will not be able to get high enough temperatures to ionize elements with high ionization energy like Hf.

3.6 Importance of leaching for accurate isotopic analysis

This part is included in this thesis for some reason. For laboratory work, sources of error and evaluation of the result is important if the procedure is going to be used again. In this study, two leaching methods were used to extract alteration effects.

Method I was done by adding 6M HCl to the samples and then they were put in a warm (50^oC) ultrasonic bath for 20 minutes. Liquid phase was removed by pipette. Solid residue was added ultrapure water and put on a hotplate(120^oC) over night. This method was initially done just for Pb. The following dissolution was was done by mixing HF and HBr in a 3:1 ratio.

Method II differs from method I in adding a much less concentrated HCl solution to the samples. We used 0,25M HCl and this was put in a room temperature(25^oC) bath in 10 minutes. This method was initially made for Sr, Nd and Hf. These were digested by adding a mix of 28M HF and 14M HNO_3 in a 3:1 ratio.

When dealing with different isotopic systems, different leaching methods needs to be used. Generally, Pb are much more susceptible for environmental contamination than Sr, Nd and Hf. Therefore, it was done as a single leaching and dissolution for this element.

How acid-leaching are affecting the isotopic composition of Sr, Nd and Hf in ocean island basalts was investigated by experiments done by (Nobre Silva, Weis, & Scoates, 2010). Nd and Hf being relatively immobile elements makes them resistant to alteration. Sr and Pb on the other hand needs thorough leaching prior to dissolution. The article by (Nobre Silva et al., 2010) did experiments on Hawaiian basalts and Kerguelen basalts and how the isotopic composition changed after acid-leaching.

Basaltic samples from Hawaii lost up to 35% and 40% of their Sr and Hf, respectively. For the basalts from Kerguelen, loss of Sr and Hf was 63% and 70%, respectively. The loss of Nd was significantly higher with up to 90% for both types of basalt.

Sr isotopic composition measured by TIMS showed that the Sr residues were significantly less radiogenic than its corresponding unleached powders. For Nd and Hf, both were within the analytical uncertainty. This means that Nd and Hf are more reliable results than Sr when leaching has been done.

For Pb, acid-leaching is an important step in getting good results. Acid-leaching removes most of the environmental and altered Pb, and thus will give more reliable data than unleached samples(Todd, Stracke, & Scherer, 2015).

4. RESULTS

Our data set consists of a compilation of trace element and isotopic analysis of the 14 collected samples from IODP expedition 350 in Izu Bonin, in addition to 11 samples analyzed from JAMSTEC. Trace elements was analyzed by X-ray fluorescence (XRF) done by JAMSTEC and by ICPMS in UiB. Normalization values for the different isotopes were as follows;

(Sr)NBS987 = 0.710240

(^{206}Pb, ^{207}Pb, ^{208}Pb) NBS981 = 16.9416, 15.5000, 36.7262

(Hf) JMC475 = 0.282160

(Nd)JNdi = 0,512115

A plot showing the concentration of the rare-earth elements normalized to a chondrite, show how each specific element have been affected by fractionation processes like melting or crystallization. For the analysis carried out in the laboratory at UiB and collaboration with JAMSTEC, some patterns and trends is observed. Greater incompatibility of the LREE compared to HREE, show a pattern much more enriched in LREE. Compared with data from the volcanic front of Izu – Bonin, they are inversely correlated, as seen in figure 12. Samples from the arc front is depleted in LREE. Also, REE pattern from the rear arc samples show a much more similarity with the average continental crust.

These graphs show variation in REE and multi element spider diagrams within unit IV, unit V, unit VI and unit VII, covering an interval of 800 m in total. This section represents an age interval of approximately 6 Ma. Normalizing values are from (Sun & McDonough, 1989) for both chondritic value and N-MORB value.

4.1 Trace element analysis

4.1 1 Unit IV

REE data from unit IV has been normalized to chondrite, (Sun & McDonough, 1989). All samples within unit IV lies in an age interval of 6,2 – 7,5 Ma. Unit IV show an enrichment of LREE compared to MREE and HREE. The heavier REE are approaching a more chondritic value. This gives a negative REE slope. Different samples have different absolute values, even though the trends are the same.

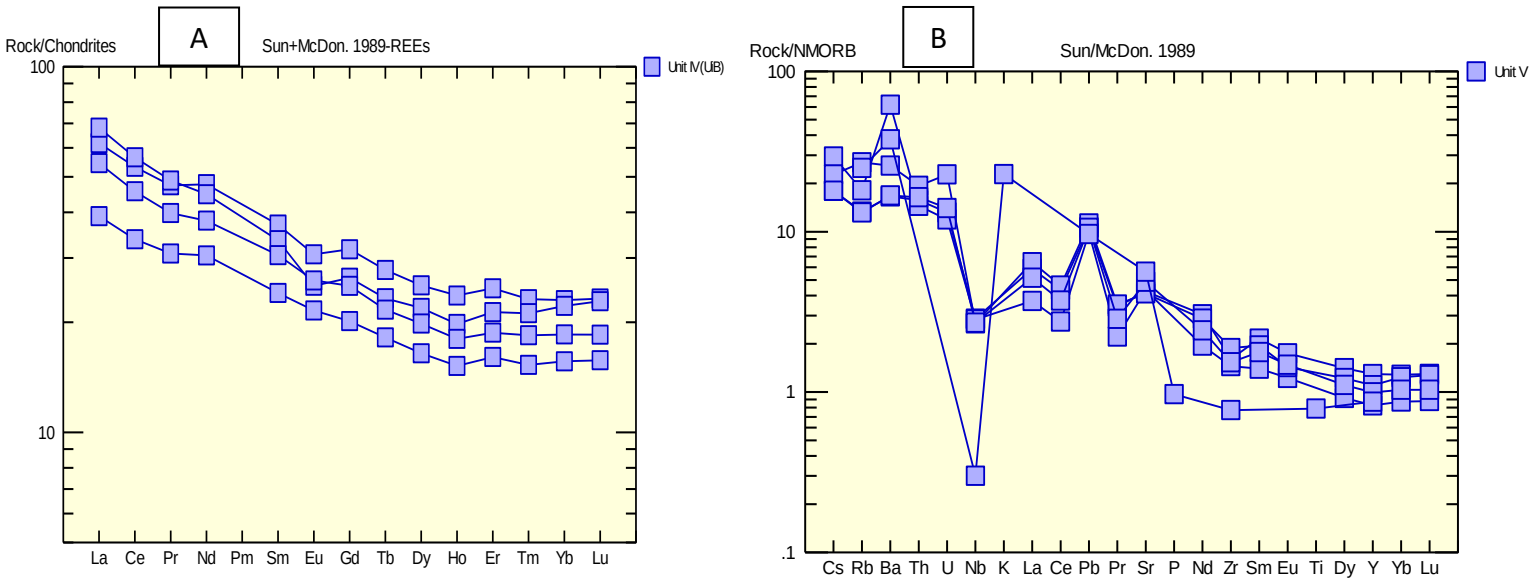

Figure 21 ***A.*** *Samples analyzed at UiB is shown in this spider diagram. It shows the variation of the chondrite normalized REE values within unit IV. An enrichment of LREE relative to MREE and HREE is observed.****B.*** *High LILE/HFSE ratio in unit IV.*

What is seen from the multi element spider diagram in figure 23, is typical subduction zone pattern. Typical strong enrichments of fluid mobile LILE. It shows high concentration of large ion lithophile elements like Cs, Rb, Ba, K and Sr. HFSE are much more depleted relative to LILE. A drop in the Nb concentration is also typical for the subduction zone pattern. We see a enrichment of Pb and Sr relative to elements with similar incompatibility such as La, Ce and Pr.

4.1.2 Unit V

Unit V, from 9 My to 7,5 My, show an enrichment of LREE compared to MREE and HREE and therefore producing the negative sloping trend line observed in figure 24. Although having the same trend, unit IV has higher values of LREE and thus a stronger enrichment.

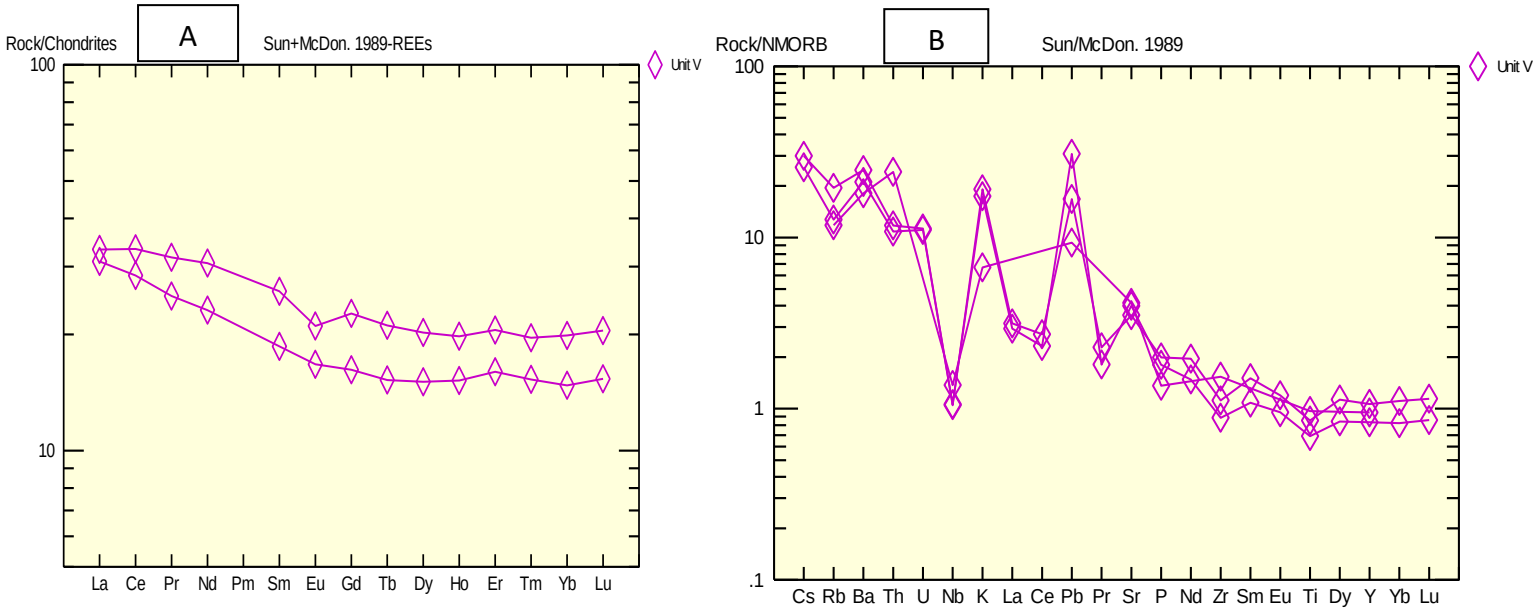

Figure 22 ***A.*** *Chondrite normalized REE pattern for unit V. Pattern is showing the LREE enrichment over the MREE and HREE.* ***B.*** *High LILE/HFSE ratio*

Multi element spider diagram for unit V show a typical subduction zone pattern, with strong enrichment of fluid mobile LILE. Enrichments of the large ion lithophile elements Cs, Rb, Sr, K, Ba compared to elements like Nb, La, Ce and other HFSE. As with unit IV, enrichments of Sr and Pb relative to elements with similar incompatibility are present.

4.1.3 Unit VI

Unit VI samples represent ages that are greater than 9 My, but lower than 10,97 My. For this unit, two very different trend lines are observed. One having the same positive slope as the samples in unit IV and V, which is the enrichment of LREE compared to HREE. The other sample show a slightly depletion of LREE compared to HREE, and thus produces a flatter line than the other units.

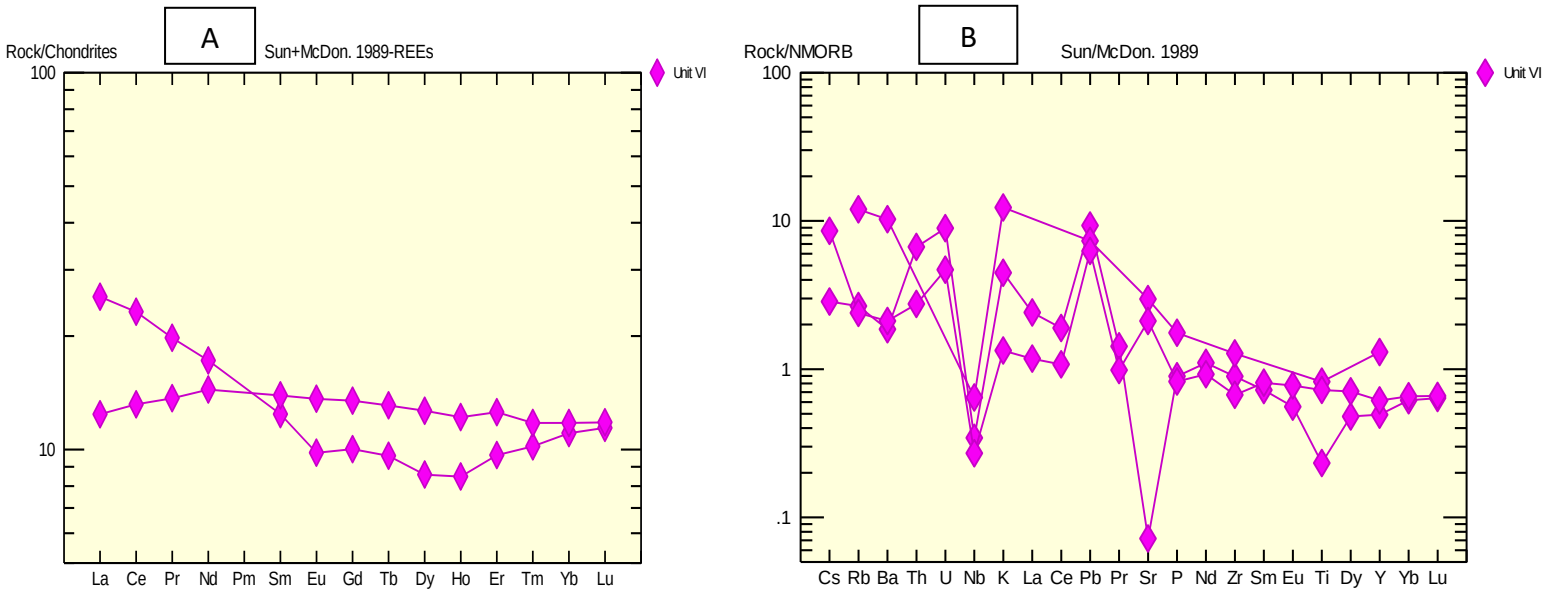

Figure 23 ***A.*** *REE spider diagram for unit VI. Two different REE pattern are observed.* ***B.*** *High LILE/HFSE ratio*

Unit VI show an unusual multi element pattern compared to unit V and unit IV. A higher spread in the relative enrichment of LILE to HFSE. A strong depletion in Nb, with enrichments in Sr and Pb is observed. These are the same as with units IV and V. The degree of LILE enrichment is also lower than for both unit IV and V.

4.1.4 Unit VII

Unit VII is represented by samples older than 10,97-11,85 My. All the samples within unit VII show much more flattening of the REE patterns compared to the other units. There is no specific enrichment of LREE or HREE. The samples in unit VII show a higher variation in their absolute values even though their trends are coherent.

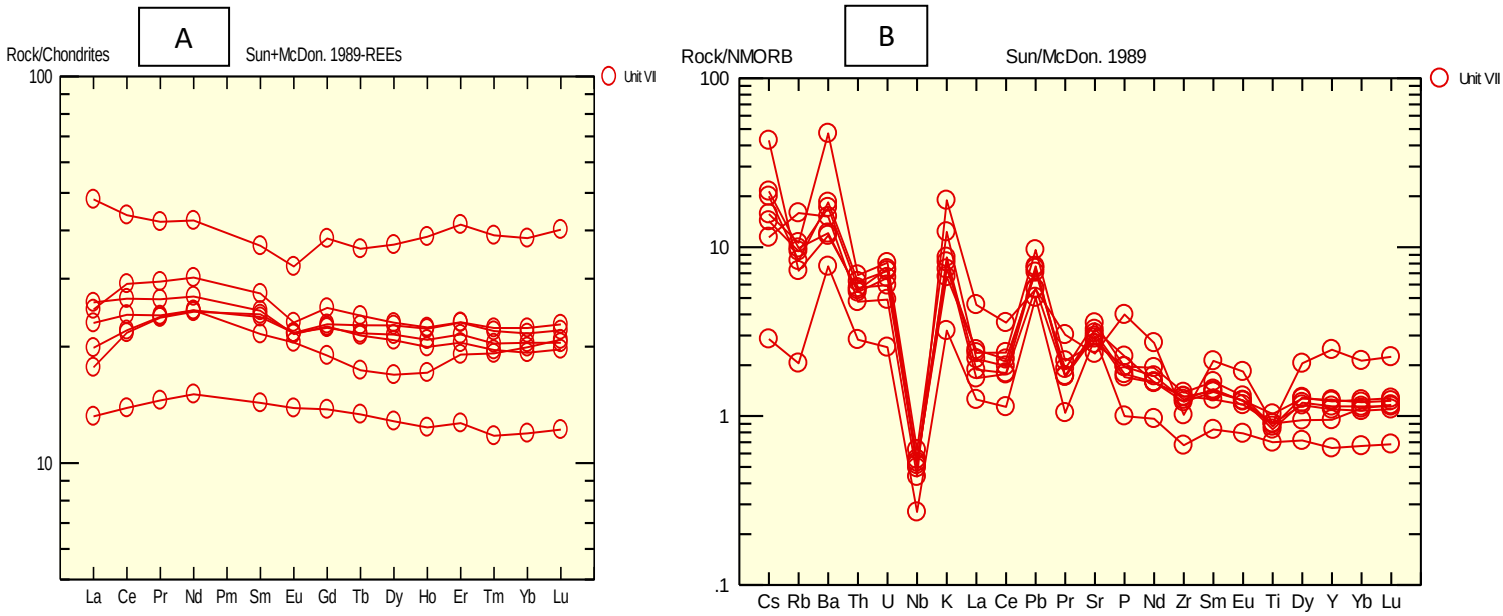

Figure 24 ***A.*** *Flat, MORB like REE pattern.* ***B.*** *High LILE/HFSE ratio.*

The multi element spider diagram for unit VII show a typical subduction zone pattern, with strong enrichment of fluid mobile LILE compared to HFSE. Higher concentrations of large ion lithophile elements like K, Sr, Rb, Ba, Cs. As with the other units, depletion in Nb and enrichments in Sr and Pb are shown in the diagram.

4.2 Isotopes results

Analyzed $^{207}Pb/^{204}Pb$ and $^{208}Pb/^{204}Pb$ from JAMSTEC and UiB was plotted against $^{206}Pb/^{204}Pb$. In each plot, the younger units become more radiogenic. However, if we look closer on how the units are distributed in the plots, there are some irregularities that will be mentioned.

$^{207}Pb/^{204}Pb$ show values ranging from 15,4813 to 15,6001. Values for $^{206}Pb/^{204}Pb$ are ranging from 18,2158 to 18,4489. Unit VII, with the age estimated to be > (10,97-11,85) Ma, show the lowest values for both $^{207}Pb/^{204}Pb$ and $^{206}Pb/^{204}Pb$, with the values 15,4813 and 18,2158, respectively. Unit VI (>9 Ma) show higher values than unit VII for both $^{207}Pb/^{204}Pb$ and $^{206}Pb/^{204}Pb$. One value strikes out to be much higher than the rest, with a $^{206}Pb/^{204}Pb$ = 18,53. For both $^{207}Pb/^{204}Pb$ and $^{206}Pb/^{204}Pb$, unit V, with an age of 7,5-9 Ma, show a more coherent increase in radiogenic Pb. Unit IV (6,2-7,5 Ma) has values that are increasing in both $^{207}Pb/^{204}Pb$ and $^{206}Pb/^{204}Pb$, and lie closer to unit VII than the other units. By looking at the age of the units and how they vary in radiogenic Pb, there are some changes in the isotopic composition of Pb in the short time interval of roughly 6 Ma.

Values for $^{208}Pb/^{204}Pb$ varies from 38,0312 to 38,5712. Unit VII shows the lowest values in $^{208}Pb/^{204}Pb$ and $^{206}Pb/^{204}Pb$, with 38,0312 for $^{208}Pb/^{204}Pb$ and 18,2158 for $^{206}Pb/^{204}Pb$. Unit VI show an increase in both $^{208}Pb/^{204}Pb$ and $^{206}Pb/^{204}Pb$ relative to unit VII. Samples from unit V show the highest values in both $^{208}Pb/^{204}Pb$ and $^{206}Pb/^{204}Pb$. Values in unit IV is closer to unit VII values.

Similar geochemical properties of $^{206}Pb/^{204}Pb$, $^{207}Pb/^{204}Pb$ and $^{208}Pb/^{204}Pb$ can be seen in the plot of $^{208}Pb/^{204}Pb$ vs $^{206}Pb/^{204}Pb$. Although the values are different for each species, the trends are the same. Although the trends are the same, $^{208}Pb/^{204}Pb$ vs $^{206}Pb/^{204}Pb$ show a steeper increase. Thus, the plot of $^{207}Pb/^{204}Pb$ vs $^{206}Pb/^{204}Pb$, which is described above, show the same trends and pattern as $^{208}Pb/^{204}Pb$ vs $^{206}Pb/^{204}Pb$.

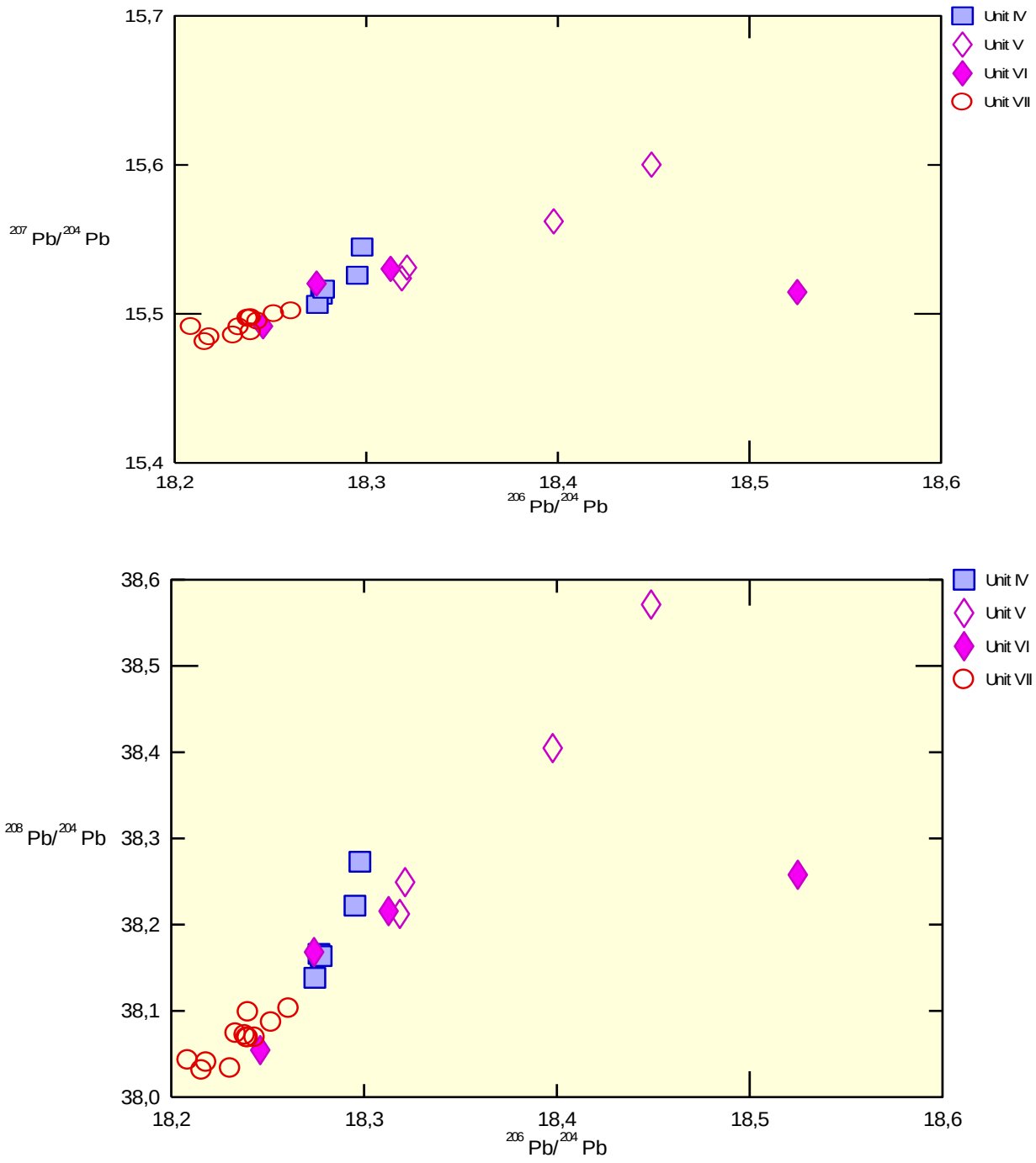

Figure 25 *Figures above show how $^{207}Pb/^{204}Pb$ and $^{208}Pb/^{204}Pb$ vary with $^{206}Pb/^{204}Pb$. Both graphs show an increasing trend with time. Unit VII has the lowest radiogenic values in both plots whereas unit V and VI has the highest values of radiogenic Pb.*

The figure below show $^{207}Pb/^{204}Pb$ vs $^{206}Pb/^{204}Pb$, where the colored areas show the range of $^{207}Pb/^{204}Pb$ and $^{206}Pb/^{204}Pb$ of the different geochemical provinces in the Izu Bonin. Comparison between data analyzed at UiB and JAMSTEC show that samples from units IV, V, VI and VII are similar with the rear arc seamount chains, volcanic front and active rift. What also can be seen is that Shikoku/Parece Vela basin is different from the samples taken from the rear arc basin. Vertical trend from unit VII to units IV and V show a transition from a rear arc volcanism to a more volcanic front like magmatism.

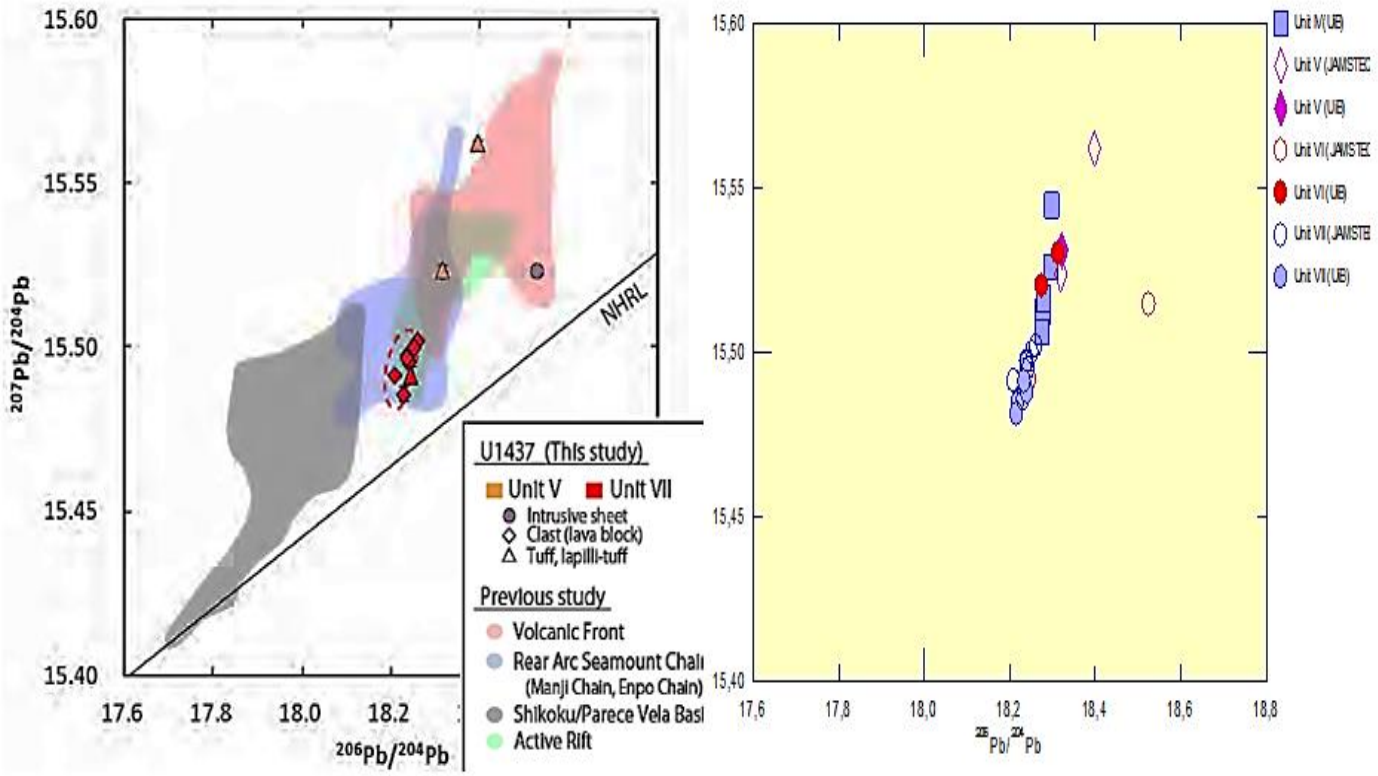

Figure 26 *This figure show how the $^{207}Pb/^{204}Pb$ vary with $^{206}Pb/^{204}Pb$, and how this variation is distributed in the geochemical sources of the Izu Bonin subduction zones. Grey area represents Shikoku Basin, blue is rear arc, green is active rift and red is the volcanic front. This is based in previous studies.*

Isotopic plot of $^{206}Pb/^{204}Pb$ and $^{87}Sr/^{86}Sr$ show a much more linear and horizontal trend than the Pb-Pb plots. Comparing the age of units with $^{206}Pb/^{204}Pb$ one can observe a $^{206}Pb/^{204}Pb$ enrichment with decreasing age, when going from unit VII to unit IV. This is also observed for the Pb-Pb plots.

Unit VII show the lowest values of $^{206}Pb/^{204}Pb$ while units VI, V and IV show higher and more enriched $^{206}Pb/^{204}Pb$. The highest enrichment of $^{206}Pb/^{204}Pb$ is in unit V. $^{87}Sr/^{86}Sr$ values do not vary as much as $^{206}Pb/^{204}Pb$ throughout the units.

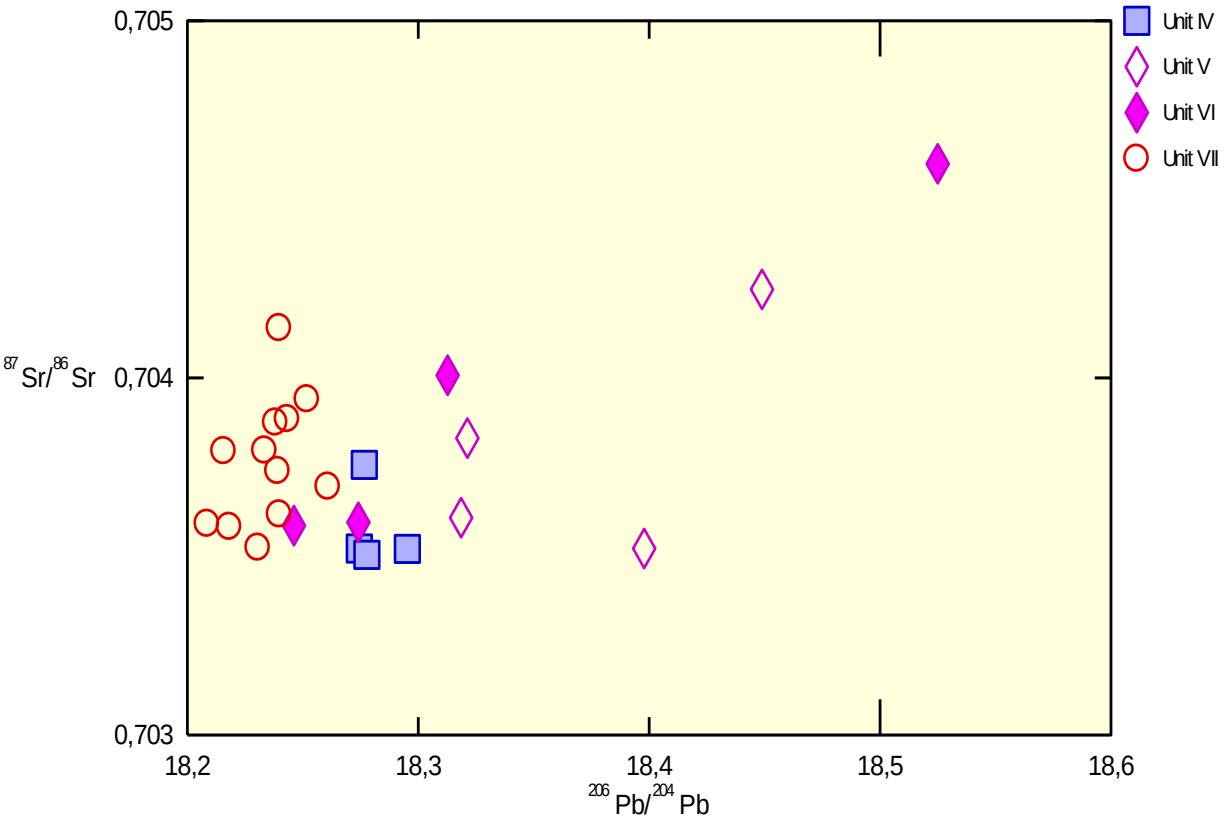

Figure 27 *An isotopic plot of ^{87}Sr and ^{206}Pb.*

Comparing these analyzed units with the isotopic composition of subduction related suits in the Izu Bonin area, we see how both $^{87}Sr/^{86}Sr$ and $^{206}Pb/^{204}Pb$ are more radiogenic than the Shikoku/Parece Vela basin.

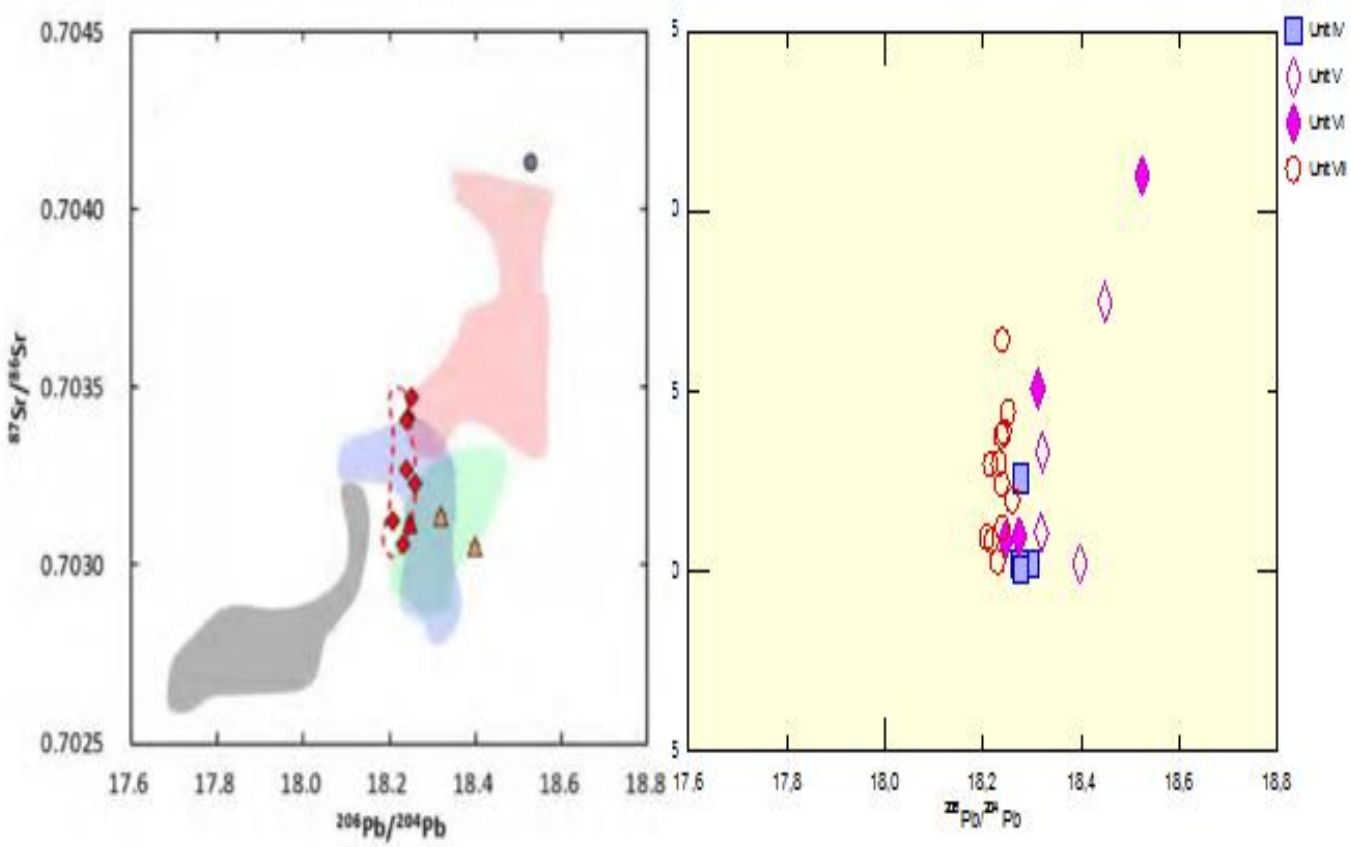

Figure 28 *This figure show how the $^{87}Sr/^{86}Sr$ vs $^{206}Pb/^{204}Pb$ vertical trend is distributed among the different geochemical provinces in Izu Bonin. Samples from JAMSTEC and UiB are different from the Shikoku Basin. Unit VII to IV show a Sr and Pb isotopic composition that resembles rear arc, active rift and the volcanic front. Grey area represents the Shikoku Basin, blue is rear arc, green is active rift and red is the volcanic front.*

The isotopic plot of $^{176}Hf/^{177}Hf$ vs $^{143}Nd/^{144}Nd$ are shown in the figure below. It shows a decreasing/horizontal trend throughout the units. Unit VII and unit VI make a rather constant cluster, with one highly deviating sample. Unit V and unit IV seems to decrease relative to the older units. Overall there is a lowering in the values of both $^{176}Hf/^{177}Hf$ and $^{143}Nd/^{144}Nd$ within the time interval of approximately 5 Ma.

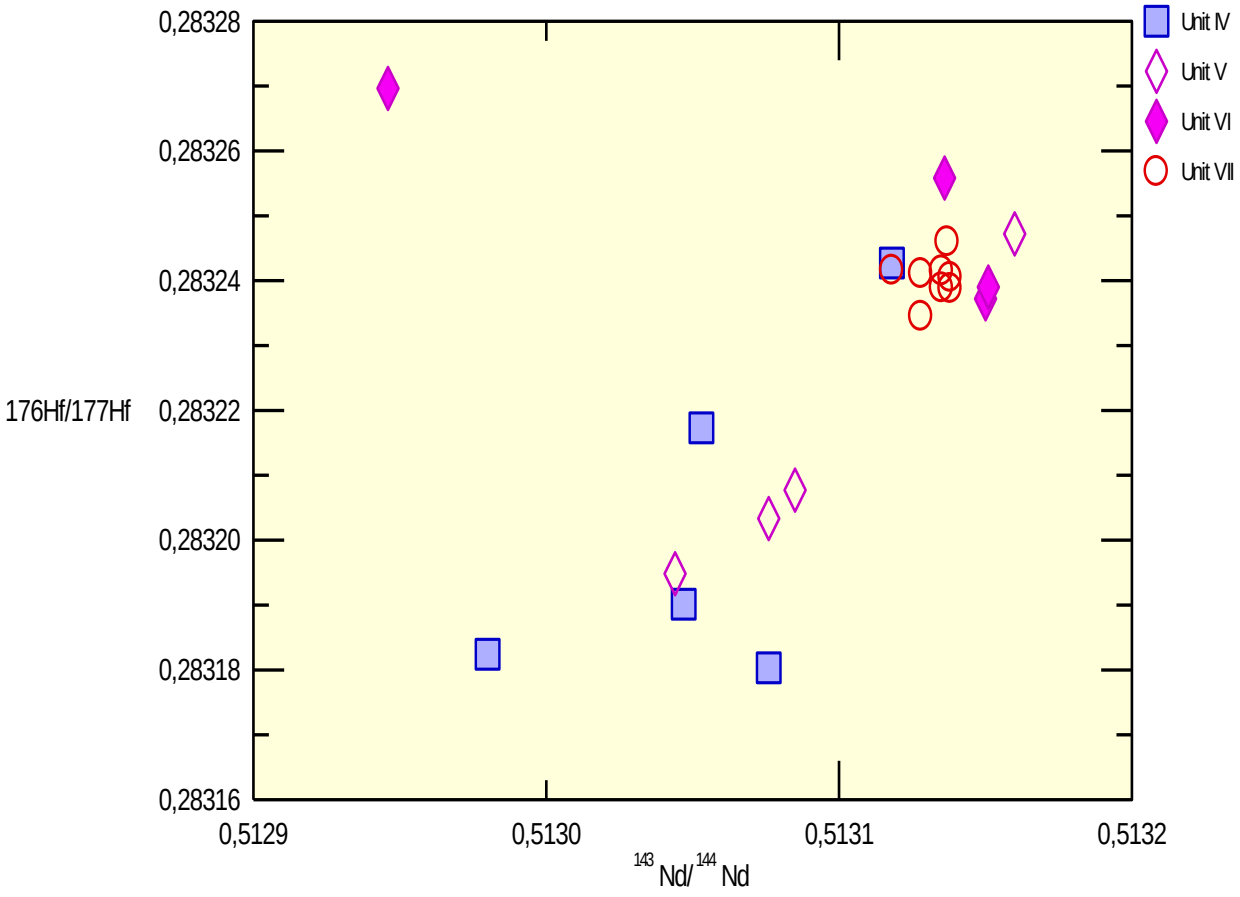

Figure 29 *Isotopic plot of $^{176}Hf/^{177}Hf$ vs $^{143}Nd/^{144}Nd$. This graphical representation show a slightly decreasing trend with time, when going from unit VII to IV.*

The figure below is based on previous studies published by JAMSTEC, and show the different geochemical sources in the Izu Bonin subduction zone. Samples drilled from the 350 IODP expedition show a gradual decrease in $^{176}Hf/^{177}Hf$ and $^{143}Nd/^{144}Nd$, a trend that goes from a more volcanic front like signature, in unit VII and unit VI, to a more rear arc like signature in units V and IV.

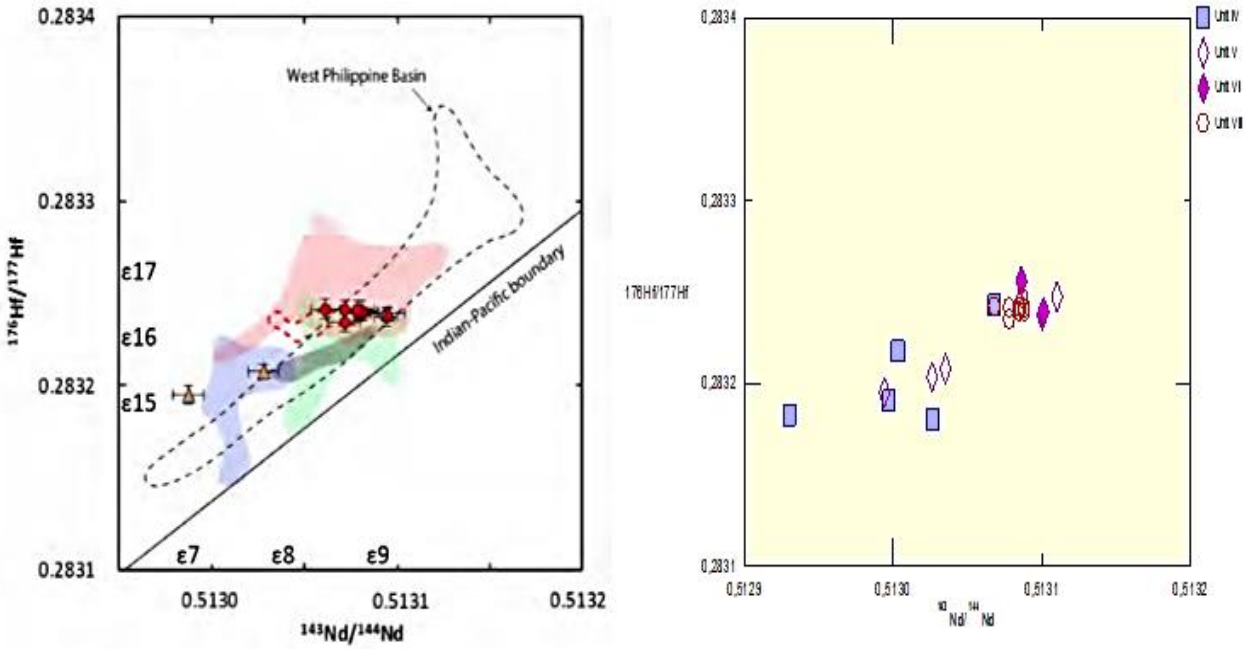

Figure 30 *Comparison between samples analyzed from the 350 IODP expedition with previous studies. Grey area represents the Shikoku Basin, blue is rear arc, green is active rift and red is the volcanic front.*

4.3 Downhole variations

4.3.1 Strontium (Sr)

Results from laboratory work and measurements from TIMS at UiB and from JAMSTEC show that values for Sr are ranging from 0,703012 to 0,706166 down the drill hole. One sample shows particularly elevated $^{87}Sr/^{86}Sr$ values at the transition between unit IV and V. Such a higher deviation from the average is probably a consequence of errors from preparation and laboratory techniques such as leaching or from the mass spectrometer itself. Since Sr is very sensitive to seawater alteration(Nobre Silva et al., 2010), it is a possibility that the leaching was not strong enough to exclude most of the alteration minerals. Jim email !

With an average value of 0,703259 it is a bit higher than the values (A. Hochstaedter et al., 2001) got from the same study area, but in the same time lower than the measured values from Izu arc front samples.

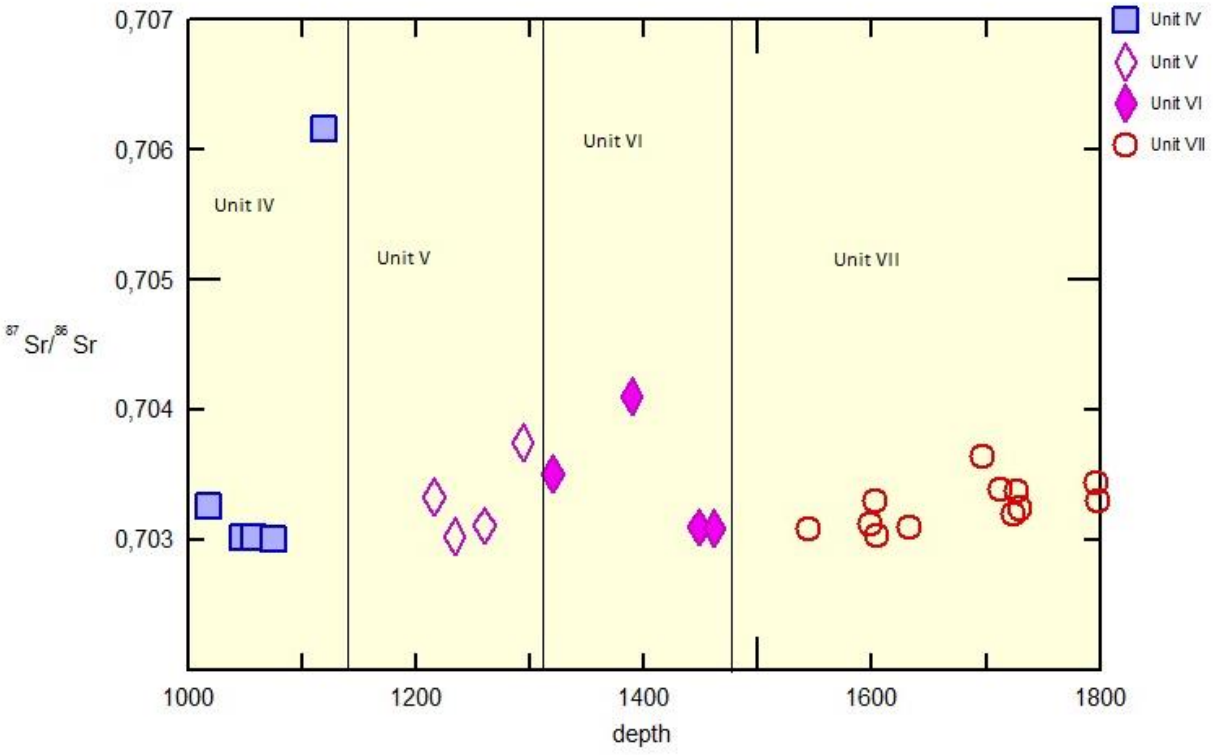

Figure 31 *Figure showing the variation of Sr with depth. Combined data from UiB and JAMSTEC. Slightly sinusoidal trend down the drill hole.*

4.3.2 Lead (Pb)

$^{206}Pb/^{204}Pb$, $^{207}Pb/^{204}Pb$ and $^{208}Pb/^{204}Pb$. Plots showing isotopic ratio with depth display a slight increase in the beginning followed by a steady decrease towards the bottom of the drill hole. All Pb isotopes show similar pattern, with the larges values in the corresponding units. Patterns showing Pb isotopic composition and how it varies with depth are shown in figure 22.

For all three species, unit V strikes out as the most enriched one. $^{206}Pb/^{204}Pb$ has values ranging from 18,2158 to 18,4489, $^{207}Pb/^{204}Pb$ from 15,4813 to 15,6001 and $^{208}Pb/^{204}Pb$ from 38,0312 to 38,5712.

Compared to values from (A. Hochstaedter et al., 2001) all species of Pb in this study show a lower ratio and thus a more depleted Pb pattern than in the volcanic front.

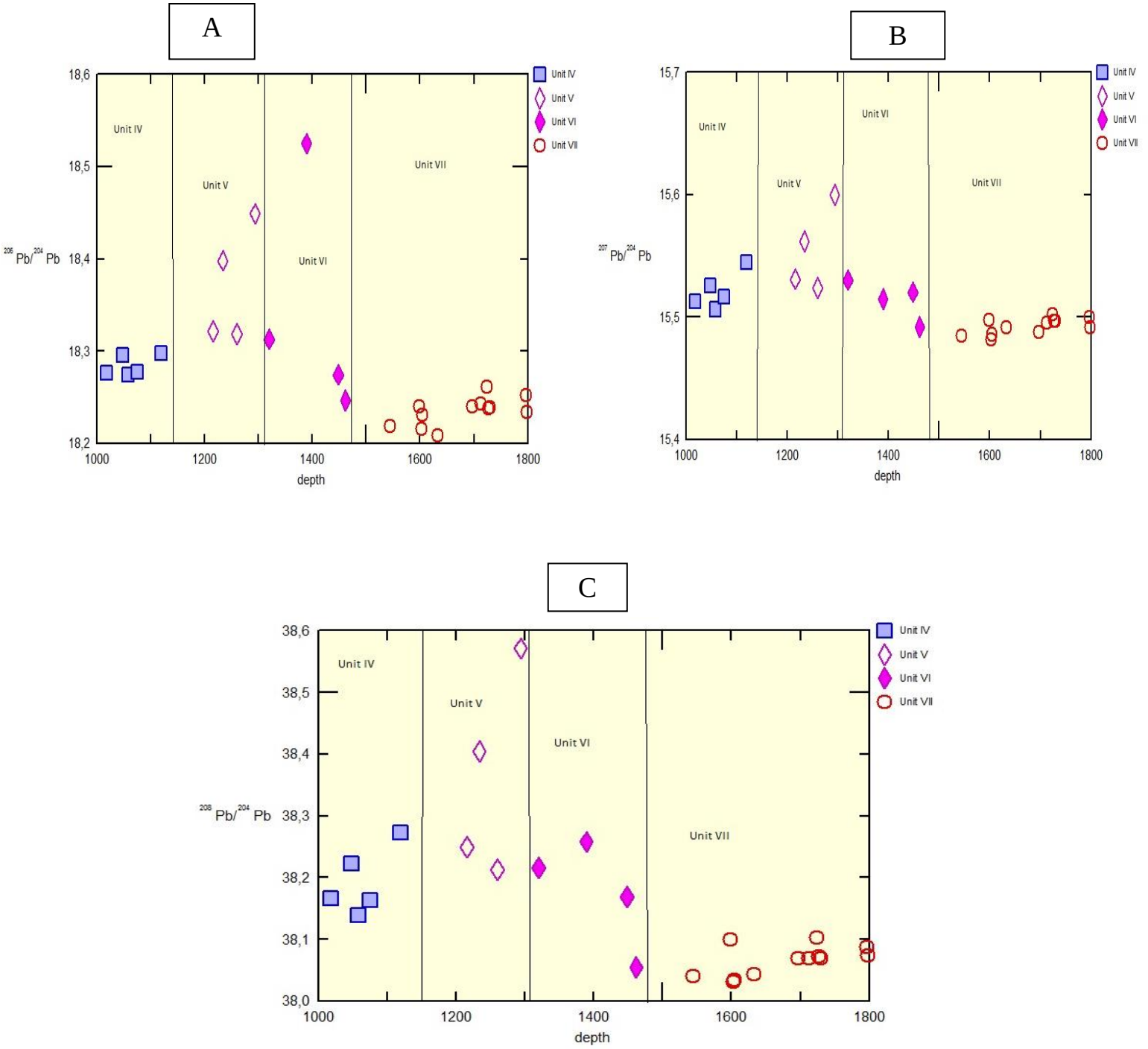

Figure 32 *Down hole measurement of ^{206}Pb, ^{207}Pb and ^{208}Pb show similar trends. Higher variations in the middle section of the drill hole. Data is from UiB and JAMSTEC.* ***A****. ^{206}Pb vs ^{204}Pb* ***B****. ^{207}Pb vs ^{204}Pb* ***C****. ^{208}Pb vs ^{204}Pb*

4.3.3 Neodymium (Nd)

Results from UiB and JAMSTEC show that Nd values are ranging from 0,512877 to 0,513095. One value strikes out among the others. It is the lowest value. Reasons for this will be discussed in section 3.6.

Generally, the core goes from low $^{143}Nd/^{144}Nd$ in unit IV to high $^{143}Nd/^{144}Nd$ in unit VII. If the value 0,512877 is not considered, a marked flattening of the trend is observed in the transition from unit V to unit VI. There is also a much higher variation in units IV and V compared to units VI and VII. Taking the age aspect in to consideration, the Nd isotopic composition is lowered in younger volcanoclastic material.

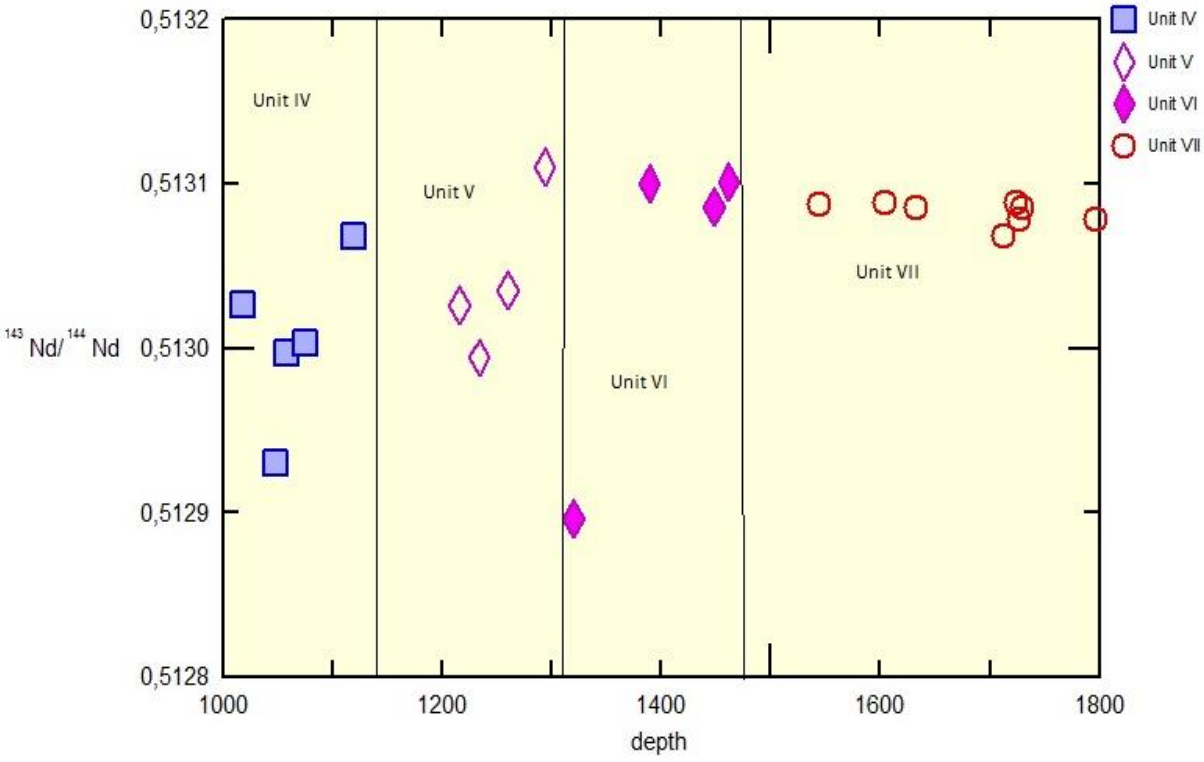

Figure 33 *Graph showing variation of $^{143}Nd/^{144}Nd$ with depth. The $^{143}Nd/^{144}Nd$ becomes flatter from unit VI to VII. More variation and lower values in units IV and V.*

4.3.4 Hafnium (Hf)

$^{176}Hf/^{177}Hf$ shows values ranging from 0,2831803 to 0,2832696. The plot showing composition of $^{176}Hf/^{177}Hf$ with depth has a sharp increase in the beginning of the unit IV followed by a decrease in the transition between unit IV and V. From unit V to the end of VII there is less variations.

As the age of the units decrease, the Hf isotopic composition is decreasing. This is also seen for the Nd isotopic composition, making Nd and Hf positively correlated with each other.

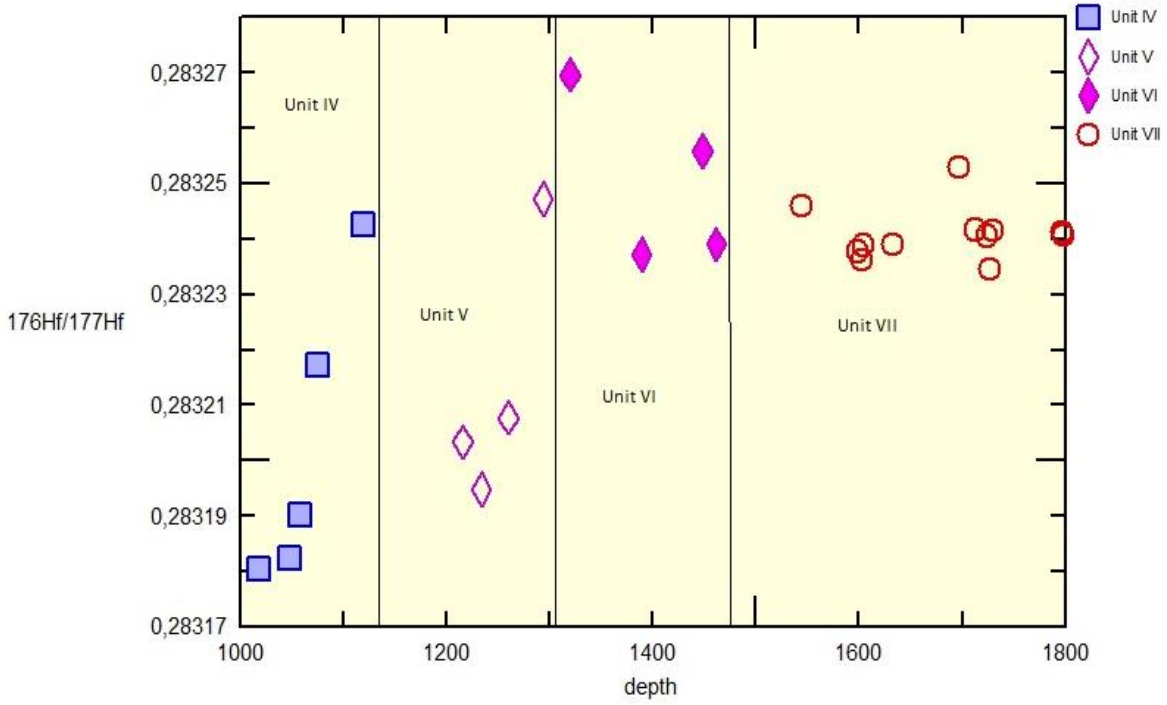

Figure 34 *Down hole measurements of $^{176}Hf/^{177}Hf$ show great variation in the start of the drill hole, but then the variation is reduced. Smaller variation in the end of the drill hole.*

5. DISCUSSION

By performing trace element and isotopic analyses, we are expecting to get valuable insight in what sources are involved in the rear arc environment. Izu Bonin subduction zone is an environment having a characteristic geochemical fingerprint, which is generated by a mix of slab derived materials interacting with the mantle wedge. Recent studies also states that magma formation in subduction zones can be affected by other geological regimes that is not common to the general subduction environment (Martinez & Taylor, 2003), such as back arc spreading. The process of back arc spreading is thought to influence the subduction zone processes by depleting the mantle.

Here, the rear arc part of Izu Bonin is studied by analyzing drilled holes between two seamount chains. Geochemical heterogeneity between the rear arc and volcanic front can be seen in REE pattern and major element chemistry (figure 11). Results from our study give new insight in the production of rear arc magmatism and how it has change with time.

5.1 Trace element geochemistry

5.1.1 Reduction in melting during 12 My to 6 My?

The temporal variations in REE patterns from this study, spans over a time interval of roughly 6 Ma. Unit VII is estimated to represent ages older than 11,87 Ma. Unit IV represent an age of 6,2 – 7,5 Ma. REE patterns, when going from the oldest unit VII to the youngest unit IV, show a gradual enrichment in the LREE compared to MREE and HREE. A more flat, less enriched REE pattern of unit VII show similarity with a mid-ocean ridge basalt (MORB), and suggest a source that is more depleted than for unit IV. The gradual increase in the enrichment of LREE can be seen in units VI and V. Unit VI marks a change in the REE geochemistry, where this can be seen as one of the samples show a more slightly enriched pattern compared to the other sample, which is flatter and less enriched (figure 23). The LREE enrichment starts to be more obvious when reaching unit V.

The enriched LREE pattern of unit IV strongly differs from unit VII. (Ishizuka, Yuasa, Taylor, & Sakamoto, 2009) showed the similar progressively LREE enrichment pattern for the Kinan Seamount chain, which is located further west of the Enpo and Manji seamount chains. Ishizuka et al. (2009) concluded that this change from a depleted to an enriched source was a result of a stop in back arc spreading. Consequently, this changed the thermal regime in the mantle wedge. Back arc spreading allows melt to be erupted and this might gradual reduce the mantle wedge temperature. When back arc spreading stops, lower melting degree at the

spreading ridge results in a higher thermal gradient in the mantle wedge, thereby enhancing the process of sediment melting(Ishizuka et al., 2009).

The transition from a flat to enriched LREE pattern may be linked to melting. MORB like pattern is observed in magmatic regimes where there is a high degree of melting. When the degree of melting is reduced, a LREE enriched pattern will be generated. When the fraction of melt becomes smaller, the more incompatible LREE becomes more enriched compared to HREE. This can be seen in following equation for Batch melting;

$$\frac{CL}{C0} = \frac{1}{D(1-F)+F} \qquad Eq.\ 10$$

C_L is concentration in melt produced, C_0 is concentration before melting, D is distribution coefficient and F is the melt fraction. The explanation to this transition in REE pattern from unit VII to IV may be consequence of the reduction in the degree of melting form approximately 12 Ma to 7 Ma.

5.1.2 Presence of a subduction component in the rear arc?

Multielement spider diagrams usually gives more information than just normal REE plots. By incorporating additional elements like the large ion lithophiles and high field strength elements, it is possible to see if there have been any fluids present during the magma formation. The multielement spider diagrams in figure 27 and 28, show a clear enrichment of LILE compared to HFSE. The decoupling of these two groups of elements indicate presence of fluids(Hanyu et al., 2006).

For units IV to V, high LILE/HFSE and enrichment of LREE compared to MREE and HREE, indicate the addition of fluids in to the mantle wedge. For units VI and VII, high LILE/HFSE is observed with reduced enrichment of LREE. The fact that unit VII has MORB like pattern and high LILE/HFSE may indicate that different types of geochemical environments are mixed, such as subduction zone magmatism and tholeiitic magmatism.

High LILE/HFSE ratio is present in all units in this study. A study by Bryant et al. (2003) also showed that this high LILE/HFSE ratio was present before back arc spreading. This contradict the hypotheses of (Ishizuka et al., 2009) and (Gill et al.,1994), which believed that the enriched signature developed after back arc spreading.

(Elliot et al.,1997) did a study where they observed different patterns in LILE and LREE and concluded that the chemical properties of these elements represent the subduction component with the characteristics ranging from aqueous fluid to sediment dominated. These

characteristics are monitored using ratios of elements that have similar partition coefficient during melting of the mantle, but different partition coefficient in fluids (Turner & Hawkesworth, 1997).

A plot of Ba/La vs La/Sm can be used to discriminate between how great the fluid and sediment contribution is in a magmatic system. Ba/La vs La/Sm plot of analyzed samples from the Izu Bonin rear arc is shown in the figure below.

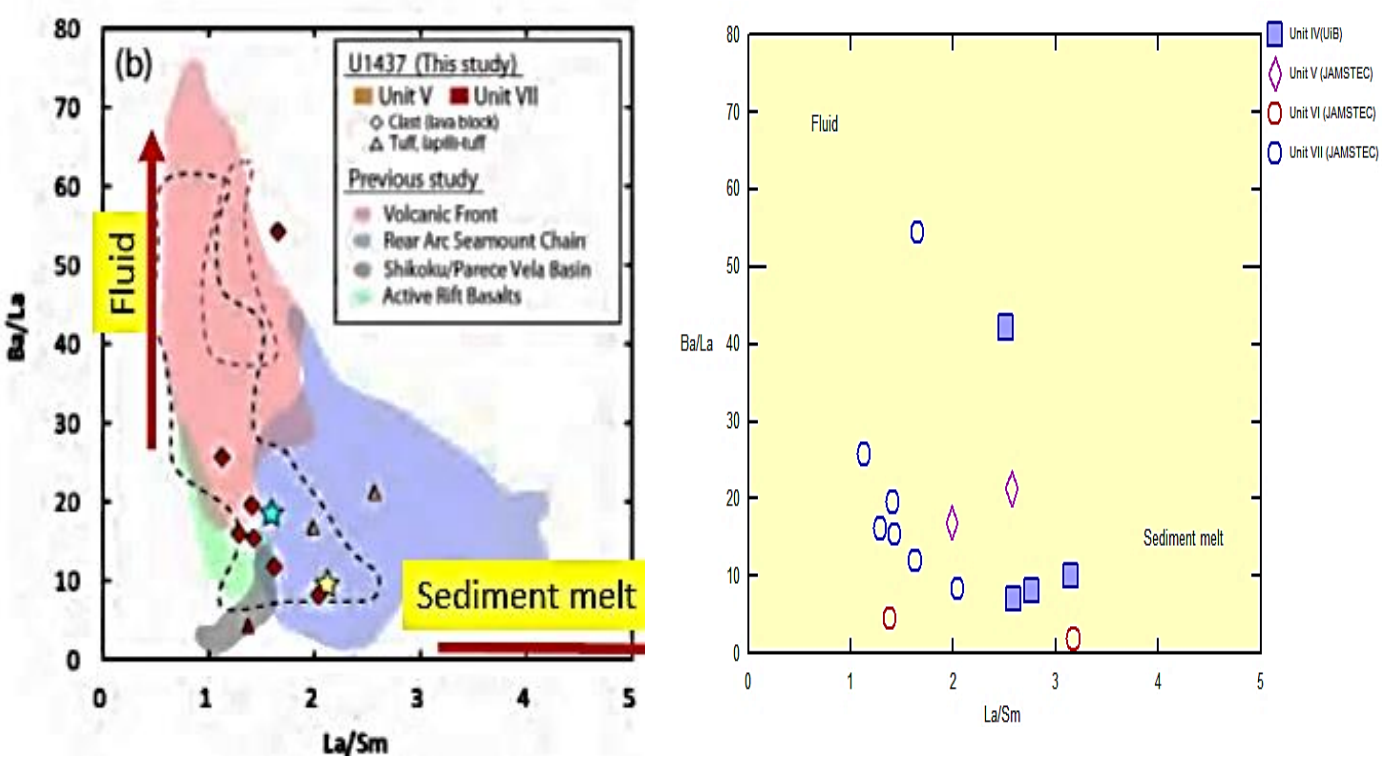

Figure 35 *Figure showing fluid and sediment melt contribution in the different units studied.*

The oldest unit VII, show the highest contribution from the slab derived fluids and at the same time the lowest contribution from sediment melts. Unit VI show very low fluid input compared to unit VII. Contribution from a potential sediment melt is higher for unit VI than for unit VII. Unit V show elevated Ba/La ratio compared to unit VI, but is similar to unit VII. Sediment melt contribution in unit V is higher than for unit VII. The youngest unit IV show the highest contribution from sediment melt. The trending patter, when going from unit VII to unit IV, is higher La/Sm and lowered Ba/La. This indicate that sediments melt has increased during the period from unit VII to IV.

Addition of fluids into the mantle wedge happens in the shallower part of the subduction, whereas the melting of sediments occurs at deeper depths(Ishizuka et al., 2009). This transition can be linked to the physical process of slab roll back. Through time, the slab will sink down in the mantle and the P-T conditions will be higher. This change the thermal environment along the slab-mantle interface. Further down, the temperature gets higher and may induce melting of sediments. Small changes are observable compared to the volcanic front, which has much higher values. Overall, figure show a weak input of the slab derived material compared to the VF.

The HFSE provide valuable insight in the relative depletion in the mantle wedge (Bryant et al., 2003). By plotting HFSE element ratio against the different units it is possible to see how enriched or depleted the mantle source is. Figure 40 show Nb/Zr variation with the different units. Unit IV show the most elevated Nb/Zr ratios. Unit V show decreasing ratios compared with unit IV. Nb/Zr ratios for unit VI and unit VII show lower ratios than for both unit V and IV. Nb/Zr ratios from (Bryant et al., 2003) estimated that N-MORB has a ratio of Nb/Zr=0,03. Comparing this with figure 36, only units IV and V has Nb/Zr ratios over the N-MORB value of 0,03. Elevated values in units IV and V suggest an enriched mantle source. For units VI and VII, lower Nb/Zr ratios than N-MORB indicate a depleted mantle source. Studies from J. B. Gill et al. (1994) and (Ewart et al.,1998) suggest that this depletion can be consequence of back arc spreading, which may directly deplete the magma as it is further advected under the arc.

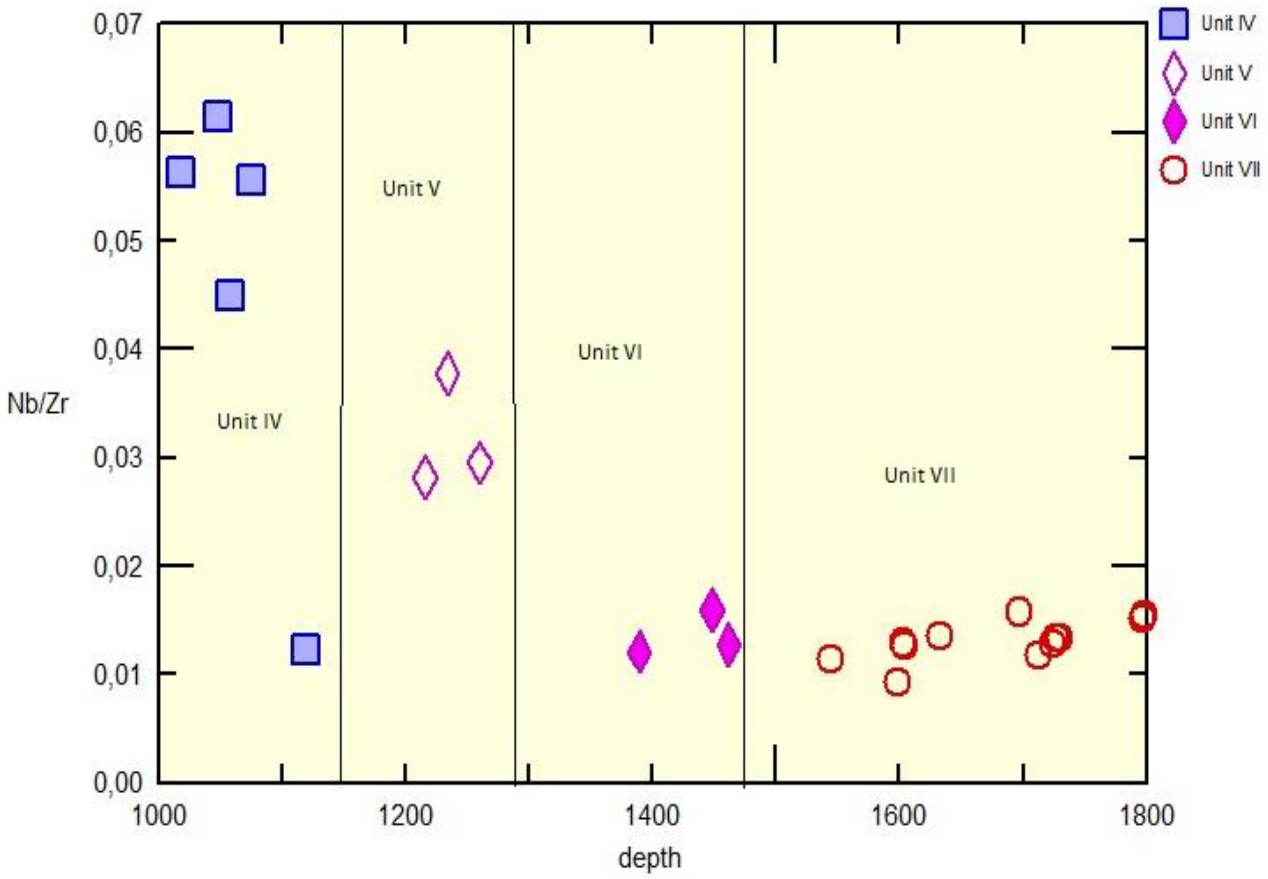

Figure 36 *Figure showing the Nb/Zr ratio plotted against the different units. High values for unit IV to low values for unit VII. May suggest a more depleted source for unit VII than unit IV, which is more enriched.*

Multielement spider diagrams are useful to give a more complete overview of the sources involved. What is observed in these diagrams is that all units studied has a subduction component. Enrichment of fluid mobile elements such as the LILE (Cs,Ba,Pb,Sr) compared to HFSE (Nb,Zr,Nd,Hf). All units from VII to IV are showing the typical high LILE/HFSE geochemical pattern, and implies that there has been a subduction component present in the time interval from 6 Ma to 12 Ma. What can be deduced from these results is that the subduction component was present in the system, even when the magmatic system was depleted.

5.2 Isotope Geochemistry

Not affected by fractionation processes, radiogenic isotopes are well used to characterize the major sources involved in magma formation. Sr, Pb, Nd and Hf have different properties during a process like dehydration. Sr and Pb are highly mobile in aqueous fluid, while Nd and Hf are both immobile. Enrichments of Sr and Pb will reflect slab fluids and Nd and Hf will reflect the mantle wedge(Straub et al.,2010). Sr and Pb are both mobile in hydrous fluids and are good proxies for the subduction component. Nd and Hf are immobile during dehydration and reflect the mantle. Looking at the different trends we see that Sr and Pb correlate well with each other and the same can be seen for Nd and Hf. Trends of Sr and Pb are vertical and are increasing towards a volcanic front like magmatism. For Nd and Hf, the trends are more horizontal and decreasing towards a more rear arc like magmatism.

5.2.1 Addition of slab derived material to the mantle wedge

Both Sr and Pb are mobile when a hydrous phase is involved in magma genesis. The down hole variation of Sr and Pb are very similar. The most interesting interval lies in between unit V and VI, approximately 1120 m – 1460 m down the drill hole. Although the variation of these isotopes are relative uniform, a sudden increase is observed at this depth. An increase of radiogenic isotopes like Sr and Pb can be linked to addition of slab derived fluids or the mixing between two different geochemical sources having different geochemical signature.

Isotopic plot of $^{206}Pb/^{204}Pb$ vs $^{87}Sr/^{86}Sr$ are shown in figure 35. Unit V and unit VI strikes out to be the area with most variation. By looking at units V and VI, and how they vary in both $^{206}Pb/^{204}Pb$ and $^{87}Sr/^{86}Sr$, we see that the increase in $^{206}Pb/^{204}Pb$ is more important than for $^{87}Sr/^{86}Sr$. This decoupling effect may be explained by the relative abundance of Sr and Pb in the slab derived materials. The principal reservoirs for Sr and Pb in subduction zones are sediments and igneous crust. These two components of the slab, have different abundance of Sr and Pb. Unradiogenic Sr from the subducted igneous crust (66% of arc Sr) and mantle (31%) buffer minor amounts of radiogenic Sr contributed from subducted sediment or altered oceanic crust(Straub et al., 2010). The opposite can be seen for Pb. Isotopic composition of Pb from the mantle is easily overpowered by the addition of slab derived materials.

When comparing the isotopic composition of Sr and Pb with earlier studies from JAMSTEC, we see that both $^{207}Pb/^{204}Pb$ vs $^{206}Pb/^{204}Pb$ and $^{87}Sr/^{86}Sr$ vs $^{206}Pb/^{204}Pb$ plots show a vertical trend and are different from Shikoku/Parece Vela Basin in composition (figure 34 and 36). The Shikoku/Parece Vela Basin represents the composition of a Philippine Sea MORB. As

seen from Sr and Pb results, they suggest fluid addition and indicate that Sr and Pb is added by a geochemical source that is not Philippine Sea MORB.

How the subduction component is varying with the measured Nb/Zr ratios can be seen by plotting Nb/Zr against fluid mobile elements like Sr and Pb. In figure 38, we see that $^{87}Sr/^{86}Sr$ is relatively constant with increasing Nb/Zr. $^{207}Pb/^{204}Pb$ is enriched in unit VI, V and IV compared to unit VII. This enrichment occurs as the units becomes higher in Nb/Zr. Addition of Pb to the magmatic system can thus be seen in contrast to Sr. This may indicate that Pb is slab derived. As mentioned in section 5.2, Pb isotopic composition in the mantle wedge is easily overpowered by the addition of slab derived materials. This is not the case for Sr, where the Sr isotopic composition in the mantle wedge acts as a buffer against slab derived materials.

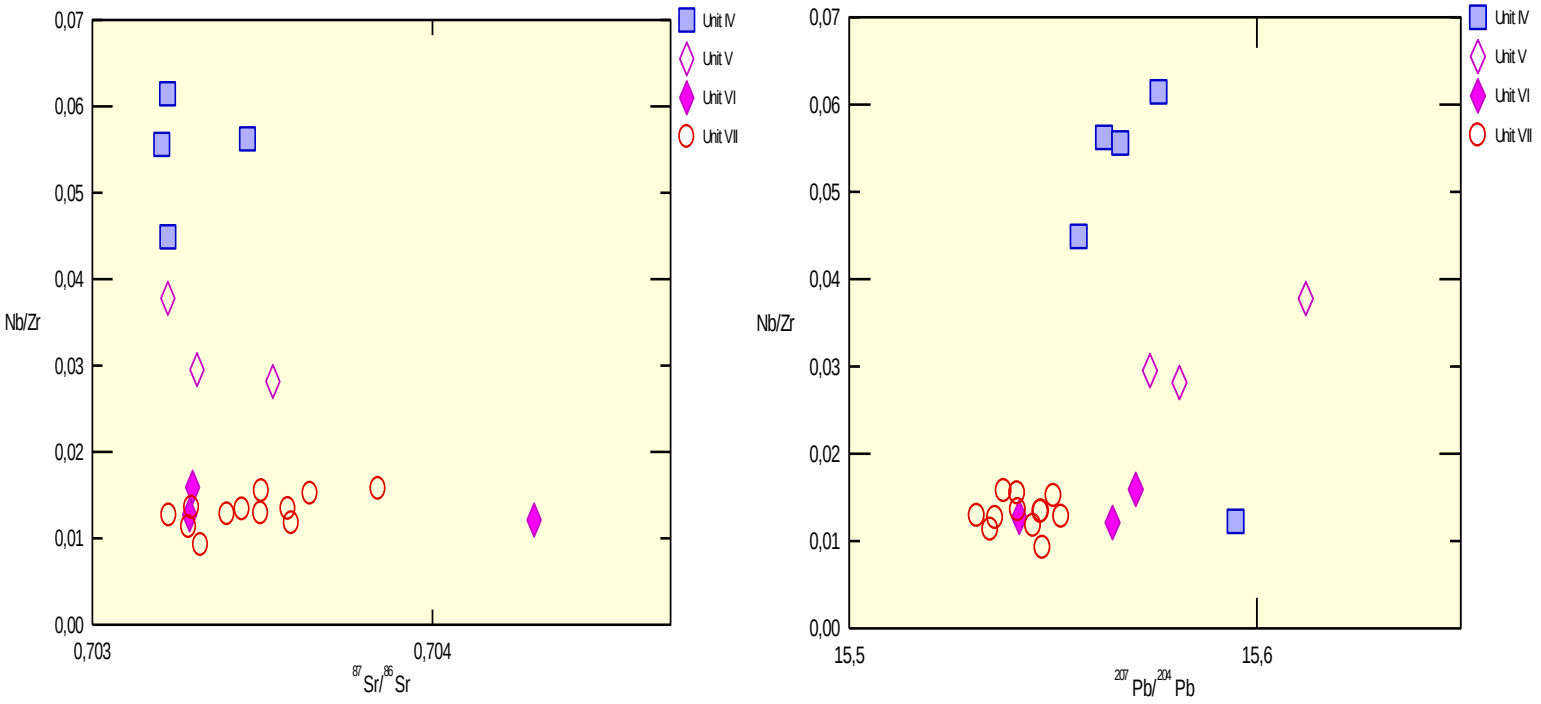

Figure 37 *$^{87}Sr/^{86}Sr$ and $^{207}Pb/^{204}Pb$ plotted against Nb/Zr.*

5.2.2 Changes in the ambient mantle

Both Nd and Hf immobile incompatible elements that are immobile during dehydration. Downhole variation in Nd and Hf isotopes show somewhat similar trends. Both have an increase in isotopic composition when going from unit IV to VII. Compared to the Sr and Pb picture, the increase is much more obvious. Nd and Hf isotopic composition show a horizontal/decreasing trend. These plots resemble the Shikoku/Parece Vela Basin more than Sr and Pb, in which these isotopes are quite different from the Shikoku Basin.

The variation in Nd and Hf show a decreasing trend from the volcanic front towards a more rear arc like magmatism when going from unit VII to unit IV. These lowered values for Nd and Hf are also observed by Tollstrup et al. (2010), which measured the Nd and Hf isotopic composition for the Neogene rear arc. These decreasing values may be explained by changes in the mantle because of their immobile property during dehydration.

The transition from a depleted to enriched mantle signature observed by the REE patterns can also be shown in a plot of Nb/Zr against $^{143}Nd/^{144}Nd$. As the units get younger, higher values of Nb/Zr is observed with decreasing $^{143}Nd/^{144}Nd$. The depleted signature has higher $^{143}Nd/^{144}Nd$ and lower Nb/Zr.

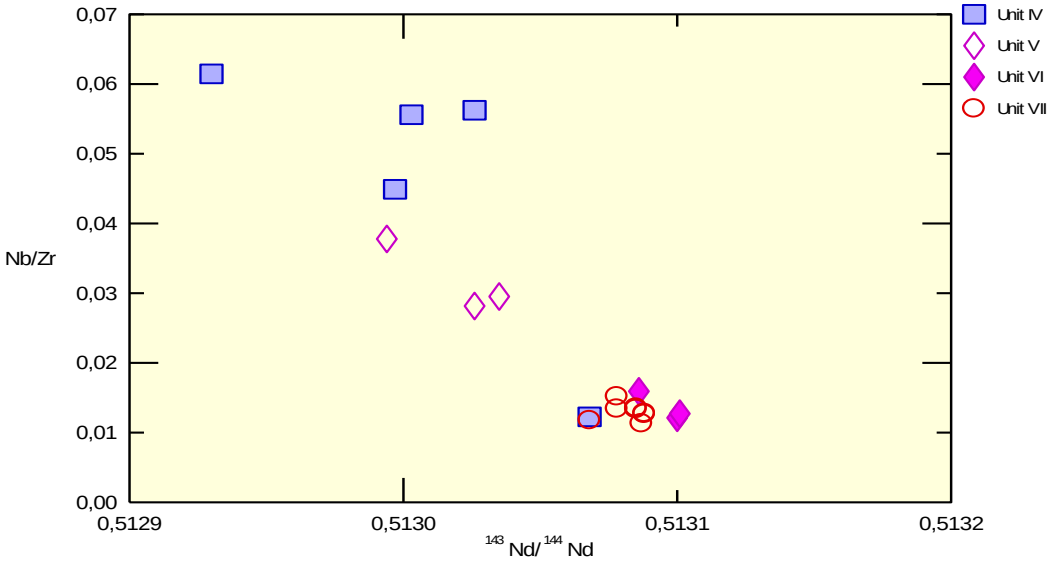

Figure 38 *Nb/Zr vs $^{143}Nd/^{144}Nd$.*

Ishizuka et al. (2009) studied the Kinan Seamount chain. They proposed that a LREE enrichment is consistent with the reduction in melting, as explained in section. Also, the change from a high to low $^{143}Nd/^{144}Nd$ is observed when going from unit VII to unit IV. An explanation for the LREE enrichment, lowering of $^{143}Nd/^{144}Nd$ may be explained by the cessation of back arc spreading at 15 Ma. Reduction in the upwelling magma during back arc spreading would progressively generate smaller melt fractions. These smaller blobs are able to sample more enriched blobs. Thereby explaining the lowering of $^{143}Nd/^{144}Nd$. The increase in Nd composition with time was also observed by J. B. Gill et al. (1994), by the study of turbidites. J. B. Gill et al. (1994) concluded that this increase in Nd, and the transition from an enriched to a depleted mantle was related to back arc spreading.

What is seen from the analyses from the volcanoclastic material recovered from the basin located between Enpo and Manji seamount chains is enriched in LREE and has high LILE/HFSE ratio. Sr and Pb isotopic composition has a vertical trend and is different from Philippine sea MORB. Hf and Nd isotopic composition show a slightly decreasing/ horizontal trend. All these observations are occurring when going from the oldest unit VII to the youngest unit IV.

Results from this study show that Nd isotopic composition was higher in unit VII (figure 31), which represent the ending of the back arc spreading. Bryant et al. (2003) analyzed the trace element compositions from the same area and concluded with the LILE/HFSE ratio was the same before and after the back arc spreading. Compared with results from this study, a high LILE/HFSE is uniform throughout the units.

The plot from figure 39 show that both fluid and sediment melt is not very high for all units. Izu Bonin tephras analyzed by Bryant et al. (2003) also indicate low sediment input to the mantle wedge during the last 30 Ma. Processes occurring at the slab-mantle interface are highly dependent on temperature and pressure. Decompression melting during back arc spreading would reduce the mantle wedge temperature, and thus generate a much gentle steeping geothermal gradient. This temperature reduction might reduce the process of sediment melting and thereby by the sediment melt contribution to the resulting magma.

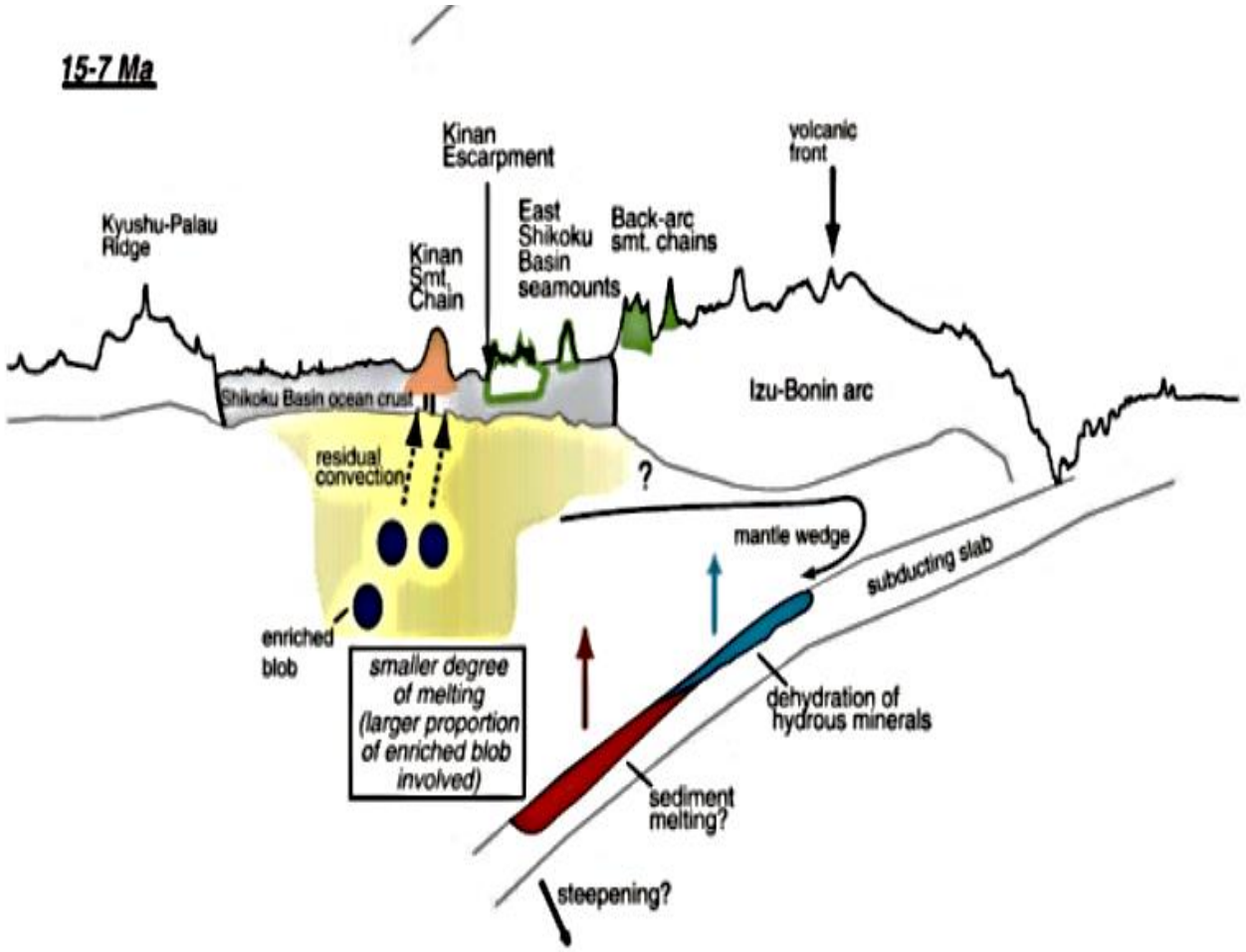

Figure 39 *This figure show an overview of the Izu Bonin magmatic setting. Small degrees of melt generate more enriched blobs. Figure from (Ishizuka et al., 2009).*

The different units recovered in the drilled core at Izu Bonin, show a change from a depleted to enriched source. This enrichment is also observed by others (e.g. (Machida et al.,2008), A. G. Hochstaedter et al. (2000), Tollstrup et al. (2010)). The origin of this enriched signature is still debated.

Some (Machida et al. (2008), Ishizuka et al. (2009)) believe that an involvement of an enriched OIB type material in the upper mantle generates this enriched rear arc signature. Others (Tollstrup et al. (2010), A. G. Hochstaedter et al. (2000)) believe that there may be an additional enrichment by partial melts derived from the slab. The temporal variations down the drill hole in this study do show that there is a shift from depleted to enriched signature in the rear arc magmatism.

A proposed model for the results in our study is that there has been a reduction in the melting regime, probably as a consequence of the stop in back arc spreading at 15 My. This led to a change from a depleted MORB like pattern to a more enriched type of mantle. This change can also be seen in Nb/Zr ratios. REE patterns from units V and VI show that this change was a gradual change, where they show REE patterns that is both slightly enriched and depleted. Advection of this enriched source under the arc, where slab derived material is added. The nature of the added slab material leaves a much clearer imprint of Pb than for Sr, where this can be seen in figure 37. Pb correlates better with the observed Nb/Zr than Sr does.

6. CONCLUSION

This study has investigated the geochemical signals inherited by volcanoclastic material recovered from the rear arc of Izu Bonin. Main conclusions reached through the study are:

- Temporal variations in REE patterns show that there is a change in the melting regime of the mantle source region. Unit VII goes from a flat MORB like pattern to a LREE enriched pattern in unit IV. This pattern can be explained by the reduction in the degree of melting through this time interval. This is consistent with the cessation of back-arc spreading, which happened shortly after 15 Ma.
- Both endmembers, unit VII and unit IV, of the studied samples show a high LILE/HFSE ratio. This decoupling effect of LILE and HFSE is explained by the presence of two different sources in the magmatic regime, that is slab-derived materials and mantle materials. Although the ratio of LILE/HFSE is present, it is much lower than for the volcanic front.
- Based on Nb/Zr ratios, there is a gradual increase in the ratio when going from unit VII to unit IV. Increase in Nb/Zr indicate that magmas older than 11 Ma was much more depleted than the 6 Ma magmas. This observation coincides with the changes observed in REE patterns.
- $^{87}Sr/^{86}Sr$ is constant throughout the units. Pb isotopic composition show an increase when going from unit VII to IV. This means that there is a certain contribution from the subducted slab to the mantle wedge.
- Hf and Nd isotopic composition decreases through time. These are related to the decrease in the magma budget when going from unit VII to unit IV.

6.1 Future work

For increased knowledge, it would be useful to do some geochemical modelling related to the mixing process of the different sources. This would give more insight in how the different slab derived components, such as fluids and sediments, are contributing to the resulting magma. Comparison of data with other parts of the core will be essential to get the whole picture regarding the rear arc magmatism.

References

Arculus, R. J., Ishizuka, O., Bogus, K. A., Gurnis, M., Hickey-Vargas, R., Aljahdali, M. H., . . . Zhang, Z. (2015). A record of spontaneous subduction initiation in the Izu-Bonin-Mariana arc. *Nature Geoscience, 8*(9), 728-0894. doi:10.1038/NGEO2515

Armstrong, R. L. (1991). The persistent myth of crustal growth. *Australian Journal of Earth Sciences, 38*(5), 613-630. doi:10.1080/08120099108727995

Bandy, W. L., & Hilde, T. W. C. (1983). Structural features of the bonin arc: Implications for its tectonic history. *Tectonophysics, 99*(2), 331-353. doi:10.1016/0040-1951(83)90111-7

Bryant, C. J., Arculus, R. J., & Eggins, S. M. (2003). The geochemical evolution of the Izu-Bonin arc system: A perspective from tephras recovered by deep-sea drilling. *Geochemistry, Geophysics, Geosystems, 4*(11), n/a-n/a. doi:10.1029/2002gc000427

Bureau, H., & Keppler, H. (1999). Complete miscibility between silicate melts and hydrous fluids in the upper mantle: experimental evidence and geochemical implications. *Earth and Planetary Science Letters, 165*(2), 187-196. doi:10.1016/S0012-821X(98)00266-0

Cosca, M., Arculus, R., Pearce, J., & Mitchell, J. (1998). 40Ar/ 39Ar and K–Ar geochronological age constraints for the inception and early evolution of the Izu–Bonin – Mariana arc system. *Island Arc, 7*(3), 579-595. doi:10.1111/j.1440-1738.1998.00211.x

Cosca, M. A., Arculus, R. J., Pearce, J. A., & Mitchell, J. G. (1998). Ar-40/Ar-39 and K-Ar geochronological age constraints for the inception and early evolution of the Izu-Bonin-Mariana arc system. *Island Arc, 7*(3), 579-595. doi:DOI 10.1046/j.1440-1738.1998.00211.x

Crawford, A. J. (1989). *Boninites*. London: Unwin Hyman.

Dickinson, W. R. (1975). Potash-Depth (K-h) Relations in Continental Margin and Intra-Oceanic Magmatic Arcs. *Geology (Boulder)*(2), 53-56.

Elliott, T. R., Plank, T., Zindler, A., White, W., & Bourdon, B. (1997). Element transport from slab to volcanic front at the Mariana arc. *Journal of Geophysical Research. Solid Earth*.

Ewart, A., Collerson, K. D., Regelous, M., Wendt, J. I., & Niu, Y. (1998). Geochemical Evolution within the Tonga–Kermadec–Lau Arc–Back-arc Systems: the Role of Varying Mantle Wedge Composition in Space and Time. *Journal of Petrology, 39*(3), 331-368. doi:10.1093/petroj/39.3.331

Fyfe, W. S. (1978). The evolution of the earth's crust: Modern plate tectonics to ancient hot spot tectonics? *Chemical Geology, 23*(1), 89-114. doi:10.1016/0009-2541(78)90068-2

Gill, J. B. (1981). *Orogenic andesites and plate tectonics* (Vol. 16). Berlin: Springer.

Gill, J. B., Hiscott, R. N., & Vidal, P. (1994). Turbidite geochemistry and evolution of the Izu-Bonin arc and continents. *LITHOS, 33*(1), 135-168. doi:10.1016/0024-4937(94)90058-2

Haeckel, M., van Beusekom, J., Wiesner, M. G., & König, I. (2001). The impact of the 1991 Mount Pinatubo tephra fallout on the geochemical environment of the deep-sea sediments in the South China Sea. *Earth and Planetary Science Letters, 193*(1), 151-166. doi:10.1016/S0012-821X(01)00496-4

Hanyu, T., Tatsumi, Y., Nakai, S. i., Chang, Q., Miyazaki, T., Sato, K., . . . Yoshida, T. (2006). Contribution of slab melting and slab dehydration to magmatism in the NE Japan arc for the last 25 Myr: Constraints from geochemistry. *Geochemistry, Geophysics, Geosystems, 7*(8), n/a-n/a. doi:10.1029/2005gc001220

Hochstaedter, A., Gill, J., Peters, R., Broughton, P., Holden, P., & Taylor, B. (2001). Across-arc geochemical trends in the Izu-Bonin arc: Contributions from the subducting slab. *Geochem. Geophys. Geosyst., 2*.

Hochstaedter, A. G., Gill, J., Taylor, B., Ishizuka, O., Yuasa, M., & Morita, S. (2000). Across-arc geochemical trends in the Izu-Bonin arc: Constraints on source composition and mantle melting. *J. Geophys. Res.-Solid Earth, 105*(B1), 495-512.

Horwitz, E. P., & Chiarizia, R. (1992). A NOVEL STRONTIUM-SELECTIVE EXTRACTION CHROMATOGRAPHIC RESIN*. *Solvent Extraction and Ion Exchange, 10*(2), 313-336. doi:10.1080/07366299208918107

Hubisz, J. L. (2014). Fundamental Planetary Science: Physics, Chemistry, and Habitability. *The Physics Teacher, 52*(6), 383-383. doi:10.1119/1.4893112

Hurley, P. M., & Rand, J. R. (1969). Pre-drift continental nuclei. *Science, 164*(3885), 1229-1242. doi:10.1126/science.164.3885.1229

Ishizuka, O., Taylor, R. N., Milton, J. A., & Nesbitt, R. W. (2003). Fluid–mantle interaction in an intra-oceanic arc: constraints from high-precision Pb isotopes. *Earth and Planetary Science Letters, 211*(3-4), 221-236. doi:10.1016/s0012-821x(03)00201-2

Ishizuka, O., Taylor, R. N., Yuasa, M., Milton, J., Nesbitt, R. W., Uto, K., & Sakamoto, I. (2003). Along-arc geochemical variation of the southern Izu-Bonin arc - Transition from the Izu-Bonin to Mariana arc. *Geochim. Cosmochim. Acta, 67*(18), A176-A176.

Ishizuka, O., Yuasa, M., Taylor, R. N., & Sakamoto, I. (2009). Two contrasting magmatic types coexist after the cessation of back-arc spreading. *Chemical Geology, 266*(3), 274-296. doi:10.1016/j.chemgeo.2009.06.014

Machida, S., Ishii, T., Kimura, J.-I., Awaji, S., & Kato, Y. (2008). Petrology and geochemistry of cross-chains in the Izu-Bonin back arc: Three mantle components with contributions of hydrous liquids from a deeply subducted slab. *Geochemistry, Geophysics, Geosystems, 9*(5), n/a-n/a. doi:10.1029/2007gc001641

Martinez, F., & Taylor, B. (2003). Controls on back-arc crustal accretion: insights from the Lau, Manus and Mariana basins. *Geological Society, London, Special Publications, 219*(1), 19-54. doi:10.1144/GSL.SP.2003.219.01.02

Nobre Silva, I. G., Weis, D., & Scoates, J. S. (2010). Effects of acid leaching on the Sr-Nd-Hf isotopic compositions of ocean island basalts. *Geochemistry, Geophysics, Geosystems, 11*(9), n/a-n/a. doi:10.1029/2010GC003176

Rapp, R. P., Shimizu, N., Norman, M. D., & Applegate, G. S. (1999). Reaction between slab-derived melts and peridotite in the mantle wedge: experimental constraints at 3.8 GPa. *Chemical Geology, 160*(4), 335-356. doi:10.1016/S0009-2541(99)00106-0

Reymer, A., & Schubert, G. (1984). Phanerozoic addition rates to the continental crust and crustal growth. *Tectonics*(1), 63-77. doi:10.1029/TC003i001p00063

Rudnick, R. L., & Gao, S. (2014). *4.1 - Composition of the Continental Crust*: Elsevier Ltd.

Smith, G., & Landis, C. (1995). Intra-arc basins, Tectonics of Sedimentary Basins CJ Busby, RV Ingersoll, 263–298: Blackwell Sci., Malden, MA.

Stern, R. (2007). When and how did plate tectonics begin? Theoretical and empirical considerations *Chin. Sci. Bull.* (Vol. 52, pp. 578-591).

Stern, R. J. (2002). SUBDUCTION ZONES. *Reviews of Geophysics, 40*(4), 3-1-3-38. doi:10.1029/2001RG000108

Stern, R. J. (2004). Subduction initiation: spontaneous and induced. *Earth and Planetary Science Letters, 226*(3), 275-292. doi:10.1016/j.epsl.2004.08.007

Stern, R. J., Fouch, M. J., & Klemperer, S. L. (2003). An overview of the Izu-Bonin-Mariana subduction factory. *Inside the subduction factory*, 175-222.

Straub, S. M. (2003). The evolution of the Izu Bonin - Mariana volcanic arcs (NW Pacific) in terms of major element chemistry. *Geochemistry, Geophysics, Geosystems, 4*(2), n/a-n/a. doi:10.1029/2002GC000357

Straub, S. M., Goldstein, S. L., Class, C., Schmidt, A., & Gomez-Tuena, A. (2010). Slab and Mantle Controls on the Sr–Nd–Pb–Hf Isotope Evolution of the Post 42 Ma Izu–Bonin Volcanic Arc. *Journal of Petrology, 51*(5), 993-1026. doi:10.1093/petrology/egq009

Sun, S. S., & McDonough, W. F. (1989). Chemical and isotopic systematics of oceanic basalts: implications for mantle composition and processes. *Geological Society, London, Special Publications, 42*(1), 313-345. doi:10.1144/GSL.SP.1989.042.01.19

Suyehiro, K., Takahashi, N., Ariie, Y., Yokoi, Y., Hino, R., Shinohara, M., . . . Taira, A. (1996). Continental Crust, Crustal Underplating, and Low-Q Upper Mantle Beneath an Oceanic Island Arc. *Science, 272*(5260), 390-392. doi:10.1126/science.272.5260.390

Tamura, Y., Tani, K., Chang, Q., Shukuno, H., Kawabata, H., Ishizuka, O., & Fiske, R. S. (2007). Wet and Dry Basalt Magma Evolution at Torishima Volcano, Izu Bonin Arc, Japan: the Possible Role of Phengite in the Downgoing Slab. *Journal of Petrology, 48*(10), 1999-2031. doi:10.1093/petrology/egm048

Tamura, Y., & Tatsumi, Y. (2002). Remelting of an Andesitic Crust as a Possible Origin for Rhyolitic Magma in Oceanic Arcs: an Example from the IzuBonin Arc. *Journal of Petrology, 43*(6), 1029-1047.

Tatsumi, Y. (2003). Slab melting: Its contribution to continental crust formation and mantle evolution. *Geochim. Cosmochim. Acta, 67*(18), A478-A478.

Tatsumi, Y. (2005). The subduction factory: How it operates in the evolving Earth. *GSA Today, 15*(7), 4. doi:10.1130/1052-5173(2005)015[4:TSFHIO]2.0.CO;2

Tatsumi, Y., & Kogiso, T. (2003). The subduction factory: its role in the evolution of the Earth's crust and mantle. *Geological Society, London, Special Publications, 219*(1), 55-80. doi:10.1144/GSL.SP.2003.219.01.03

Taylor, B., & Natland, J. (1995). *Active margins and marginal basins of the western Pacific* (Vol. vol. 88). Washington, DC: American Geophysical Union.

Taylor, R. N., & Nesbitt, R. W. (1998). Isotopic characteristics of subduction fluids in an intra-oceanic setting, Izu–Bonin Arc, Japan. *Earth and Planetary Science Letters, 164*(1), 79-98. doi:10.1016/S0012-821X(98)00182-4

Taylor, S. R. (1967). The origin and growth of continents. *Tectonophysics, 4*(1), 17-34. doi:10.1016/0040-1951(67)90056-X

Taylor, S. R., McLennan, S. M., Armstrong, R. L., & Tarney, J. (1981). The Composition and Evolution of the Continental Crust: Rare Earth Element Evidence from Sedimentary Rocks [and Discussion]. *Philosophical Transactions of the Royal Society of London. Series A, Mathematical and Physical Sciences (1934-1990), 301*(1461), 381-399. doi:10.1098/rsta.1981.0119

Todd, E., Stracke, A., & Scherer, E. E. (2015). Effects of simple acid leaching of crushed and powdered geological materials on high-precision Pb isotope analyses. *Geochemistry, Geophysics, Geosystems, 16*(7), 2276-2302. doi:10.1002/2015GC005804

Tollstrup, D., Gill, J., Kent, A., Prinkey, D., Williams, R., Tamura, Y., & Ishizuka, O. (2010). Across-arc geochemical trends in the Izu-Bonin arc: Contributions from the subducting slab, revisited. *Geochemistry, Geophysics, Geosystems, 11*(1), n/a-n/a. doi:10.1029/2009gc002847

Turner, S., & Hawkesworth, C. (1997). Constraints on flux rates and mantle dynamics beneath island arcs from Tonga-Kermadec lava geochemistry. *Nature, 389*(6651), 568-573. doi:10.1038/39257

White, W. M. (2013). *Geochemistry*. Hoboken: Wiley.

Wiesner, M., Wetzel, A., Catane, S., Listanco, E., & Mirabueno, H. (2004). Grain size, areal thickness distribution and controls on sedimentation of the 1991 Mount Pinatubo tephra layer in the South China Sea. *Bulletin of Volcanology, 66*(3), 226-242. doi:10.1007/s00445-003-0306-x

Winter, J. D. (2010). *An introduction to igneous and metamorphic petrology* (2nd ed. ed.). New York: Prentice Hall.

Yoshihiko, T., Takeshi, S., Toshiya, F., Shuichi, K., & Alexander, N. (2016). Advent of Continents: A New Hypothesis. *Scientific Reports, 6*. doi:10.1038/srep33517

Yoshihiko Tamura, P. B., Cathy J. Busby. (2014). The missing half of the subduction factory: shipboard results from the Izu rear arc, IODP Expedition 350.

Zhao, D., Wang, Z., Umino, N., & Hasegawa, A. (2007). Tomographic imaging outside a seismic network; application to the northeast Japan Arc. *Bulletin of the Seismological Society of America, 97*(4), 1121-1132. doi:10.1785/0120050256

http://cobblab.blogspot.no/2012/09/enter-george-weve-spent-many-nights.html

(Downloaded 03.04.2017)

http://pcigr.eos.ubc.ca/instrumentation/multi-collector-icp-ms/

(Downloaded 03.04.2017)

https://online.science.psu.edu/chem101_sp1/node/6357

(Downloaded 03.04.2017)

APPENDIX 1 Overview of samples

Table 1. Overview of samples from UiB and JAMSTEC

Sample Number (UiB samples)	Nr	Unit	Depth	Description
350-U1437D-64R-1-W 118/121-HAME	1	IV	1018,98	Single clast handpicked, highly altered
350-U1437D-67R-CC-W 1/4-HAME	2	IV	1048,43	Collection of moderately altered small clasts handpicked
350-U1437D-69R-2-W 64/67-HAME	3	IV	1058,24	Single clast, but not big enough for Major/Trace/Isotopes
350-U1437D-70R-CC-W 19/20-HAME	4	IV	1075,06	Fresh looking single clast picked
350-U1437E-6R-3-W 106/109-HAME	5	IV	1119,95	Very fined grain consolidated
350-U1437E-17R-2-W 122/124-HAME	6	V	1216,01	Highly altered small clasts
350-U1437E-25R-3-W 59/60-HAME	7	V	1293,91	Single, fresh looking, grey clast picked for chemistry
350-U1437E-28R-1-W 9/11-HAME	8	VI	1320,09	Single clast picked
350-U1437E-41R-2-W 19/21-HAME	9	VI	1448,19	Moderately altered single clast
350-U1437E-51R-1-W 78/81-HAME	10	VII	1544,58	Fresh looking single clast picked
350-U1437E-56R-5-W 123/125-HAME	11	VII	1598,48	Part of a large clast, handpicked
350-U1437E-57R-1-W 58/60-HAME	12	VII	1602,78	Part of a large clast, handpicked
350-U1437E-66R-5-W 103/105-HAME	13	VII	1696,57	Part of a large clast, handpicked
350-U1437E-79R-2-W 37/41-HAME	14	VII	1798,58	Part of a large clast, handpicked

Sample Number (JAMSTEC samples)	Nr	Unit	Depth	Description
350-U1437E-19R-2-W 0/2-SATO	1	IV	1234,04	lapilli-tuff
350-U1437E-21R-6-W 43/44-SATO	2	IV	1259,89	tuff
350-U1437E-35R-1-W 123/125-SATO	3	V	1389,35	rhyodacite
350-U1437E-42R-4-W 106/112-SATO	4	V	1461,71	lapilli-tuff
350-U1437E-58R-2-W 36/38-SATO	5	VII	1604,08	andesite
350-U1437E-60R-2-W 60/66-SATO	6	VII	1633,45	andesite
350-U1437E-69R-3-W 9/11-SATO	7	VII	1712,28	andesite
350-U1437E-70R-4-W 129/131-SATO	8	VII	1724,5	andesite
350-U1437E-70R-6-W 35/37-SATO	9	VII	1726,51	andesite
350-U1437E-71R-2-W 69/71-SATO	10	VII	1730,48	Andesite
350-U1437E-79R-1-W 46/48-SATO	11	VII	1797,28	Andesite

APPENDIX 2 Trace element data

Table 2. Trace element data from UiB

Sample nr	1	2	3	4	5	6	7	8	9	10	11	12	13	14
Ba	104,6	390	162,8	106,1	237,3	114,1	50	NA	64,6	NA	26,2	74,9	86	90
Ce	32,57	20,65	34,58	27,92	NA	NA	NA	NA	NA	NA	NA	NA	NA	NA
Co	17,85	18,29	13,04	19,15	NA	NA	NA	NA	NA	NA	NA	NA	NA	NA
Cr	29,11	122,6	6,7	7,23	13,8	21,6	8,6	NA	64,4	112,3	85,4	159	45,3	23,3
Cs	0,126	0,206	0,159	0,126	NA	NA	NA	NA	NA	NA	NA	NA	NA	NA
Cu	26,19	39,61	10,97	36,23	126,3	47,6	41,2	NA	48,9	64,5	89,8	40,5	33,3	20,7
Dy	6,41	4,18	5,56	5,04	NA	NA	NA	NA	NA	NA	NA	NA	NA	NA
Er	4,1	2,66	3,53	3,1	NA	NA	NA	NA	NA	NA	NA	NA	NA	NA
Eu	1,78	1,25	1,46	1,51	NA	NA	NA	NA	NA	NA	NA	NA	NA	NA
Gd	6,51	4,14	5,44	5,17	NA	NA	NA	NA	NA	NA	NA	NA	NA	NA
Hf	3,32	2,94	3,73	3,14	NA	NA	NA	NA	NA	NA	NA	NA	NA	NA
Ho	1,34	0,86	1,12	1,02	NA	NA	NA	NA	NA	NA	NA	NA	NA	NA
La	14,65	9,25	16,14	12,91	NA	NA	NA	NA	NA	NA	NA	NA	NA	NA
Li	9,69	9,7	10,88	10,61	NA	NA	NA	NA	NA	NA	NA	NA	NA	NA
Lu	0,59	0,40	0,58	0,47	NA	NA	NA	NA	NA	NA	NA	NA	NA	NA
Mn	1117	990,2	1001	1076	NA	NA	NA	NA	NA	NA	NA	NA	NA	NA
Nb	6,68	6,6	6,25	6,31	0,7	3,2	NA	NA	1,5	0,9	0,5	1	1,4	1,5
Nd	22,28	14,23	20,92	17,71	NA	NA	NA	NA	NA	NA	NA	NA	NA	NA
Ni	8,44	27,39	3,24	5,5	13,2	27,9	6,4	NA	22,4	46,4	32,1	50,7	21,7	20,9
Pb	3,2	2,94	3,38	3,17	2,9	2,8	6,5	NA	2,2	NA	1,9	3,1	2,9	3,2
Pr	4,5	2,93	4,64	3,78	NA	NA	NA	NA	NA	NA	NA	NA	NA	NA
Rb	7,48	10,15	15,17	7,38	14	6,6	5,4	NA	6,7	1,9	2,9	5,1	8,2	3,6
Sc	22,95	26,38	16,99	24,12	NA	NA	NA	NA	NA	NA	NA	NA	NA	NA
Sm	5,66	3,68	5,13	4,67	NA	NA	NA	NA	NA	NA	NA	NA	NA	NA
Sr	381,7	388,1	371,1	438,9	507,4	373	67,2	NA	267	254,3	274	223,3	220,6	286,2
Ta	NA	NA	NA	NA	NA	NA	NA	NA	NA	NA	NA	NA	NA	NA
Tb	1,04	0,68	0,87	0,81	NA	NA	NA	NA	NA	NA	NA	NA	NA	NA
Th	1,89	1,74	2,32	1,97	NA	2,90	NA	NA	NA	NA	NA	NA	NA	NA
Tl	NA	NA	NA	NA	NA	NA	NA	NA	NA	NA	NA	NA	NA	NA
Tm	0,59	0,39	0,54	0,47	NA	NA	NA	NA	NA	NA	NA	NA	NA	NA
U	0,62	0,56	1,07	0,66	NA	NA	NA	NA	NA	NA	NA	NA	NA	NA
V	155,9	190,5	141,3	216	337,8	295,2	88	NA	311,1	292,7	349,9	275,4	234,5	254,5
Y	36,26	23,12	30,87	27,88	24,4	26,6	37,8	NA	36,5	27,7	21,5	26,7	27,9	23,8
Yb	3,91	2,66	3,77	3,15	NA	NA	NA	NA	NA	NA	NA	NA	NA	NA
Zn	94,1	91,3	81,2	88,8	111,8	102,5	137,8	NA	95,3	90,6	90,9	129,1	92,8	62,5
Zr	118,8	107,4	139,2	113,5	57,1	113,7	76,2	NA	94,3	79,4	54	77,4	88,9	96,8

Table 3. Trace element data from JAMSTEC

Sample nr	1	2	3	4	5	6	7	8	9	10	11
Ba	156	133	11,7	13,3	48,5	95,4	116	76,2	108	73,8	297
Ce	17,4	20,4	14,2	8,07	8,5	26,8	17,8	13,5	13,3	16,3	14,8
Co	33,4	29	1,78	19,6	27,6	20	18,8	17,4	23,8	21,7	16,1
Cr	NA	NA	NA	NA	NA	NA	NA	NA	NA	NA	NA
Cs	0,21	0,18	0,02	0,06	0,02	0,08	0,14	0,15	0,1	0,3	0,11
Cu	42,9	38,6	3,15	57,4	50,7	56,1	37,5	49,1	40,8	35,1	44,1
Dy	3,83	5,14	2,18	3,22	3,26	9,33	5,86	5,46	5,77	5,28	4,3
Er	2,65	3,4	1,6	2,08	2,1	6,85	3,83	3,56	3,82	3,39	3,16
Eu	0,971	1,22	0,569	0,791	0,805	1,87	1,34	1,26	1,26	1,25	1,19
Gd	3,33	4,66	2,06	2,77	2,83	7,83	5,18	4,6	4,7	4,64	3,9
Hf	1,79	2,38	2,13	1,49	1,5	2,23	2,96	2,62	2,76	2,67	2,72
Ho	0,86	1,12	0,48	0,69	0,70	2,18	1,27	1,18	1,26	1,13	0,97
La	7,33	7,87	6,03	2,94	3,13	11,4	5,92	4,71	4,19	6,17	5,46
Li	NA	NA	NA	NA	NA	NA	NA	NA	NA	NA	NA
Lu	0,39	0,52	0,29	0,30	0,31	1,02	0,58	0,52	0,56	0,50	0,53
Mn	NA	NA	NA	NA	NA	NA	NA	NA	NA	NA	NA
Nb	2,47	2,44	0,8	0,63	0,63	1,02	1,2	1,15	1,29	1,24	1,47
Nd	10,8	14,3	8,05	6,74	7,04	19,8	14,1	11,6	11,5	12,6	11,6
Ni	27,8	16,2	1,11	9,64	31,4	8,35	11,2	15,6	13,5	9,9	21,4
Pb	9,24	5,03	2,79	1,88	1,51	1,69	2,89	2,24	1,71	2,13	2,31
Pr	2,39	3,01	1,88	1,3	1,38	4	2,8	2,27	2,26	2,52	2,29
Rb	10,92	7,12	1,49	1,34	1,15	8,92	4,66	5,53	5,3	4,06	5,94
Sc	24,7	29,6	3,85	22,3	30,4	32,1	26,8	23,8	32,5	28,3	26
Sm	2,85	3,96	1,9	2,13	2,19	5,58	4,2	3,65	3,71	3,79	3,3
Sr	359	316	6,47	190	260	211	242	279	267	320	293
Ta	0,19	0,17	0,08	0,04	0,04	0,08	0,09	0,08	0,09	0,09	0,11
Tb	0,57	0,79	0,36	0,49	0,50	1,34	0,90	0,81	0,85	0,80	0,65
Th	1,41	1,30	0,80	0,33	0,34	0,57	0,75	0,65	0,69	0,67	0,82
Tl	0,19	0,07	0,01	0,02	0,01	0,08	0,04	0,06	0,06	0,04	0,06
Tm	0,39	0,50	0,26	0,30	0,30	0,99	0,57	0,52	0,56	0,50	0,49
U	0,53	0,52	0,42	0,22	0,12	0,23	0,34	0,31	0,28	0,35	0,38
V	NA	NA	NA	NA	NA	NA	NA	NA	NA	NA	NA
Y	23,3	29,8	13,8	17,2	18,1	69,2	34,2	32	34,9	30,7	26,6
Yb	2,51	3,38	1,88	2,00	2,03	6,49	3,80	3,48	3,68	3,28	3,39
Zn	NA	NA	NA	NA	NA	NA	NA	NA	NA	NA	NA
Zr	65,4	82,7	66,1	49,6	49,7	75,2	102	89,8	96	92,7	96,8

APPENDIX 3 Isotopic data

Table 4. Isotopic data from UiB

Sample nr	1	2	3	4	5	6	7	8	9	10	11	12	13	14
$^{87}Sr/^{86}Sr$	0,703264	0,703029	0,703030	0,703012	0,706166	0,703339	0,703756	0,703515	0,703103	0,703091	0,703126	0,703303	0,703648	0,703305
2SE	0,000007	0,000009	0,000009	0,000009	0,000009	0,000010	0,000008	0,000008	0,000009	0,000012	0,000008	0,000009	0,000011	0,000006
$^{143}Nd/144Nd$	0,513007	0,512911	0,512978	0,512984	0,513049	0,513007	0,513091	0,512877	0,513067	0,513068	NA	NA	NA	NA
2SE	0,000007	0,000007	0,000009	0,000007	0,000008	0,000012	0,000009	0,000009	0,000011	0,000014	NA	NA	NA	NA
$^{206}Pb/^{204}Pb$	18,2767	18,2953	18,2745	18,2778	18,2979	18,3213	18,4489	18,3128	18,2741	18,2182	18,2399	18,2158	18,2398	18,2335
2SE	0,0003	0,0003	0,0004	0,0003	0,0003	0,0003	0,0003	0,0003	0,0003	0,0003	0,0004	0,0003	0,0002	0,0002
$^{207}Pb/^{204}Pb$	15,5125	15,5259	15,5063	15,5165	15,5448	15,5310	15,6001	15,5302	15,5203	15,4846	15,4974	15,4813	15,4879	15,4912
2SE	0,0002	0,0003	0,0004	0,0002	0,0002	0,0003	0,0002	0,0002	0,0002	0,0003	0,0002	0,0003	0,0002	0,0002
$^{208}Pb/^{204}Pb$	38,1660	38,2220	38,1382	38,1634	38,2729	38,2492	38,5712	38,2155	38,1681	38,0403	38,0987	38,0312	38,0689	38,0740
2SE	0,0007	0,0009	0,0014	0,0007	0,0007	0,0007	0,0007	0,0007	0,0007	0,0008	0,0008	0,0009	0,0007	0,0007
$^{207}Pb/^{206}Pb$	0,8488	0,8486	0,8485	0,8489	0,8495	0,8477	0,8456	0,8481	0,8493	0,8500	0,8496	0,8499	0,8491	0,8496
$^{208}Pb/^{206}Pb$	2,0882	2,0892	2,0870	2,0880	2,0917	2,0877	2,0907	2,0868	2,0886	2,0880	2,0888	2,0878	2,0871	2,0881
$\Delta^{207}Pb$	4,03	5,17	3,43	4,42	7,03	5,39	10,92	5,41	4,84	1,88	2,92	1,57	1,97	2,37
$\Delta^{208}Pb$	44,25	47,61	41,73	43,86	52,38	47,18	63,95	44,83	44,77	38,75	41,97	38,13	38,99	40,27
176Hf/177Hf	0,2831803	0,2831824	0,2831901	0,2832173	0,2832427	0,2832033	0,2832472	0,2832696	0,2832558	0,2832460	0,2832377	0,2832361	0,2832530	0,2832407
2SE	0,000004	0,000004	0,000003	0,000004	0,000003	0,000003	0,000004	0,000004	0,000004	0,000004	0,000004	0,000003	0,000004	0,000003

..

Table 5. Isotopic data from JAMSTEC

Sample nr	1	2	3	4	5	6	7	8	9	10	11
$^{87}Sr/^{86}Sr$	0,703054	0,703139	0,704130	0,703118	0,703056	0,703123	0,703417	0,703227	0,703407	0,703271	0,703472
2SE	0,000008	0,000008	0,000007	0,000007	0,000006	0,000007	0,000007	0,000007	0,000008	0,000007	0,000006
$^{143}Nd/144Nd$	0,512987	0,513028	0,513094	0,513095	0,513081	0,513078	0,513061	0,513081	0,513071	0,513078	0,513072
2SE	0,000008	0,000008	0,000006	0,000009	0,000009	0,000008	0,000008	0,000009	0,000009	0,000009	0,000008
$^{206}Pb/^{204}Pb$	18,3979	18,3186	18,5250	18,2462	18,2306	18,2086	18,2433	18,2609	18,2382	18,2392	18,2519
2SE	0,0013	0,0009	0,0010	0,0025	0,0024	0,0010	0,0010	0,0010	0,0008	0,0011	0,0011
$^{207}Pb/^{204}Pb$	15,5620	15,5238	15,5146	15,4917	15,4858	15,4914	15,4951	15,5020	15,4971	15,4969	15,5001
2SE	0,0011	0,0009	0,0009	0,0026	0,0025	0,0009	0,0009	0,0008	0,0007	0,0010	0,0009
$^{208}Pb/^{204}Pb$	38,4047	38,2123	38,2577	38,0545	38,0335	38,0429	38,0691	38,1030	38,0719	38,0690	38,0868
2SE	0,0035	0,0023	0,0024	0,0042	0,0034	0,0024	0,0024	0,0023	0,0020	0,0027	0,0023
$^{207}Pb/^{206}Pb$	0,8459	0,8474	0,8375	0,8490	0,8494	0,8508	0,8494	0,8489	0,8497	0,8496	0,8492
$^{208}Pb/^{206}Pb$	2,0875	2,0860	2,0652	2,0856	2,0862	2,0893	2,0867	2,0866	2,0875	2,0872	2,0867
$\Delta^{207}Pb$	7,67	4,71	1,55	2,28	1,86	2,66	2,66	3,15	2,90	2,88	3,06
$\Delta^{208}Pb$	53,47	43,81	23,40	36,78	36,56	40,16	38,59	39,85	39,49	39,08	39,32
176Hf/177Hf	0,2831948	0,2832077	0,2832372	0,2832390	0,2832388	0,2832389	0,2832416	0,2832405	0,2832345	0,2832415	0,2832411
2SE	0,000005	0,000004	0,000005	0,000004	0,000004	0,000004	0,000005	0,000005	0,000005	0,000005	0,000005